Exploring the role of 4-hydroxy-2-nonenal and mitochondrial dysfunction in diabetic neuropathy

by

Eli Kwaku Akude

A Thesis submitted to the Faculty of Graduate Studies of

The University of Manitoba

in partial fulfillment of the requirements of the degree of

DOCTOR OF PHILOSOPHY

Department of Pharmacology and Therapeutics

University of Manitoba

Winnipeg

Contributions

Dr. Elena Zherebitskaya performed the fluorescence imaging described in Figs. 20 and 35. Dr. Subir Roy Chowdhury performed the mitochondrial respiration and complex activity studies described in Fig. 30 and Table 6, and the Western blot described in Fig. 36. Dr. Rick Dobrowsky performed the proteomics work described in Figs. 27 and 28, and Table 4. Induction of diabetes and maintenance of animal groups, analysis of blood glucose or glycated hemoglobin was performed by Dr. Darrel Smith.

Acknowlegdements

This work was supported by a grant from NSERC to Dr. Paul Fernyhough, Manitoba Health Research Council, St. Boniface General Hospital Research Foundation and the Alzheimer's Society of Manitoba. I wish to thank: Dr. Gordon Glazner, University of Manitoba and St Boniface Hospital Research Centre, for permitting access to the Carl Zeiss LSM 510; Dr. Elena Zherebitskaya, St Boniface Hospital Research Centre, for the training provided on the confocal microscope; Dr. Rick Dobrowsky, University of Kansas, Dept of Pharmacology and Toxicology, for the proteomics analysis; and Dr. Paul Fernyhough, University of Manitoba and St Boniface Hospital Research Centre, for his patience and wonderful supervision.

Table of contents

Abstract

In diabetes hyperglycemia and lack of insulin signaling are key factors in the induction of diabetic sensory neuropathy. The combination of these factors in diabetes may enhance oxidative stress and trigger distal nerve damage in the peripheral nervous system. The link between elevated reactive oxygen species (ROS) levels and nerve degeneration is not clear. We tested the ***hypothesis*** that elevation of 4-hydroxy-2-nonenal (4-HNE) induced by oxidative stress in diabetes impairs mitochondrial activity and axonal regeneration in dorsal root ganglion (DRG) neurons. Also, we investigated the association between mitochondrial dysfunction and altered mitochondrial proteome in the axons of streptozotocin–induced diabetic rats.

Research design and methods. Cultured adult rat DRG sensory neurons were treated exogenously with 4-HNE, and cell survival, axonal morphology, and level of axon outgrowth assessed. Western blot and fluorescence imaging were used to determine changes in the levels of adducts of 4-HNE and abnormalities in the mitochondria. Proteomic analysis using stable isotope labeling with amino acids in cell culture (SILAC) determined expression of proteins in the mitochondria.

Results. 4-HNE impaired axonal regeneration, mitochondrial activity and induced aberrant axonal structures along the axons, which mimicked axon pathology observed in nerve isolated from diabetic rats and replicated aspects of neurodegeneration observed in human diabetic neuropathy. Proteins associated with mitochondrial dysfunction, oxidative phosphorylation and biosynthesis were

down regulated in diabetic samples. The axons of diabetic neurons exhibited oxidative stress and depolarized mitochondria. CNTF and resveratrol reversed abnormalities in the mitochondrial membrane potential induced by diabetes and treatment of neurons with 4-HNE.

CONCLUSIONS. Elevation of 4-HNE levels in diabetes was associated with impaired mitochondrial function and might be an important link between increased ROS levels and nerve degeneration in diabetic neuropathy**.** Abnormal mitochondrial function correlated with a down-regulation of mitochondrial proteins, with components of the respiratory chain targeted in lumbar DRG in diabetes. The reduced activity of the respiratory chain was associated with diminished superoxide generation within the mitochondrial matrix and did not contribute to oxidative stress in axons of diabetic neurons.

List of tables

List of figures

28. Expression of components of the electron transport chain are reduced in DRG from STZ- induced diabetic rats.
29. The mitochondria of DRG sensory neurons exhibited lower respiratory chain activity.
30. The mitochondria in the axons of normal neurons show greater levels of FCCP-induced depolarization compared with neurons from diabetic rats.
31. Low micromolar concentrations of FCCP do not affect the plasma membrane potential in cultured DRG neurons.
32. The mitochondria in the axons of normal neurons show greater levels of depolarization compared with neurons from diabetic rats.
33. Oligomycin induces greater hyperpolarization levels in the axons of STZ-induced diabetic neurons compared with controls.
34. Impaired respiratory function is associated with reduced ROS generation in the mitochondrial matrix of cultured neurons isolated from STZ-induced diabetic rats.
35. Expression of some proteins that regulate cellular energy metabolism is reduced in DRG from STZ- induced diabetic rats.
36. CNTF normalizes abnormalities in the rate of depolarization in the axons of diabetic neurons.
37. CNTF normalizes abnormal levels of hyperpolarization induced by oligomycin in the axons of STZ- induced diabetic neurons.
38. Resveratrol normalizes abnormalities in the rate of depolarization in the axons of diabetic neurons.

39. Resveratrol normalizes abnormal levels of hyperpolarization induced by oligomycin in the axons of STZ-induced diabetic neurons.
40. Rate of mitochondrial depolarization is slower in DRG neurons treated with 4-HNE.
41. CNTF normalizes abnormalities in the rate of depolarization in the axons of 4-HNE treated neurons.

Chapter 1:

Background and literature review

1.1. Diabetes

Diabetes mellitus is a disease considered by the world health organization as one of the main threats to human health in the 21st century (Zimmet 2000). It affects over 150 million people worldwide, and with profound changes in human behavior, life style and the environment, this figure could increase to about 300 million by the year 2025 (Amos, McCarty et al. 1997; King, Aubert et al. 1998).

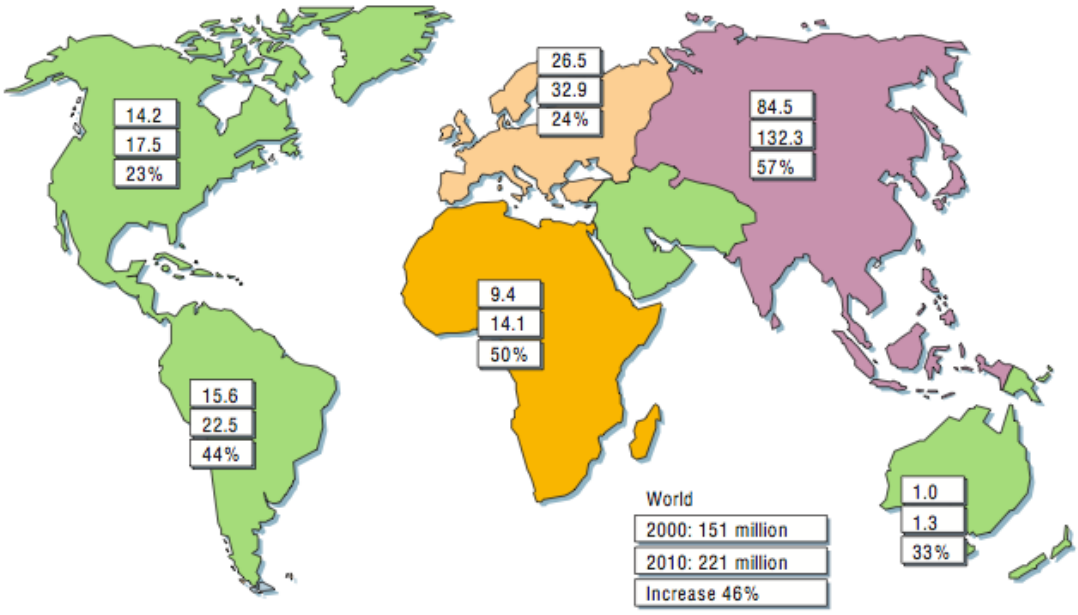

Fig. 1. Number of people with diabetes (millions) for 2000 (top) and 2010 (middle), and the percentage increase worldwide. (Adapted from (Zimmet 2000)).

Type 1 diabetes also known as insulin dependent diabetes mellitus (IDDM), is a T-cell mediated autoimmune disorder. It is characterized by selective destruction of the pancreatic β cells, resulting in absolute insulin deficiency (Kelly, Rayner et al. 2003). Susceptibility to type 1 diabetes is attributed to environmental and genetic factors. The environmental factors believed to contribute to the risk of developing type 1 diabetes include viral infections (Dahlquist 1997), dietary factors in early infancy (Ellis and Atkinson 1996), vaccination, climate influences, toxins, and stress (Akerblom, Knip et al. 1997). The interaction between the environmental factors and genetic factors is poorly understood. While some investigators believe environmental agents trigger disease development in genetically susceptible individuals, others suggest that environmental factors may modify the developing immune system in an age dependent manner irrespective of genetic susceptibility, and may therefore promote or attenuate disease at different stages of development, depending on the timing and the number of exposures (Dahlquist 1997; McKinney, Parslow et al. 1999). None of these environmental agents have been conclusively implicated in the etiology of type 1 diabetes; however, an infection with rubella or coxsackie B4 virus is frequently associated with an increased risk of developing the disease (Ou, Mitchell et al. 2000; Varela-Calvino, Ellis et al. 2002).

The genetic risk factors of the disease are better understood. Two genes believed to be associated with the development of this disease are the human leucocyte antigen (HLA, designated IDDM1) located on chromosome 6p21 (Nerup, Platz et al. 1974) and insulin gene region (designated IDDM2) located

on chromosome 11p (Bain, Prins et al. 1992). The IDDM1 locus is a major risk factor for the disease and accounts for approximately 42% of familial inheritance; it encompasses the HLA genes and consists of about 200 genes subdivided into three sub-regions, classes I, II, and III. The HLA class II genes provide the strongest genetic risk, in that, specific structural modification determines their ability to activate the auto-reactive T cells responsible for β cell destruction. The IDDM2 locus contributes a further 10% of genetic susceptibility (Davies, Kawaguchi et al. 1994). The variable number of tandem repeats (VNTR) region upstream of the insulin gene also makes an important contribution to the disease, although the mechanism is not known (Kelly, Rayner et al. 2003).

The frequency of type 1 diabetes is low compared with type 2 diabetes, which accounts for about 90 % of cases globally (Zimmet 2000). People with type 2 diabetes are not dependent on exogenous insulin, but may require insulin to stabilize blood glucose levels if diet and exercise fails. The risk factors for this disease include sedentary life styles, obesity, family history, impaired glucose tolerance and ethnicity. Type 2 diabetes is characterized by insulin resistance and defective pancreatic β cell function resulting in hyperglycemia. The mechanism of insulin resistance or β cell failure is not well understood (Todd 1996). However, recent studies in obese mice with homozygous null mutation at the tumor necrosis factor alpha (TNFα) loci showed improved insulin receptor signaling capacity and sensitivity (Lorenzo, Fernandez-Veledo et al. 2008; Nieto-Vazquez, Fernandez-Veledo et al. 2008). Other factors include mutations in the insulin receptor and hepatocyte nuclear factor -1α gene (Yamagata, Oda et al.

1996). In both type 1 and type 2 diabetes uncontrolled hyperglycemia results in development of degenerative complications of the eye (retinopathy), heart, kidneys (nephropathy) and the nerves (neuropathy), thereby reducing the quality of life.

1.2. Epidemiology of diabetic neuropathy

One of the commonest complications of diabetes is peripheral neuropathy (Tesfaye, Stevens et al. 1996). It affects about 20-30 million people worldwide, and with the increase in rates of obesity and associated prevalence of type 2 diabetes this figure could double by the year 2025 (Said 2007). In young adults with uncontrolled type 1 diabetes, neuropathy develops shortly after the onset of diabetes (Said, Bigo et al. 1998). Neuropathy comprises a cross range of syndromes, and the classification of the various syndromes into distinct groups has been difficult due to the overlap in etiology, clinical features, natural history and prognosis. Nonetheless, attempts at classification enhance our understanding of the etiology of the disease and aids in the design of strategies for patient management (Table 1;Tesfaye, 2007).

Distal symmetrical neuropathy, the primary focus of this work, is the most common neuropathic syndrome, affecting about 80% of patients with clinical neuropathy (Said 2007). The disease is characterized by a ‘length-related pattern of sensory loss’ with symptoms beginning and remaining pronounced in the toes and then extending to involve more proximal parts of the lower limbs, indicating that the longest nerves are affected first during the progression of the disease

(Said 2007; Yagihashi, Yamagishi et al. 2007). Similar progression is also observed in the upper limbs. In rare cases, symptoms can extend over the entire body including the head and face (Said, Slama et al. 1983).

Table. 1. Classification of diabetic neuropathy

Symmetrical neuropathies	Asymmetrical neuropathies
Distal sensory and sensory-motor neuropathy	Mononeuropathy
Large-fiber type of diabetic neuropathy	Mononeuropathy multiplex
Small-fiber type of diabetic neuropathy	Radiculopathies
Distal small-fiber type diabetic neuropathy	Lumbar plexopathy or radiculoplexopathy
Chronic inflammatory demyelinating polyradiculoneuropathy	

(Adapted from (Tesfaye, 2007))

1.3. Clinical presentation

The main clinical presentation of distal neuropathy is sensory loss described as numbness or a 'dead feeling'. Some patients may also experience a progressive build up of unpleasant sensory sensations particularly in the feet. This includes tinglings, burning pains, contact pain (allodynia) especially at bedtime, pain in walking described as 'walking bare foot on marble or hot sands' (Tesfaye, 2007). Occasionally, symptoms extend above the feet and may involve the leg and upper limbs. Some patients do not show the above symptoms, and the first presentation of neuropathy is foot ulceration (Yagihashi, Yamagishi et al.

2007). This predisposes patients to thermal and mechanical injury, and more importantly infection, which could result in gangrene and foot amputations. Proper foot management of patients is paramount under these conditions (Yagihashi, Yamagishi et al. 2007). Indeed, a great proportion of all foot amputations are attributed to neuropathy in the advanced world (Abbott, Vileikyte et al. 1998).

1.4. Pathology of diabetic neuropathy

The pathology of diabetic neuropathy has been extensively studied in human diabetic patients. Most of the pathological studies have been performed on autopsy or biopsied materials mainly from the sural nerve in diabetic patients with established neuropathy (Yagihashi, Yamagishi et al. 2007). Underpinning these pathological changes are several morphological alterations in nerves, ganglia and the microvascular system. Studies in human subjects and experimental models of diabetes have attempted to correlate the pathological changes to the pathophysiological and functional deficits observed in neuropathy; however, the link between these factors is still not clear.

1.5. Peripheral nerve abnormalities in human diabetic neuropathy

The early pathological features in human diabetic neuropathy observed in teased fibers from the sural nerve include an increase in abnormal fibers due to paranodal abnormalities, segmental demyelination and remyelination. There is no evidence of axonal degeneration, regeneration, changes in myelinated fiber density and fiber diameter (Sugimura and Dyck 1981; Dyck, Zimmerman et al.

1988; Ziegler, Mayer et al. 1988; Malik, Veves et al. 2001; Malik, Tesfaye et al. 2005). Qualitative assessment of unmyelinated fibers demonstrates an increase in unassociated Schwann cell profiles (indicative of degeneration) and higher axon density, but the axon show reduced diameter suggestive of axonal regeneration (Ziegler, Mayer et al. 1988; Said, Goulon-Goeau et al. 1992; Malik, Tesfaye et al. 2005). Also, the early morphological changes in myelinated and unmyelinated fibers are associated with mild but progressive changes in nerve conduction velocity, neuropathic symptoms, neurological deficits and cardiac autonomic function (Ziegler, Mayer et al. 1988; Malik, Tesfaye et al. 2005).

In human diabetic patients with established neuropathy, nerve biopsy and teased fiber studies demonstrate segmental demyelination, remyelination, fiber loss and paranodal abnormalities. (Dyck, Zimmerman et al. 1988; Llewelyn, Gilbey et al. 1991; Malik, Veves et al. 2001). The process of demyelination could be primarily due to Schwann cell dysfunction or secondarily related to impairment of axonal control of myelination (Kalichman, Powell et al. 1998), proliferation of Schwann cells and hypertrophy of the basal lamina (Kalichman, Powell et al. 1998). Segmental demyelination in teased fibers is recognized by axons with inappropriately thin myelin sheath or splitting of myelin sheath with the accumulation of granular vesicular debris (Yagihashi and Matsunaga 1979). Reports of segmental demyelination without prominent axonal degeneration contributed to the view that demyelination was the primary lesion of diabetes induced injury (Thomas and Lascelles 1965), but detailed neurophysiological studies in sural and peroneal nerves in human subjects have shown that the

process of demyelination precedes axonal loss and that the latter may be responsible for the clinical symptoms (Valls-Canals, Povedano et al. 2002). In fact, certain clinical features of diabetic neuropathy are best explained by both demyelination and nerve degeneration (Said 1983). Remyelination following demyelination is recognized in the axons by the formation of onion bulbs - clusters of Schwann cells in concentric arrangements (Thomas and Lascelles 1965; Chopra, Hurwitz et al. 1969). Onion bulbs are believed to be a result of recurrent segmental demyelination and remyelination (Thomas and Lascelles 1965). Loss of small and large myelinated nerve fibers is evident in diabetic patients with established neuropathy; however, this does not correlate with demyelination (Behse, Buchthal et al. 1977; Dyck, Zimmerman et al. 1988; Llewelyn, Gilbey et al. 1991; Malik, Veves et al. 2001). Paranodal abnormalities described in diabetic neuropathy include demyelination, paranodal swelling and axoglial dysjunction (Sima, Nathaniel et al. 1988; Sima, Prashar et al. 1993). Paranodal swellings have been suggested to precede paranodal demyelination and associated with axoglial dysjunction (Sima, Nathaniel et al. 1988; Sima, Prashar et al. 1993); however, these abnormalities have not been observed in other studies (Giannini and Dyck 1996; Thomas, Beamish et al. 1996). Axonal atrophy has been described by some investigators, but there is no convincing evidence of this occurring in diabetic subjects (Engelstad, Davies et al. 1997).

Nerve fiber loss in sensory neuropathy is length-dependent and predominates distally, progressing towards the more proximal parts of the body (Said 2007). The involvement of small sensory myelinated and unmyelinated sensory fibers in

the ‘dying-back’ process is supported by recent morphological and physiological studies in the epidermis and dermis of lower limb skin of diabetic subjects, which presents clinically as reduced intraepidermal nerve fiber (IENF) density. This is demonstrated by skin biopsy studies in diabetic patients with neuropathy (Kennedy and Zochodne 2005; Wendelschafer-Crabb, Kennedy et al. 2006; Ebenezer, McArthur et al. 2007), HIV patients with neuropathy (Polydefkis, Yiannoutsos et al. 2002), skin of calf in subjects with impaired glucose tolerance (IGT) (Polydefkis, Griffin et al. 2003; Sumner, Sheth et al. 2003), and structural abnormalities in the IENF (Lauria, Morbin et al. 2003). The extent of skin denervation increases with the duration of diabetes (Shun, Chang et al. 2004). Whereas, loss of small nerve fibers have been associated with the loss of sensation and elevation of warm threshold in sensory neuropathy, the loss of large fibers in the dermis results in disturbance of light touch sensation, sensibility to pressure and vibration, and joint position sense (Said 2007; Yagihashi, Yamagishi et al. 2007).

1.6. Peripheral nerve abnormalities in animal models of diabetic neuropathy

Experimental animals have been extensively employed to mimic functional and morphological changes observed in human patients with diabetic neuropathy. The most commonly used rat model of neuropathy is the streptozotocin (STZ)-induced diabetic rat (a model of type 1 diabetes); much of our understanding of diabetic neuropathy has been gained from this model. Deficits in nerve conduction velocity, abnormalities in nerve blood flow and changes in pain perception threshold develop within weeks of induction of

diabetes in STZ diabetic rats, (Kennedy, Quick et al. 1982; Sharma, Thomas et al. 1983; Calcutt, Jorge et al. 1996; Cotter, Jack et al. 2002). Despite the development of these early functional and metabolic abnormalities, STZ diabetic rats do not reproduce structural changes observed in the human condition (Wright and Nukada 1994; Walker, Carrington et al. 1999). For example, The STZ-rat model does not demonstrate loss of myelinated and unmyelinated fibers in a number of peripheral nerves including the sural nerves (Sharma and Thomas 1974; Brown, Sumner et al. 1980), tibial nerves (Sharma and Thomas 1974), peroneal (Jakobsen 1976; Jakobsen 1976), and sciatic nerves (Wright and Nukada 1994) . Reports of changes in myelinated fiber size in this model are conflicting; while some studies find no abnormalities in the mean fiber diameter (Sharma, Bajada et al. 1981; Wright and Nukada 1994), others report a decrease in fiber size in myelinated fibers, which is attributed to axonal atrophy (Jakobsen 1976; Jakobsen 1976). Experimental studies show nodal and paranodal degeneration with axo-glial dysfunction (Sima, Zhang et al. 2004), but no evidence of paranodal and segmental demyelination has been reported in STZ diabetic rats (Jakobsen 1976; Jakobsen 1976). Nerve fiber loss has been reported in the epidermis of STZ-induced diabetic rats (Bianchi, Buyukakilli et al. 2004), but several groups have not replicated this finding.

The STZ diabetic mouse model has several advantages over the rat model, in that, some strains develop severe hyperglycemia without the characteristic weight loss associated with the rat model, thereby minimizing the sources of variability (Kennedy and Zochodne 2000; Qi, Fujita et al. 2005). There is a

slowing of motor and sensory nerve conduction velocity in the sciatic (Obrosova, Mabley et al. 2005) and tibial nerves despite normal axon caliber (Kennedy and Zochodne 2000). Morphometric studies on the sural nerve of these mice demonstrate demyelination, axonal loss at the distal ends of the nerve and impairment of axonal regeneration (Kennedy and Zochodne 2000). Some STZ-diabetic mice show significant reduction in epidermal nerve fibers. For example, STZ-induced diabetic inbred C57BL and MrgD mice show significant reduction in epidermal nerve fibers and behavioral deficits in mechanical and thermal sensitivity following the induction of diabetes (Christianson, Ryals et al. 2003; Johnson, Ryals et al. 2008).

Unlike the rat and mouse models of neuropathy, myelinated nerve fiber pathology in the feline diabetic model is similar to that present in human neuropathy. Work by Mizisin et al. on the peroneal nerve in diabetic cats demonstrates axonal and Schwann cell injury, demyelination and remyelination, and extensive fiber loss (Mizisin, Shelton et al. 2002; Mizisin 2003; Mizisin, Nelson et al. 2007). Structural abnormalities in other models of type 1 diabetes such as the BB/ Wor-rat include nodal and paranodal swellings with progressive axonal atrophy more pronounced distally (Sima and Kamiya 2006). These structural abnormalities ultimately result in axonal degeneration with secondary myelin break down and fiber loss.

Abnormalities in the peripheral nerves of animal models of type 2 diabetes appear to be milder compared with animal models of type 1 diabetes. The most prominent abnormality is the loss of epidermal nerve fibers, demonstrated in the

skin of Zucker diabetic fatty (ZDF) rats (long-term model of type 2 related diabetic neuropathy) (Brussee, Guo et al. 2008) and the leptin deficient (ob/ob) mouse (Drel, Mashtalir et al. 2006). Mild axonal atrophy, demyelination and axonal degeneration have also been reported in other models of type 2 diabetes (Norido, Canella et al. 1984; Sima, Zhang et al. 2000; Murakawa, Zhang et al. 2002; Iizuka, Suzuki et al. 2005).

1.7. Abnormalities in the ganglia of human diabetic neuropathy

Although neuropathies primarily involve peripheral nerves, other parts of the neuraxis including projections within the central nervous system and the dorsal root ganglia (DRG) may play a role. Abnormalities in the DRG may account for the early sensory abnormalities in human polyneuropathy. The major ultrastructural change in the DRG of human diabetics is neuroaxonal dystrophy (axonal sprouting). This is characterized by swollen terminal axons and enlarged proximal segments of axons or cell body projections (Schmidt, Dorsey et al. 1997). Neuroaxonal dystrophy affects a subpopulation of intraganglionic axons containing calcitonin gene regulated peptide (CGRP) and substance P, while the noradrenergic sympathetic axons are largely spared. Some larger diameter neurons have been shown to be targets of dystrophic swellings, indicating the involvement of this subpopulation of neurons in the pathology of the disease (Schmidt, Dorsey et al. 1997). Other pathological changes include increased amounts of lipofuscin and neuromelanin and accumulation of neurofibrillary tangles (Kawasaki, Murayama et al. 1987). Disorganization of the rough endoplasmic reticulum and Golgi bodies has been reported in the DRG of human

diabetics. Despite these ultrastructural changes, the cell bodies within the lumbar DRG appear normal (Sidenius and Jakobsen 1980), and no evidence of apoptotic dependent loss of neurons have been demonstrated in human diabetics (Schmidt, Dorsey et al. 1997). Although, the loss of DRG neurons have been reported in some human diabetics (Nagashima and Oota 1974), detailed morphometric evaluation of the first sacral ganglion show no evidence of neuronal loss (Ota, Offord et al. 1974).

1.8. Abnormalities in the ganglia of animal models of diabetic neuropathy

Various ultrastructural abnormalities have been reported in animal models of neuropathy. In a study on lumbar DRG neurons, Jakobsen et al demonstrates a reduction in the volume of the cell body after 4 weeks of induction of diabetes in adult rats. The reduced cell body size in the DRG was believed to be due to a combination of shrinkage of nerve cell bodies and inhibition of normal increase of the cell body volume during the experimental period (Sidenius and Jakobsen 1980). Also, some studies have reported apoptosis of neurons in the DRG of STZ-induced diabetic rats as a prominent feature of diabetic sensory neuropathy (Russell, Sullivan et al. 1999), while this study might correctly identify activation of caspase -3 and -9 and some DNA damage associated with apoptosis in diabetic sensory neurons, clear evidence of neuronal loss is lacking. Examination of DRG's isolated from BB/Wor rats show no evidence of apoptosis (Kamiya, Zhangm et al. 2005; Kamiya, Zhang et al. 2006), further, a rigorous study using the physical dissector counting method clearly demonstrates the absence of sensory neuronal loss at 2 months of experimental diabetes, although some loss

of small neurons, probably as a result of aging, occurred over a longer time point (Zochodne, Verge et al. 2001). Additionally, cell loss has been observed in the BB rat model at 10 months, however, there is little evidence to suggest that apoptosis was involved in this process. It is not clear whether these structural abnormalities observed in the ganglia of animal model models of type 1 diabetes are replicated in models of type 2 diabetes.

1.9. Microvascular system in diabetic neuropathy

Microangiopathy, a hallmark of diabetes is believed to induce hypoxia and resultant neuropathy (Fagerberg 1959). Several microvascular factors have been implicated in the pathogenesis of diabetic neuropathy. In human diabetics, nerve blood capillaries show markedly greater abnormalities compared with capillaries in other tissues like the muscle and the skin, and the severity of these abnormalities increases with the severity of neuropathy (Malik, Newrick et al. 1989; Bradley, Thomas et al. 1990; Malik, Veves et al. 1992). Early in the onset of neuropathy, a reduction in the endoneurial capillary density without an increase in the mean fascicular area occurs (Malik, Veves et al. 1992), and this might be associated with reduced nerve blood flow and hypoxia. As the disease progresses, endothelial cell hyperplasia and hypertrophy become evident (Dyck, Hansen et al. 1985; Timperley, Boulton et al. 1985; Yasuda and Dyck 1987). Endothelial hypertrophy may be a late feature of neuropathy since there is no evidence of endothelial cell hypertrophy in human subjects with mild neuropathy. Thickening of the basement membrane area and decrease in endothelial cell profile numbers per capillary have been reported; this correlates with

neurophysiological and neuropathological measures of neuropathic severity (Giannini and Dyck 1995). Other abnormalities in nerve blood capillaries include luminal occlusions and reduced nerve blood flow (Yasuda and Dyck 1987; Malik, Newrick et al. 1989). Endoneurial changes correlate with reduction of peroneal, sural nerve conduction velocities and myelinated fiber density in human diabetic subjects (Malik, Metcalfe et al. 1992).

Evidence for the involvement of microvascular abnormalities in the pathology of diabetic neuropathy in experimental animals is rather confusing. Tuck and colleagues reported a substantial reduction in nerve blood flow, increased microvascular resistance and lowered nerve oxygenation in 4 months STZ-induced diabetic rats (Tuck, Schmelzer et al. 1984). This finding was corroborated in subsequent studies by other investigators, thus replicating the microvascular abnormalities in human diabetic subjects. However, Williamson and colleagues consistently demonstrated early rises in nerve blood flow in STZ-induced diabetic rats (Sutera, Chang et al. 1992; Tilton, Chang et al. 1995). This is supported by studies which failed to identify reduction in nerve blood flow in 4 months old STZ-induced diabetic rats (Zochodne and Nguyen 1999). Also, this study showed increased numbers of whole nerve and endoneurium microvessels with associated rise in vessel densities and total luminal areas. Despite this controversy there is evidence to the effect that nerve hypoxia develops in early experimental models of neuropathy (Zochodne and Nguyen 1999).

1.10. Pathogenesis of diabetic neuropathy

There is evidence to show a strong link between the morphological severity of neuropathy and glycemic control in both type 1 and type 2 diabetes (Perkins, Greene et al. 2001). Complex metabolic processes downstream of high glucose are involved in the etiology of diabetic neuropathy; these include enhanced polyol pathway activity, increased nonenzymatic glycation of proteins, elevated oxidative stress, impaired neurotrophic support and changes in protein kinase C activation (Yagihashi, Yamagishi et al. 2007; Calcutt, Jolivalt et al. 2008; Tomlinson and Gardiner 2008). Hyperglycemia-induced generation of reactive oxygen species (ROS) by the mitochondria has been proposed to link these mechanisms, suggesting a role for mitochondrial dysfunction in the etiology of this disease (Brownlee 2001).

1.10.1. Polyol pathway activation

Neurons have a constantly high demand for glucose and neuronal uptake of glucose is independent of insulin. Thus, glucose uptake in the nerve depends on the extracellular glucose concentration. Diabetes-induced hyperglycemia can result in a four-fold increase in glucose levels in the nerve compared with other tissues (Tomlinson and Gardiner 2008); the persistence of high glucose levels in nerves could result in nerve damage, a phenomenon referred to as glucose neurotoxicity (Tomlinson 1999). While there is mounting evidence for the role of hyperglycemia in the etiology of neuropathy, the mechanisms that link hyperglycemia and nerve damage in diabetes are poorly understood (Oates

2002). The polyol pathway activation provides the first plausible link between hyperglycemia and nerve dysfunction in diabetes (Tomlinson and Gardiner 2008). Evidence for this hypothesis originates from work by Heyningen and Gabbay, showing the elevation of polyols and free sugars in the lens and nerve of diabetic rats (Gabbay, Merola et al. 1966). The first enzyme in this pathway, aldose reductase (AR), has a lower affinity for glucose compared with hexokinase, a key enzyme in the glycolytic pathway (Hers 1960). Therefore, under normal conditions, the majority of glucose is converted into glucose-6-phosphate through the hexokinase pathway with trace amounts being converted to sorbitol by the polyol pathway. However, under hyperglycemic conditions, it is believed the hexokinase pathway becomes saturated and the rise in intracellular glucose concentration approaches the K_m of AR. This may result in the accumulation of sorbitol, which can lead to nerve damage (Oates 2002; Tomlinson and Gardiner 2008). Although an osmotic effect of sorbitol may play an important role in nerve dysfunction (Kinoshita 1990; Lee and Chung 1999), the preponderance of literature favors the metabolic flux hypothesis. The polyol pathway compromises the glutathione cycle by converting NADPH to NADP, which reduces the capacity of glutathione peroxidase to metabolize hydrogen peroxide to water (Cheng and Gonzalez 1986; Williamson, Chang et al. 1993). This could result in the increase in production of superoxide and hydroxyl radicals through the Fenton reaction leading to oxidative stress (Oates and Mylari 1999).

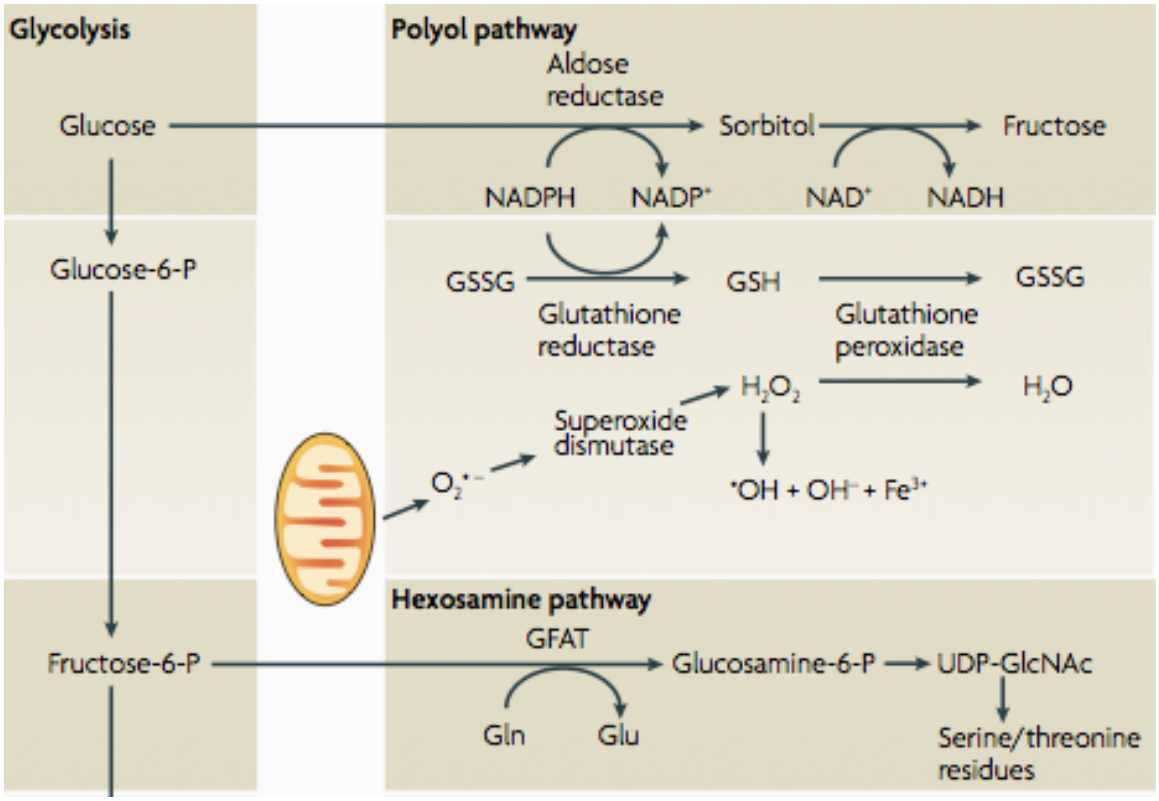

Fig. 2. Schematic representation of metabolic pathways favored by raised intracellular glucose levels. (Adapted from (Tomlinson and Gardiner 2008)).

Direct evidence for the involvement of the polyol pathway in oxidative stress comes from the observation that treatment of diabetic rats with aldose reductase inhibitors results in normalization of various markers of oxidative stress (Obrosova, Van Huysen et al. 2002). The second enzyme in the polyol pathway, sorbitol dehydrogenase (SDH), converts sorbitol to fructose. AR and SDH are predominantly in the cytoplasm and are believed to catalyze metabolic steps in the polyol pathway sequentially. Because both enzymes and their metabolites are found in peripheral nerve tissue extracts, it was assumed that they were in communication through their metabolites. However, there is no published data showing in vivo colocalization of the two enzymes in peripheral neurons (Oates

2002). AR immunoreactivity is observed in Schwann cell, pericytes, and smooth muscle cell of endo- and epineurial microvessels in postmortem human sciatic nerve (Kasajima, Yamagishi et al. 2001). In this study, immunoassayed AR content of the sciatic nerve of human diabetics was found to be 1.8 fold higher in diabetic compared with normal sciatic nerves. The localization of AR in human sciatic tissue is consistent with previous work in rat, mouse and rabbit peripheral nerves (Gabbay and O'Sullivan 1968; Ludvigson and Sorenson 1980; Chakrabarti, Sima et al. 1987). Strong SDH immunoreactivity is present in tubular cells of the renal cortex, but only trace amounts have been detected in postmortem human sciatic nerves (Mizisin, Li et al. 1997; Kasajima, Yamagishi et al. 2001; Cunha, Jolivalt et al. 2008).

Several studies have reported the protective effects of aldose reductase inhibitors (ARI) in diabetic rats. ARI's have been demonstrated to suppress nerve polyol levels, protect and correct nerve conduction velocity and other neuronal abnormalities (Yue, Hanwell et al. 1982; Schmidt, Plurad et al. 1991; Tomlinson, Willars et al. 1992; Cameron, Cotter et al. 1994; Yagihashi 1997). ARI's have direct antioxidant effects, protect nerve glutathione levels and normalize various markers of oxidative stress such as protein adducts of 4-hydroxy-2-nonenal and malondialdehyde (Lowitt, Malone et al. 1995; Obrosova, Cao et al. 1998; Jiang, Calcutt et al. 2006).

1.10.2. Nonenzymatic glycation of proteins

Another effect of hyperglycemia is the non-enzymatic glycation of proteins (Brownlee 2001). It is caused by the direct addition of open chain glucose to lysine groups on proteins resulting in the formation of a Schiff base. This undergoes a slow, spontaneous rearrangement to form a stable advanced glycation end-product (AGE) (Singh, Barden et al. 2001; Jakus and Rietbrock 2004). AGE's have been detected in sural, peroneal, and saphenous nerves of human diabetics (Sugimoto, Nishizawa et al. 1997) and sciatic nerves of STZ-diabetic rats (Sensi, Morano et al. 1998). AGE's have the capacity to alter cellular responses through the receptor for AGE (RAGE) (Li, Mitsuhashi et al. 1996). Activation of RAGE can lead to the activation of NF-κB and the disruption of intracellular signals, which destabilizes several processes in the nerve (Thornalley 1988; Haslbeck, Neundorfer et al. 2007). Oxidative stress enhances the process of protein glycation, which in-turn increases oxidative stress. The lack of molecules that directly inhibit glycation have limited our understanding of the functional and structural effects of glycation of nerve proteins. Although aminoguanidine has been utilized to this end, its usefulness as an in vivo investigative tool is limited. New inhibitors such as pyridoxamine might provide some insight into the effects of glycation (Tomlinson and Gardiner 2008).

1.10.3. Oxidative stress

Oxidative stress occurs in cells when the generation of free radicals exceeds the antioxidant scavenging capacity. The targets of free radicals include protein, lipids and nucleic acids. Molecules modified by free radicals lose their biological properties, leading to the disruption of metabolism, cell signaling, transport, and other major functions (Vincent, Russell et al. 2004). Several studies have implicated oxidative stress in the pathogenesis of diabetic peripheral neuropathy (Obrosova 2002) . Oxidative stress possibly triggered by abnormalities in the endoneurial capillaries in the nerve is associated with abnormalities in nerve blood flow, conduction deficits, impaired neurotrophic support, changes in signal transduction, and morphological abnormalities characteristic of peripheral neuropathy (Cameron, Eaton et al. 2001; Yorek 2003; Malik, Tesfaye et al. 2005). There is a close correlation between oxidative stress and the development of complications associated with diabetic neuropathy. Oxidative stress occurs in both type 1 and type 2 diabetes at the onset of the disease, and there are reports of decreased antioxidant potential and increased plasma lipid peroxidation as well as decreased plasma GSH and GSH metabolizing enzymes all of which are markers of oxidative stress (Vincent, Russell et al. 2004). In experimental models of diabetic neuropathy, oxidative stress is manifested in several ways including the increased generation of ROS in vascular endothelial cells (Nishikawa, Edelstein et al. 2000), increased lipid peroxidation (Obrosova 2002), protein nitrosylation and decreased levels of glutathione and ascorbate in peripheral nerves and sensory neurons (Obrosova, Ilnytska et al. 2007).

1.10.4. Reactive oxygen species

There are several forms of ROS involved in the mediation of cellular degradation in disease states such as diabetic neuropathy. Superoxides, hydrogen peroxides and peroxynitrite are different forms of ROS, which have been widely studied, in peripheral neuropathy. It is believed that superoxides are generated through the activity of the respiratory chain and by-products of many enzymes that act as oxidases (Fridovich 1995; Brownlee 2001) (a detailed description of the involvement of the mitochondria in the production of oxidative stress will be discussed later). Hydrogen peroxide is generated spontaneously following superoxide dismutase (SOD) catalyzed conversion of superoxides and it is broken down by the enzyme catalase into water. Hydrogen peroxide reacts with free Fe^{2+} to release hydyroxyl free radicals, which are believed to mediate the modification of lipids, proteins and other biological molecule in the cell (Antunes and Cadenas 2000). The activity of the cytosolic enzyme nitric oxide synthase leads to the generation of nitric oxide (NO), which has a dual role as being beneficial or detrimental to cells. NO is believed to react with excess superoxides to form a pro-oxidant known as peroxynitrite, which has been implicated in the pathogenesis of neuropathy (Obrosova, Drel et al. 2005).

1.10.5. Oxidative stress in cultured neurons

Studies in cultured embryonic neurons have demonstrated that high glucose concentration induces excessive generation of ROS and this was associated with significant neuronal loss (Russell, Golovoy et al. 2002; Vincent, McLean et al.

2005). Also, work by Brownlee and colleagues in smooth muscle endothelial cells showed hyperglycemia induced an increase in ROS generation (Brownlee 2001). However, studies on adult DRG neurons demonstrated an increase in ROS levels in axons of neurons with a diabetic phenotype following exposure to high glucose, but not in non-diabetic neurons. In this study treatment of the diabetic neurons with an antioxidant reduced ROS levels. Significantly, no neuronal loss was observed when non-diabetic or diabetic neurons were exposed to high glucose (Gumy, Bampton et al. 2008; Yu, Rouen et al. 2008; Zherebitskaya, Akude et al. 2009).

1.10.6. Oxidative stress in endoneurial capillaries

Oxidative stress might be a contributing factor to vascular abnormalities in peripheral neuropathy. These abnormalities include reduced endoneurial blood flow and impairment of acetylcholine-mediated vascular relaxation of arterioles that provide circulation to the sciatic nerve in STZ-induced diabetic rats (Coppey, Gellett et al. 2001). It has been demonstrated that these vascular abnormalities precede the slowing of sensory and motor nerve conduction velocities. Several in vivo and in vitro studies have demonstrated the accumulation of superoxides and peroxynitriles results in nitric oxide quenching in the arterioles that provide circulation to the sciatic nerves and this has been associated with the vascular abnormalities in diabetes (Yorek 2003). Indeed, treatment of diabetic rats with antioxidants such as α-lipoic acid reduces the accumulation of superoxides. This may result in the reduction of peroxynitriles and hence a reduction in the quenching of nitric oxides and an improvement in vascular function and

improving nerve ischemia. Nerve ischemia is believed to be one of the key factors in the process of nerve degeneration associated with sensory neuropathy. Taken together, these reports indicate that oxidative stress and vascular dysfunction may be major factors in the development of sensory neuropathy (Coppey, Gellett et al. 2003).

1.10.7. Oxidative stress in peripheral nerves

The manifestation of oxidative stress in peripheral neuropathy includes the accumulation of lipid peroxidation products (Lowitt, Malone et al. 1995), protein nitrosylation products, and the disruption of the antioxidant defense mechanism (Obrosova, Ilnytska et al. 2007). These changes in diabetes have been demonstrated in peripheral nerve, dorsal root and sympathetic ganglia (Obrosova 2002). Studies by Lowitt et al showed increases in levels of malondialdehyde in the sciatic nerves of STZ- induced diabetic rats and this was reversed by acetyl-carnitine and sorbinil - previously shown to clear products of lipid peroxidation (Lowitt, Malone et al. 1995). Also, elevation of the lipid peroxidation product 4-hydroxy-2-nonenal and conjugated diennes have been observed in the sciatic nerves of STZ-induced diabetic rats (Obrosova 2002). Further, work by Calcutt et al showed that the treatment of STZ-induced diabetic rats with aldose reductase inhibitors reduced the levels of hydroxy-2-nonenal in the sciatic nerves (Cunha, Jolivalt et al. 2008).

1.10.8. Disruption of the antioxidant defense mechanism in diabetes

The antioxidant defense system plays a critical role of limiting the increase in ROS levels in tissues. Abnormalities in this defense mechanism provides the most convincing evidence to date on the involvement of oxidative stress

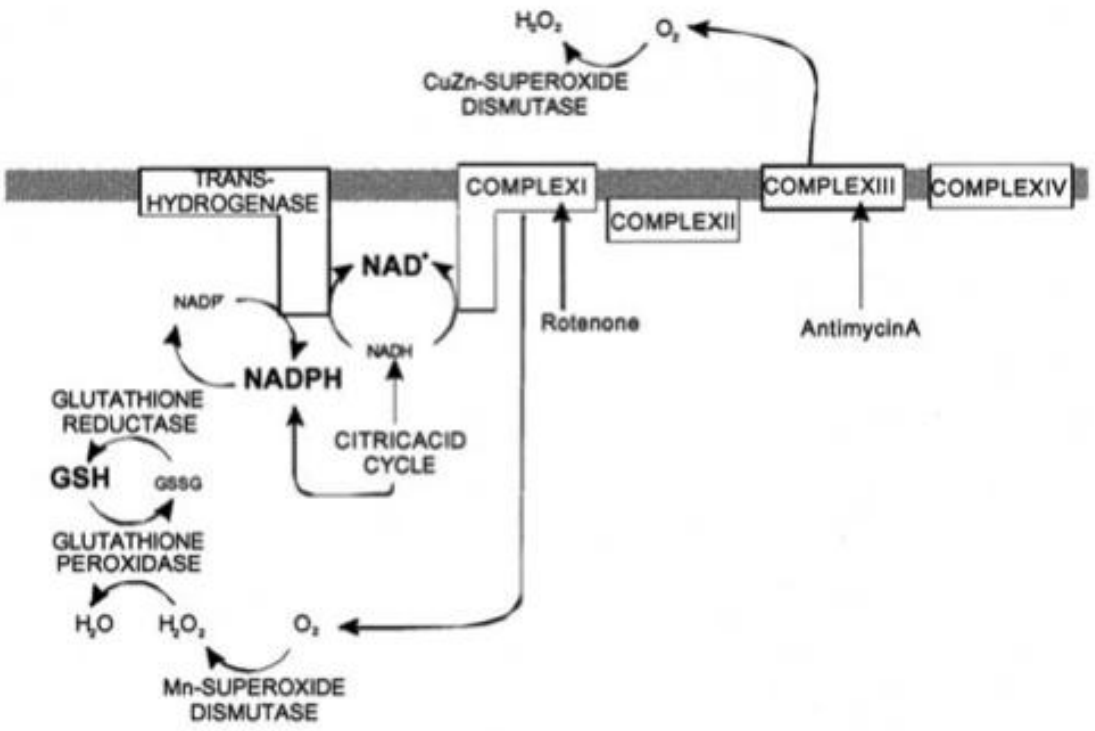

Fig. 3. Schematic representation of the antioxidant defense system in the mitochondrial matrix. Superoxide generated by the mitochondria is detoxified by Mn-superoxide dismutase to hydrogen peroxide, which is converted into water by glutathione peroxidase. The glutathione pool is maintained reduced by glutathione reductase , which utilizes NADPH formed by transhydrogenase and isocitrate dehydrogenase, (adapted from (Nicholls 2004))

in the pathogenesis of peripheral neuropathy (Obrosova 2002). The reported abnormalities in the antioxidant defense system observed in the peripheral nerves of STZ-induced diabetic rats include the depletion of reduced gluthatione

(GSH) (Nagamatsu, Nickander et al. 1995; Obrosova, Fathallah et al. 1999), ascorbate, and taurine (Nagamatsu, Nickander et al. 1995); and an increase in the oxidized gluthatione ratio and dehydroascorbate/ascorbate ratio (Nagamatsu, Nickander et al. 1995; Obrosova, Fathallah et al. 2001). Gluathione provides the main pathway for the detoxification of hydrogen peroxide, converting hydrogen peroxide into water. Also, the impairment of enzymatic antioxidants such as catalase, quinone reductase and SOD has been reported in diabetic rats (Low and Nickander 1991; Stevens, Obrosova et al. 2000). All of these changes have been observed in peripheral nerves, dorsal root and sympathetic ganglia of the peripheral nervous system and smooth muscle endothelial cells (Giardino, Edelstein et al. 1996) of STZ –diabetic rats. Moreover, treatment of diabetic rats with antioxidants reverses most of the abnormalities associated with peripheral neuropathy (Obrosova 2002).

1.11. Lipid peroxidation

Lipid peroxidation involves the free radical oxidation of polyunsaturated fatty acids such as arachidonic acid and linoleic acids in membranes to release highly reactive compounds such as 4-hydroxy-2-nonenal (4-HNE), which is one of the most widely studied products of lipid

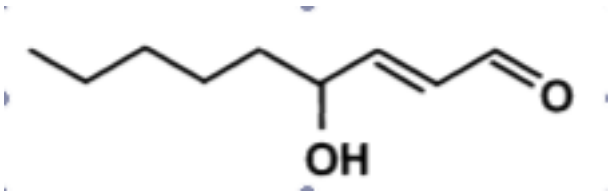

Fig. 4. Chemical structure of 4-hydroxy-2-nonenal. (Adapted from (Uchida 2003))

peroxidation (Uchida 2003). 4-HNE is an α, β - unsaturated aldehyde and contains three functional groups, a hydroxyl group, a conjugated system consisting of a C=C double bond and a carbonyl group C=O, which together provides a partial positive charge to the third carbon atom. Thus nucleophilic attack by thiols and other amino acids occur primarily at carbon three and secondarily at carbon one. 4-HNE is an electrophile, which is toxic to cells at certain concentrations (Uchida 2003; Carini, Aldini et al. 2004; Petersen and Doorn 2004); it can form protein adducts with amino acid residues such as cysteine, histamine, and lysine due to its strong electrophilic properties (Uchida 2003; Isom, Barnes et al. 2004). The presence of these protein adducts can serve as biomarkers for the occurrence and extent of oxidative stress. 4-HNE inhibits neurite outgrowth, disrupt microtubules, and modifies tubulin in Neuro 2A neuroblastoma cells (Neely, Sidell et al. 1999; Kokubo, Nagatani et al. 2008), and has cytotoxic and genotoxic effects (Karlhuber, Bauer et al. 1997). Low basal levels of 4-HNE are present in cells (< 1μM) and at this concentration it serves as a signaling molecule (Awasthi, Sharma et al. 2003). 4-HNE levels are elevated in several neurodegenerative disorders including peripheral neuropathy and

Alzheimer's disease (Petersen and Doorn 2004; Obrosova, Drel et al. 2005).

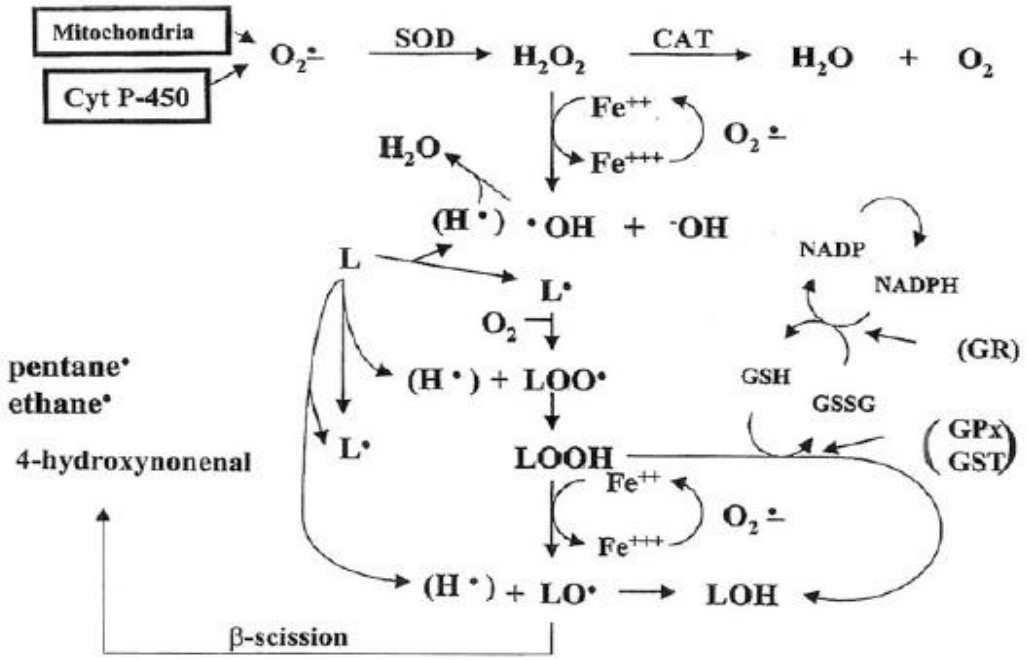

Fig. 5. Autocatalytic chain process for the production of 4-HNE. SOD: superoxide dismutase, CAT: catalase , LOOH : lipid hydroperoxide, GSH: reduced glutathione, Cyt P-450 : cytochrome P-450. (Adapted from (Yang, Sharma et al. 2003)

In diabetes, adducts of 4-HNE are elevated in the sciatic nerve and retina of STZ- diabetic rats (Obrosova, Fathallah et al. 2001; Obrosova, Drel et al. 2005). Further, modification of sorbitol dehydrogenase subunits in the mitochondrial respiratory chain has been associated with increased levels of 4-HNE in cardiomyocytes (Lashin, Szweda et al. 2006). The cellular effects of 4-HNE are dependent on the ability of a particular cell to metabolize 4-HNE. For example, isolated hepatocytes are much more resistant to the cytotoxic effects of 4-HNE because of the activities of diverse enzymatic pathways for oxidation and reduction of 4-HNE, as well as enzymes conjugating the 4-HNE with GSH. On the contrary, other cell types such as fibroblasts and neurons are much more

susceptible to the toxic effects of 4-HNE due to their limited ability to detoxify the aldehyde (Luckey and Petersen 2001). Sub-cytotoxic concentrations of 4-HNE have been reported in several studies to directly or indirectly alter a variety of cellular systems. The mitogen-activated protein kinase (MAPK) pathways involved in cellular stress responses, appear to be particularly sensitive to 4-HNE (Uchida 2003). 4-HNE has been demonstrated to activate c-jun terminal kinases (JNK) and p38, both of which can regulate several transcription factors involved in cellular responses including cell proliferation, inflammation and protein degradation (Petersen and Doorn 2004). Several studies have reported the activation of these stress-activated protein kinases in experimental models of diabetic neuropathy possibly leading to axonal degeneration. The effect of increased 4-HNE on this process is not fully understood (Uchida 2003; Yang, Sharma et al. 2003).

1.11.1. Reactions of 4-HNE with protein nucleophiles

4-HNE reacts with nucleophiles through 1,2- and 1,4- Michael addition (Esterbauer, Schaur et al. 1991).1,2- addition involves the reaction of a primary amine such as Lys with a carbonyl that has an α, β - unsaturation, resulting in the formation of a carbinolamine intermediate that rearranges and loses water to yield a Schiff base product. This reaction has been shown to occur in hydrophobic protein microenvironments (Nadkarni and Sayre 1995). 1,4- addition of 4-HNE readily occurs via the reaction of a nucleophile with C3 of the lipid aldehyde, and the net result is the addition of a nucleophile and proton across the 4-HNE carbon-carbon double bond (C=C).

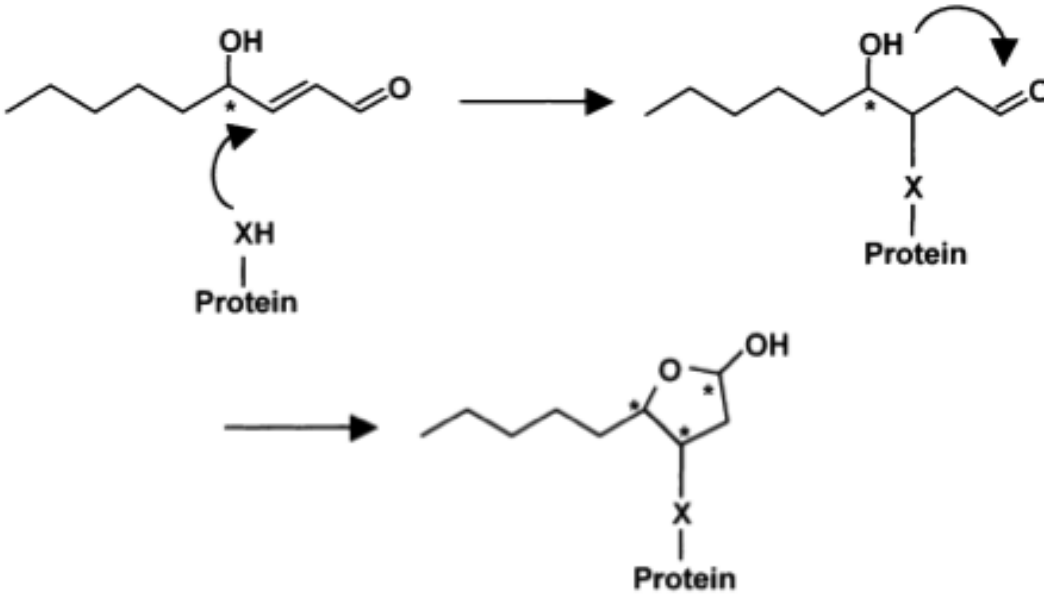

Fig. 6. Michael adduction of 4-HNE to protein. X: sulfhydryl group of cysteine, imidazole group of histidine or ε-amino group of lysine. (Adapted from (Uchida 2003))

The initial product is an enolate, which rearranges to a keto form followed by protonation of the C2 carbanion. The addition product does not contain a C=C at (C2-C3) and subsequently rearranges to a cyclic hemiacetal through the hydroxyl group reacting with C=O functional group. The final product is a protein adduct of 4-HNE (Esterbauer, Schaur et al. 1991). Protein residues known to react with 4-HNE via 1,4 addition include Cys, His, and Lys. The order of reactivity towards 4-HNE is Cys > His > Lys. Based on the measured rate constant Cys may have the greatest reactivity towards 4-HNE but may form the least stable adduct, however, 4-HNE forms the most stable adduct with His conjugates (Nadkarni and Sayre 1995; Petersen and Doorn 2004).

1.11.2. Metabolism of 4-HNE

The interaction of 4-HNE with protein nucleophiles is reflected in the ability of the cell to biotransform the aldehye into a non- toxic and less reactive form. Different mechanisms for the metabolism of 4-HNE have been described in several cell types. 4-HNE can be converted to 4-hydroxy-2-enoic acid, this reaction is catalysed by mitochondrial aldehyde dehydrogenase (ALDH2) in an NAD-dependent manner, and the resulting 4-HNA is not a Michael acceptor and hence cannot react with protein nucleophiles (Mitchell and Petersen 1987). 4-HNE can also be reduced by numerous enzymes including aldehyde reductase, aldose reductase and members of the AKR 1C subfamily. These enzyymes are efficient catalysts for NADPH-dependent reduction of 4-HNE, yeiding the inactive 1,4-dihydroxy-2-nonene (Burczynski, Sridhar et al. 2001).

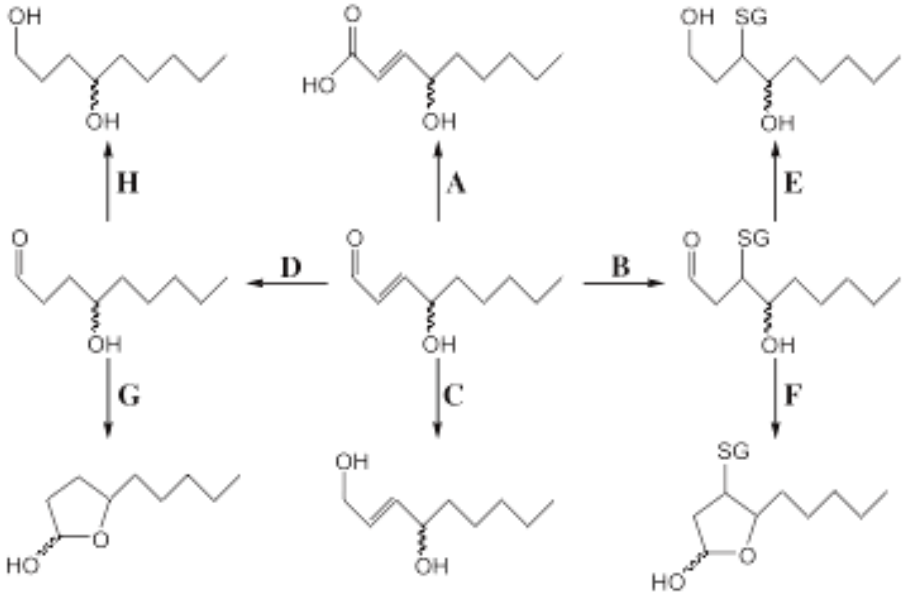

Fig. 7. Major pathways for 4-HNE biotransformation. (A) ALDH2 catalyzed oxidation to 4HNA. (B) GST mediated GSH conjugation (C) Enzyme catalyzed reduction to DHN. (D) AO mediated

reduction of C=C. (E) AR catalysed reduction to GS-DHN (F) spontaneous rearrangement to a cyclic hemiacetal adduct. (G) spontaneous rearrangemnt to a lactol. (H) Reduction of 4HNA. (adapted from (Petersen and Doorn 2004)).

Under physiological conditons GSH reacts with 4-HNE through Michael addition to yield a glutathione-4HNE conjugate. However, glutathione-s-transferase (GST) enzymes have been found to catalyze this reaction 600-fold compared with the spontaneous reaction. It is worth noting that GS-4HNE is also a substrate for AR, which catalyses NADPH-dependent reduction of the conjugate to glutathione-DHN (Alin, Danielson et al. 1985). Recent work has demonstrated enzyme catalyzed reduction of the C=C of 4-HNE by one oxidoreductase (AO). This enzyme has been found to have a high level of reactivity towards 4-HNE in the presence of NADPH, by converting it to 4-hydroxynonanal, which rearranges to a lactol form lacking free aldehyde (Dick, Kwak et al. 2001). It has been reported in hepatocytes that the cellular excretion of 4-HNE metabolites occur through the MRP2 transporter, however it is not clear how this occurs in other cell types like neurons (Reichard, Doorn et al. 2003). Several studies have attempted to quantitate intracellular 4-HNE metabolism and the degree to which it undergoes oxidation, reduction and conjugation with glutathione. From this quantitation it was observed that the major biotransformtaion pathway for 4-HNE was GSH conjugation acounting for about 60% of 4-HNE elimination. Whereas oxidation and reduction accounted for only 10% of metabolism (Hartley, Ruth et al. 1995).

1.12. Mitochondria

Mitochondria are the primary ATP generation organelles in the cell. ATP is generated through the activity of a host of proteins residing in the inner mitochondrial membrane, which forms the electron transport chain (ETC). Apart from ATP production, the mitochondria are believed to be the main source of ROS, which is known to elevate levels of 4-HNE in the cell. The elevation of ROS in the cell induces the degeneration of tissue in several disease states including diabetic neuropathy. The mitochondria have also been shown to be involved in the signaling of cell death and survival, the biosynthesis of hormones, cell signaling molecules and abnormal calcium homeostasis.

1.12.1. Structure of the mitochondrion

The mitochondrion is a very dynamic organelle of 0.1-0.5μm in diameter that occupies a substantial portion of the cytoplasm in eukaryotes. It is enclosed by two highly specialized membranes, creating two mitochondrial compartments: the internal matrix and a much narrower intermembrane space. The outer membrane contains many porin molecules, which act as non-specific pores for solutes of low molecular weight. The inner membrane is the energy-transducing portion of the mitochondria. It is highly convoluted, forming a series of in-foldings known as cristae, which projects into the matrix. This organelle contains a high proportion of the phospholipid cardiolipin and transport proteins, which makes it selectively permeable to molecules that are metabolized by the enzymes in the matrix. The enzymes of the electron transport chain are embedded in the inner mitochondrial

membrane, and they are essential to the process of oxidative phosphorylation, which generates ATP.

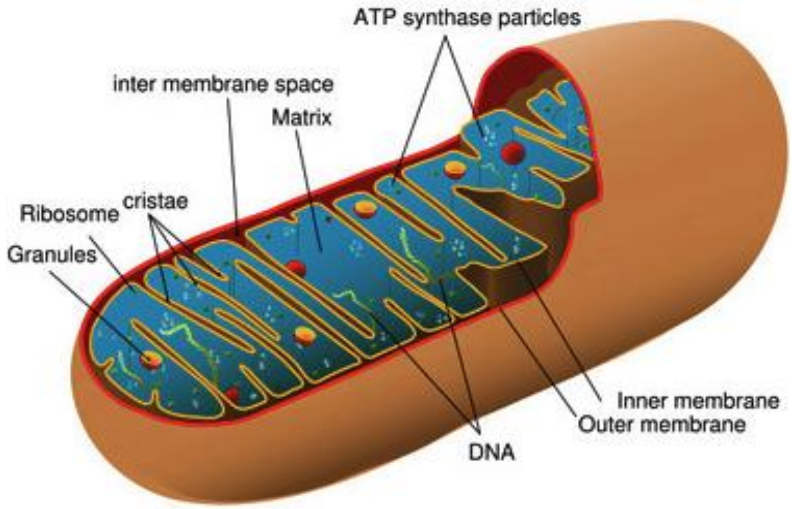

Fig. 8. Cross sectional view of the mitochondrion showing the various compartments in the mitochondrion (adapted from http://en.citizendium.org/images/c/c7/MitochondriaSMALL2.jpg)

The matrix contains enzymes that metabolize pyruvate acid and fatty acid to release acetyl CoA and those that oxidize acetyl CoA into the citric acid cycle. The main by-product of this oxidation is NADH, which is fed into the electron transport chain to generate ATP (Nicholls 2004).

Mitochondrial respiratory chain

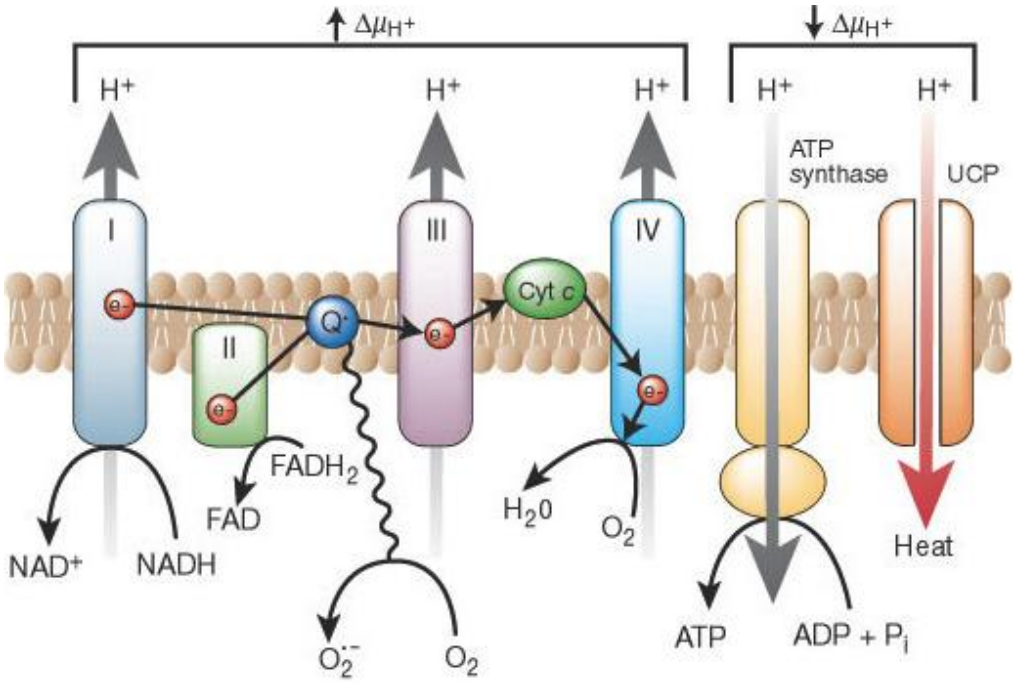

Fig. 9. Schematic diagram of the mitochondrial electron transport chain. (adapted from (Brownlee 2001))

The electron transport chain is an assembly of more than 20 discrete electron carriers that are grouped into several multi polypeptide complexes. These are NADH: ubiquinone oxidoreductase (complex 1), succinate: ubiquinone oxidoreductase (complex II), cytochrome C oxidoreductase (complex III) , cytohrome C oxidase (complex IV) and ATP synthase also known as F_1F_0-ATPase (complex V). Complexes I, III and IV serve as proton pumps, using the energy of the electron transfers to translocate protons from the matrix to the inner mitochondrial space, thereby generating and sustaining the electrochemical gradient across the inner membrane (Schultz and Chan 2001). The mitochondrial complex I is a large enzyme, it has about 43 subunits and contains

a non-covalently bound flavin mononucleotide (FMN) molecule, nine iron-sulfur clusters and two ubiquinone binding sites. It accepts electrons from NADH, which is formed from glycolysis and the TCA cycle, and transfers through flavin and seven iron-sulfur clusters to ubiquinone. The transfer of electrons is coupled with release of protons, which are pumped into the inner mitochondrial space (Sazanov and Walker 2000). Complex II has four subunits and a molecular weight of 125kDa. Although it is not a protein pump, it facilitates the entry of electrons into the respiratory chain and serves as a site for the regulation of the activity of the citric acid cycle. It oxidizes succinate to fumarate and transfers electrons from succinate to ubiquinone (Ohnishi, Moser et al. 2000). Complex III exists functionally as a dimer, with each monomer consisting of eleven subunits. Three subunits, cytochrome *b*, c_1 and an iron-sulfur protein, contain all of the redox active metal centres of the enzyme and constitute the catalytic core of the protein. The enzyme catalyses the transfer of electrons from ubiquinol to ferricytochrome C. Proton translocation involves a Q-cycle, a mechanism by which complex III serves as a proton pump. One electron from the oxidation of ubiquinol is used to reduce ferricytochrome c on the cytoplasmic side, while the other electron is used to reduce ubiquinone to ubiquinol with the associated release of protons from the matrix to the cytoplasmic side (Darrouzet, Moser et al. 2001). Complex IV has13 subunit and four redox centres: Cu_A, a binuclear copper centre located in subunit II; Cu_B, a mononuclear copper found in subunit I; and two heme, a six-cordinate low-spin heme a and a five –cordinated high spin heme a_3, both of which are located in subunit I. Dioxygen binds to heme a_3 and

$Cu_{B,}$ and is reduced to water. Cu_A serves as the initial acceptor of electrons from cytochrome c, and heme (a) mediates the transfer of electrons from Cu_A to the heme copper centre. Thus cytochrome oxidase catalyzes the transfer of electrons from cytochrome c to dioxygen in the final step of respiration. Also, this process involves the release of protons from the matrix side to the cytoplasmic side of the mitochondria increasing the electrochemical gradient (Schultz and Chan 2001). The electrochemical gradient generated by the pumping of protons from complex I, III and IV to the cytoplasmic side of the inner mitochondria membrane creates a driving force known as the mitochondrial membrane potential ($\Delta\Psi_m$), which drives ATP synthase to generate ATP (Nicholls 2004).

1.12.2. Synthesis / hydrolysis of ATP

Pyruvates and fatty acids transported across the inner mitochondrial membrane are converted to acetyl CoA by enzymes in the matrix. The acetyl groups are then oxidized by the citric acid cycle to release CO_2 and activated carrier molecules NADH and FADH2 carry electrons. These electrons are transferred to the inner mitochondrial membrane where they enter the electron transport chain. ATP synthase utilizes the electrochemical gradient across the inner mitochondrial membrane to promote the phosphorylation of ADP to ATP. ATP synthase consists of a membrane bound subcomplex F_0, a large extramembranous complex F_1 that resides in the matrix, and a stalk connecting the two complexes. The F_0 complex contains nine distinct subunits and forms an ion channel that allows the flow of protons from the cytoplasmic to the matrix side. F_1 complex has $\alpha_3 \beta_3 \gamma\delta\ \varepsilon$ subunit composition, it is involved in ATP

synthesis and hydrolysis and the active site for ATP synthesis or hydrolysis resides on the β subunits. The flow of protons through this enzyme promotes the rotation of a large subunit assembly, and the energy from this rotation is utilized for ATP synthesis. It is worth noting that ATP synthase under certain conditions can operate in the reverse direction leading to the hydrolysis of ATP. Thus the essence of the chemiosmotic theory is that the primary proton pumps (complex I, III and IV) generate a sufficient gradient of protons to force the secondary pump (ATP synthase) to synthesize ATP from ADP and P_i (Schultz and Chan 2001; Nicholls 2004).

1.12.3. Regulation of mitochondrial membrane potential (ψ_m)

The regulation of ROS production, ATP synthesis, calcium homeostasis and cell survival depends to a large extent on the gradient of protons across the inner mitochondrial membrane (Nicholls 2004). The quantitative thermodynamic measure is the proton electrochemical gradient ($\Delta\mu_H^+$). This gradient, measured in KJ/mol, has two components: one due to the concentration difference of protons across the membrane (ΔpH) and one due to the electrical potential between the two aqueous phases separated by the membrane, known as the membrane potential ($\Delta\Psi$) (Nicholls and Budd 2000). Primary pumps and secondary pumps regulate the membrane potential. The secondary pumps include ATP synthase, cation and anion carriers, the NADH/NADP transhydrogenase, uncoupling proteins (UCP1, UCP2, UCP3) and adenine nucleotide transporter (ANT). Glycolysis results in the elevation of pyruvate,

which drives the TCA cycle to generate more NADH (Schuit, De Vos et al. 1997). The increase in the NADH and $FADH_2$ increases the activity of the primary pumps of the respiratory chain leading to enhanced efflux of protons to the cytoplasmic side of the membrane, hence the mitochondrial membrane potential increases. A rise in intramitochondrial calcium levels $(Ca^{2+})_m$ can enhance the mitochondrial membrane potential by elevating the rate of NADH production by the enzymes in the Krebs cycle, including pyruvate dehydrogenase, isocitrate dehydrogenase and α-ketoglutarate (McCormack, Halestrap et al. 1990; Territo, French et al. 2001). Furthermore, increases in mitochondrial calcium levels have been shown to regulate the activity of the ATP synthase and to enhance electron transport chain activity (Territo, French et al. 2001). Cellular energy and mitochondrial membrane potential are regulated by a group of uncoupling proteins (UCP). The members of this family of proteins include UCP1, UCP2 and UCP3. These proteins have different tissue distribution and function. UCP1 is strictly restricted to brown adipose tissue and its principal function is the generation of heat. UCP3 is predominantly limited to skeletal muscle, whereas UCP2 is expression is widespread in spleen, lungs, white adipose tissue and the brain. UCP's regulate energy metabolism and possibly weight regulation. Members of this family of inner mitochondrial proteins all function as proton carriers and play an important role in dissipating the mitochondrial electrochemical gradient, thus preventing hyperpolarization of the mitochondrial inner membrane and serving to reduce the generation of ROS from the mitochondrial respiratory chain under conditions of low cellular ATP consumption

(Echtay, Winkler et al. 2000; Pecqueur, Alves-Guerra et al. 2001; Pecqueur, Couplan et al. 2001). These proteins have been proposed to be down-regulated in diabetes leading to excessive ROS generation (Vincent, Olzmann et al. 2004). However, this result has not been replicated by other studies in STZ diabetic rats. Adenine nucleotide translocase (ANT) is a family of proteins involved in the regulation of the mitochondrial membrane potential. Three isoforms of this transporter have been described in mammals. They exist as dimers with one nucleotide-binding site. ANT transports ATP out of the mitochondria while facilitating the inflow of ADP into the mitochondria for ATP synthesis. An increase in the electron transport chain activity results in the activation of ANT, which aids in the reduction of the membrane potential. Increase in mitochondrial calcium levels can also result in the activation of ANT through the enhancement of the electron transport chain activity (Heimpel, Basset et al. 2001).

1.12.4. Mitochondria and neuronal death

Some investigators have reported apoptosis of neurons in the DRG of STZ-induced diabetic rat as a prominent feature of diabetic sensory neuropathy (Russell, Sullivan et al. 1999). While this study might correctly identify caspase-3 and -9 activation, possibly theoretically associated with apoptosis in diabetic sensory neurons, clear evidence of apoptosis induced neuronal loss is lacking (Cheng and Zochodne 2003). Diabetic neuropathy is characterized by distal axonal degeneration, with no evidence of apoptosis-induced cell death in both the experimental and the human form of the disease (Sidenius and Jakobsen 1980; Schmidt, Dorsey et al. 1997; Kamiya, Zhang et al. 2006).

The mitochondria are involved in the process of apoptosis, which is an orderly shutdown of metabolism and digestion of cell content with minimal leakage of cell content. The apoptotic pathway can be triggered by a variety of physiological death signals and pathological cellular insults, and it manifests in two major execution programs downstream of the death signal. These are the caspase pathway and the organelle dysfunction pathway of which the mitochondrial dysfunction is the best characterized. Dysfunctional mitochondria, which could be in the form of abnormalities in the membrane potential, ROS generation or activation of the permeability transition pore (PTP) could result in the release of cytochrome C. Together with a cytoplasmic factor, Apaf-1, and driven by ATP hydrolysis, cytochrome C forms an apoptosome capable of aggregating procaspase 9. Procaspase 9 is then activated into caspase-9, which in-turn activates caspase -3 responsible for specific protein cleavages characteristic of apoptosis.

1.12.5. Mitochondrial dysfunction and oxidative stress

Several studies have shown that diabetes and hyperglycemia increases oxidative stress (Nishikawa, Edelstein et al. 2000; Russell, Golovoy et al. 2002). It has been proposed that isolated mitochondria generate superoxide from complex I upstream of the rotenone inhibition site and in complex III at the outer ubiquinone binding site. However, the mechanism leading to the release of superoxide from the mitochondria is not clear (Nicholls 2004). In cultured endothelial cells, it has been proposed that hyperglycemia increases electron donation to the electron transport chain in the mitochondria, resulting in

hyperpolarization of the mitochondrial inner membrane and elevated ROS production (Nishikawa, Edelstein et al. 2000; Brownlee 2001). This mitochondrial driven process has been proposed as the central mediator of oxidative stress in diabetic complications. This theory suggests that high glucose as a result of diabetes results in an increase in the supply of NADH from glycolysis and the TCA cycle to the mitochondria. This results in excessive donation of reducing equivalent to the electron transport chain by NADH, thus enhancing electron transfer through the electron transport chain and subsequent increase in the proton gradient across the inner mitochondrial membrane. It is believed that when the electrochemical gradient generated by the proton gradient is high; the lifetime of ubisemiquinone is prolonged. Aside from transferring electrons from complex II to complex III, ubiquinone is believed to mediate the reduction of O_2 to superoxide. Thus the prolongation of the semiubiquinone by enhanced activity of the electron transport chain results in the elevated production of ROS. Indeed, it was found that overexpression of manganese (Mn) SOD abolished the signal generated by the generation of ROS, and also the overexpression of uncoupling protein-1 collapsed the proton gradient and prevented hyperglycemia-induced over production of ROS (Brownlee 2001). Studies on adult sensory neurons from normal and STZ-induced diabetic rats have not replicated the responses to high glucose observed in endothelial cells and embryonic neurons. Studies by Huang et al and Wiley et al show that the inner membrane of mitochondrial in the cell body of neurons isolated from STZ-induced diabetic rats is depolarized and not hyperpolarized as demonstrated in endothelial cells and embryonic neurons

(Srinivasan, Stevens et al. 2000; Huang, Price et al. 2003). Also, mitochondrial depolarization could be prevented by systemic treatment with low dose insulin. The current study will provide more evidence of mitochondrial depolarization in DRG neurons in the results section. Extensive studies in a variety of cell types has associated the rise in mitochondrial calcium levels to the increase in the rate of NADH production by enzymes of the Krebs cycle including pyruvate dehydrogenase, isocitrate dehyrogenase and α-ketoglutarate dehydrogenase. Further studies have shown that Ca^{2+} can regulate the activity of ATP synthase, enhance electron transport and activate the adenine nucleotide translocase (McCormack and Denton 1990; Territo, French et al. 2001). Despite these associations between a rise in mitochondrial calcium levels and mitochondrial function, there is no evidence in the literature linking abnormal Ca^{2+} levels in the mitochondria and the generation of ROS under diabetic conditions in adult neurons. However, because reduced ubiquinone intermediate in the Q cycle is a significant source of ROS, both the concentration of QH, which is increased when the distal respiratory chain is inhibited, and frequency of QH, which is increased when the rate of electron transport is enhanced can regulate ROS production. Thus, it is believed that increased mitochondrial calcium could indirectly result in an increase in the generation of ROS.

1.12.6. Abnormalities in mitochondrial physiology in heart, muscle and kidney in diabetes

Abnormalities in mitochondrial physiology in both type 1 and 2 diabetes are not limited to nerves and DRG, but also the muscle, kidney and heart. The

mitochondria in the myocardium of STZ-induced diabetic mice show reduced respiration at complexes I, II and III, and this is associated with reduced enzymatic activity and mitochondrial DNA (Yu, Tesiram et al. 2007; Dabkowski, Williamson et al. 2009; Yang, Yeh et al. 2009). Also, reduced respiration rate at state 3 with glutamate and pyruvate is observed in the heart of diabetic Akita mice and this is associated with reduced ATP synthesis and decreased mRNA level of several proteins involved in oxidative phosphorylation (Bugger, Boudina et al. 2008; Bugger, Chen et al. 2009). Reduced respiration rate at state 3 with glutamate and malate, and a decrease in enzymatic activity of complex I and II (heart and gastrocnemius muscle) (Lashin, Szweda et al. 2006; Herlein, Fink et al. 2009), complex I, III and IV (kidney) (de Cavanagh, Ferder et al. 2008) (Munusamy, Saba et al. 2009) have been reported. Muscle biopsies in type 2 diabetic patients have shown decreased respiratory activity and reduced mitochondrial size (Boushel, Gnaiger et al. 2007; Mogensen, Sahlin et al. 2007; Rabol, Hojberg et al. 2009). Additionally, decreased enzymatic activity and protein expression have been reported in the skeletal muscles of the diabetic Goto-Kakizaki rats (Shen, Hao et al. 2008) and Zucker diabetic fatty rats (De Feyter, Lenaers et al. 2008). These findings generally point to a diminished function of the mitochondrial electron transport chain in these tissues. However, the diabetes-induced factors causing these abnormalities are poorly understood.

1.12.7. Ultrastructural changes in the mitochondria

There is increasing evidence for abnormal mitochondrial ultrastructure in human and animal models of type 1 and type 2 diabetes. Changes in the

mitochondria number and size have been described in Schwann cells, myelinated fibres and unmyelinated fibres in human and animal models of diabetic sensory neuropathy (Kalichman, Powell et al. 1998). A study of intraepidermal axonal swellings and dermal nerves in HIV patients with neuropathy showed accumulation of mitochondria and mildly enlarged mitochondria (Ebenezer, McArthur et al. 2007). Also, some unsual crystalline-inclusions are present in axonal mitochondria of diabetic cats (Mizisin, Nelson et al. 2007). These inclusions are believed to interfere with the functions of the mitochondria (Engel et al. 1994). Additionally, mitochondrial abnormalities are present in the pre- and post-synaptic elements in prevertebral sympathetic ganglia (Schmidt, Plurad et al. 1993; Schmidt, Dorsey et al. 2003; Schmidt, Parvin et al. 2008). The abnormalities demonstrated in the sympathetic ganglia of diabetic mice include increased number of mitochondria in autophagic vacuoles associated with synaptic vesicles and the accumulation of mitochondria without significant amount of intervening cytoplasm in post-synaptic dendrites, which often appear smaller than those in adjacent cell bodies. Additionally, studies of prevertebral sympathetic ganglia of non obese diabetic (NOD), STZ-treated and STZ-treated NOD/severe-combined immunodeficiency (SCID) mice (Schmidt, Dorsey et al. 2003), and the Akita mouse, show the accumulation of small, hyperchromatic dense mitochondria that were significantly smaller than those in the non-diabetic controls (Schmidt, Green et al. 2009).

Chapter 2:

Research design and methods

2.1. Adult rat and mouse DRG sensory neuron culture

DRG sensory neurons from adult male Sprague-Dawley rats or male Swiss Webster mice were isolated and dissociated using previously described methods (Huang, Price et al. 2003; Gardiner, Fernyhough et al. 2005; Huang, Sayers et al. 2005; Huang, Verkhratsky et al. 2005). Rats were either age matched control or 3-5 month STZ-diabetic. Rats were made diabetic with a single i.p. injection of 75 mg/kg STZ (Sigma).

Table. 2. Summary of body weights, plasma glucose and glycated hemoglobin (HbA1c) of treatment groups.

	Body weight (g)	Blood glucose (mmol/l)	HbA1c (%)
	n = 10-13	n = 10-13	n = 9-10
Control	770.9 ± 57.9*	8.24 ± 0.89*	4.39 ± 0.28*
Diabetic	415.8 ± 33.9**	30.95 ± 2.71**	11.69 ± 0.97**
Diabetic + insulin	519.1 ± 42.0	14.81 ± 4.95	8.59 ± 1.17

Values are means ±SD. *p<0.001 vs other groups; **p<0.001 vs diabetic + insulin (one way ANOVA with Tukey's test)

All animal protocols carefully followed Canadian Committee on Animal Care (CCAC) guidelines. Cells were plated onto poly-d-L-ornithine hydrobromide and laminin-coated multi-well plates (Nunclon Surface, Ottawa, Ontario) for neuronal survival and axon outgrowth studies and 25 mm glass cover slips (Electron Microscopy Sciences, Hatfield, PA, German glass #1) for immunocytochemistry and measurement of mitochondrial localization. Neurons were grown in defined Hams F-12 medium with modified Bottenstein and Sato's N2 medium (with no insulin) containing 0.1 mg/ml transferrin, 20 nM progesterone, 100 μM putrescine, 30 nM sodium selenite, 1 mg/ml BSA, and supplemented with neurotrophic factors (NTFs): 1 nM insulin, 1 ng/ml nerve growth factor (NGF), 10 ng/ml glial cell line-derived neurotrophic factor (GDNF) and 10 ng/ml neurotrophin-3 (NT-3) (all obtained from Sigma).

2.2 Assessment of neuronal survival and neurite outgrowth

For neuronal survival and axon outgrowth studies cultured DRG neurons from adult rats or mice were treated with 4-HNE concentrations ranging from 1.0 μM to 10.0 μM and assessed at 24-48 hr. Neuronal survival was assessed by established methods (Mattson, Barger et al. 1995; Fernyhough, Smith et al. 2005). Briefly, viable neurons were counted before experimental treatment and at time points following treatment. Neurons that died in the intervals between examination points were usually absent, and the viability of the remaining neurons was assessed by morphological criteria. Neurons with membranes and

soma with a smooth round appearance were considered viable; whereas neurons with fragmented or distended membranes and vacuolated soma were considered nonviable. 6 images were collected randomly from each well at 24 hours of culture using a phase-contrast light microscope (Nikon Diaphot, phase contrast inverted microscope) fitted with a 20x objective and equipped with camera (Nikon Coolpix 5000). For neurite outgrowth measurements, images of cultures were collected from 6 randomly selected fields from each well using a phase-contrast light microscope. The total number of neurons and number of intersect of their neurites with a vertical Weibel grid were counted using a morphometric approach and using SigmaScan Microsoft software as previously described (Gardiner, Fernyhough et al. 2005). The number of intersects per neuron was taken as the measure of total axon outgrowth.

2.3. Immunocytochemistry for detection of adducts of 4-HNE, manganese superoxide dismutase (MnSOD) and phosphorylated neurofialment H

Adult DRG neurons grown on glass cover slips were fixed with 4% paraformaldehyde in phosphate buffered saline (PBS, pH 7.4) for 15 min at room temperature and then permeabilized with 0.3 % Triton X-100 in PBS for 5 min. Nonspecific binding was reduced by incubation for 1 hr at room temperature in blocking buffer prepared from blocking reagent (Roche, Indianapolis, IN, Cat# 1 096 176) which was diluted with FBS and 1.0 mM PBS in proportion 3:1:1 for 1hr and washed with PBS three times. Fixed cells were then incubated with antibodies to β-tubulin isotype III (neuron specific; Sigma, Oakville, ON, 1:1000), (E)-4-hydroxy-2-nonenal adducts (anti-4-HNE adducts PAb (Alexis Biochemicals,

San Diego, CA, 1:500), (MnSOD, Abcam, 1:300) and phosphorylated neurofilament H (NFH) (neuron specific; SMI-31; Covance, Berkeley, CA, 1:500). DRG cultures were incubated overnight with primary antibody in a humidified chamber followed by FITC- and CY3-conjugated secondary antibodies (Jackson ImmunoResearch Laboratories, West Grove, PA, 1: 250) for 3 hrs at room temperature. Fluorescence signal was examined using a Carl Zeiss Axioscop-2 mot microscope with AxioVision 3 software and equipped with FITC, CY3, DAPI filters, and AxioCam camera.

2.4. Detection of mitochondria in cultured DRG neurons

Mitotracker red chloromethyl-x-rosamine (CMXRos; Molecular probes, OR) and Mitotracker green (Molecular probes, OR) were used to detect the mitochondria. These membrane permanent cationic fluorescent probes contain positively charged quarternary nitrogen and extensive π-orbital system, which enhances permeability across the membranes. At equilibrium the distribution of these cationic probes across the membrane is governed by the Nernst equation.

$$[C^+]_{matrix} = [C^+]_{cytoplasm} \times 10^{(\Delta\Psi m/\ 61.5)}$$

Where $[C^+]_{matrix}$ and $[C^+]_{cytoplasm}$ represent concentrations in the appropriate compartments.

2.5. Chloromethyl-X-Rosamine indicator

This is a permanent mitochondrion selective dye used for detecting actively respiring mitochondria. CMXRos works by passively diffusing across the plasma

membrane and accumulating in actively respiring mitochondria. The dye then binds irreversibly to thiol groups on mitochondrial proteins via a chloromethyl group, which keeps it associated with the mitochondria after fixation and permeabilization. Once in the mitochondria, CMXRos is oxidized into a fluorescence probe, which is detected with a confocal microscope. To stain mitochondria in cultured DRG neurons, an individual vial containing 50μg of CMXRos was dissolved in 94.1μl of anhydrous DMSO (protected from light) to a final concentration of 1mM, aliquoted and frozen (CMXRos stock). For spectral analysis the stock solution was thawed at room temperature and a working concentration of 1μM (Fig. 10) prepared in F12 media. Neurons were incubated with dye for 15min at 37°C and fluorescence detected with a Carl Zeiss LSM510 confocal inverted microscope.

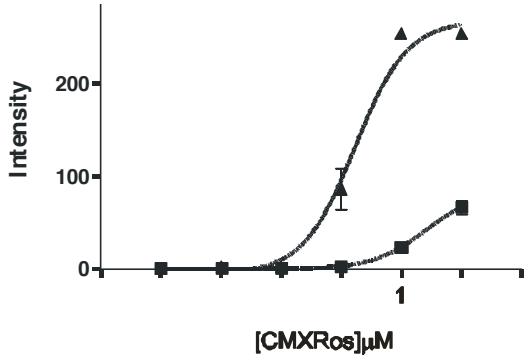

Fig. 10. CMXRos dose response in cultured DRG neurons. Cultured neurons were stained with CMXRos concentrations ranging from .0001 μM to 10 μM. Optimal concentration (EC 50) of CMXRos occurred at 1 μM. Axons – triangles, cell body – (squares).

2.6. Mitotracker green indicator

This was used to detect mitochondria irrespective of the potential across the inner mitochondrial membrane (mitochondrial mass). Mitotracker green does not fluoresce in aqueous environment, only becoming fluorescent once it accumulates in the lipid environment of the mitochondria. Hence background fluorescence is negligible, enabling the visualization of mitochondria in both live and fixed cells. This dye is substantially more photo-stable, produces a brighter signal at lower concentrations, and is well retained after fixation and permeabilization. To stain cultured DRG neurons, an individual vial containing 50μg of the probe was dissolved in 74.4μl of anhydrous DMSO (protected form light) to a final concentration of 1mM, aliquoted and frozen (stock solution). For spectral analysis, the stock solution was thawed at room temperature and a working concentration of 100 nM was prepared in F12 media. Neurons were incubated with dye for 15min at 37°C and fluorescence detected with a Carl Zeiss LSM510 confocal inverted microscope.

2.7. Simultaneous detection of active mitochondria and adducts of 4-HNE

For co-localization of actively respiring mitochondria and adducts of 4-HNE DRG neurons isolated from adult rats were cultured on 25mm glass cover slips under growth conditions for 24 h (as described), and incubated with 1μM CMXRos for 15 min under growth conditions. Cultures were washed with fresh F12 media and fixed with 4% paraformaldehyde (PFA) for 15min. Neurons were permeabilized in PBS containing 0.2% Triton X-100 at room temperature for

5mins and then blocked with a blocking buffer containing blocking solution, fetal bovine serum (FBS) and PBS in the ratio 1:1:3 respectively. Neurons were incubated with polyclonal antibody to adducts of 4-HNE (1:750) for 16h at 4° C, washed three times with PBS and incubated at room temperature with fluorescence (FITC) - conjugated AffiniPure donkey anti-rabbit IgG for 1-3 h, and mounted on glass slides for visualization. Neurons were imaged on a Carl Zeiss Axioscope-2-mot microscope equipped with FITC, CY3 and DAPI filters. Imaging was performed with a 40X objective

2.8. Simultaneous detection of active mitochondria and mitochondrial mass

For co-localization of active mitochondria and mitochondrial mass, cultured DRG neurons were stained with CMXRos, fixed with PFA and permeabilized (as described). Neurons were incubated with mitotracker green probe for 15 min at room temperature, rinsed in PBS and mounted in DAPI on glass slides for visualization. Fluorescence signals were examined using a Carl Zeiss LSM510 confocal microscope. The pinhole diameter was adjusted to give an optical slice of 1μm. Fluorescence was excited in multi-track mode with 488nm of an argon laser (mitotracker green, 3% laser power) and 543nm of helium neon (HeNe1) laser (CMXRos, 41% laser power). The emitted fluorescence was detected in channel 1 through emission filter LP 585 for mitotracker green and LP 560 for CMXRos (Fig. 12). High resolution scanning was performed with a Plan-Aprochromat 100X objective lens. Care was taken to minimize excitation of the

dyes, given their propensity to free radicals. Also the amplifier gain was kept constant throughout.

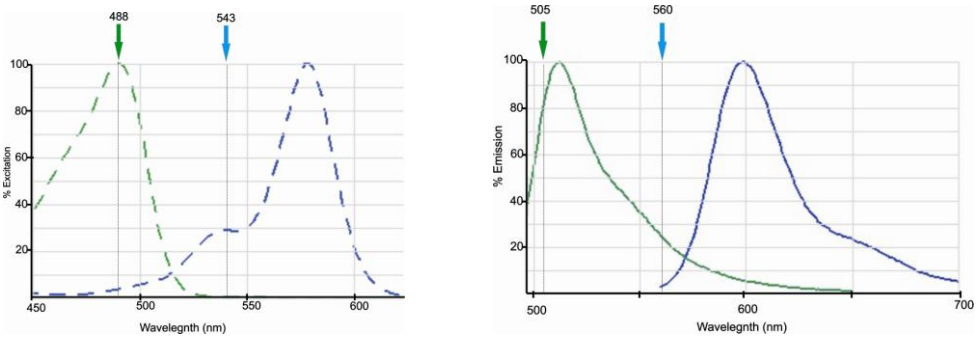

Fig.12. In vitro excitation and emission spectra for mitotracker green (green) and CMXRos (blue).

Quantification of fluorescence signal

The fluorescence intensity signal along the axons in each field of view was assessed using SigmaScan software (SPSS). For the assessment of 4-HNE and phosphorylated neurofilament levels, a line of specific width was traced along the axons and the average line pixel intensity over a distance of 150 μm measured. To assess CMXRos, Mitotracker green, and adducts of 4-HNE levels, a line of specific width was traced along each axon and the pixel intensity per μm of axonal length measured.

2.9. Assessment of mitochondrial membrane potential in cultured neurons

Absolute determination of the mitochondrial inner membrane potential is rather difficult and prone to errors. It involves the measurements of the matrix volume and activity coefficient among other parameters. However, relative

changes in the mitochondrial membrane potential can be assessed using cationic probes like tetramethyl rhodamine methyl ester (TMRM; Molecular probes, Eugene, OR). This is a lipophilic probe, which permeates membranes depending on the membrane potential. It is the least toxic of all commonly used probes and equilibrates readily across the plasma membrane and the inner mitochondria membrane. It can be used to monitor mitochondrial membrane potential in both matrix quenching and non-quenching modes. Fluorescence quenching occurs when the probe accumulates in the matrix above a certain threshold concentration; under this condition the matrix signal becomes largely independent of further probe accumulation. If fluorescent quenching occurs changes in the membrane potential will produce a transient whole-cell response as the probe re-distributes from the quenched matrix to the unquenched cytoplasm. Thus in the quench mode, depolarization produces an increase in whole-cell fluorescence followed by a slow decay as the excess probe from the mitochondria re-equilibrates across the plasma membrane. However, when the probe accumulates in the matrix at concentrations sufficiently lower than the threshold concentration so as to avoid fluorescence quenching, a decrease in membrane potential will reflect in a stable decrease in whole-cell fluorescence. Studies have shown that there is no matrix quenching when TMRM is employed at a concentration lower than 5nM, and at such low concentration toxicity is negligible. For the staining of cultured DRG neurons, 25mg of TMRM was dissolved in 50ml of anhydrous DMSO to a stock concentration of 1mM. The stock solution was aliquoted into 1ml tubes and stored at -80°C. For spectral

analysis, the stock solution was thawed at room temperature (protected from light) and a working concentration of 1μM was prepared in F12 media. Neurons were incubated with dye for at least 1hr at 37°C and fluorescence detected with a Carl Zeiss LSM510 confocal inverted microscope.

2.10 Validation of TMRM in the axons of cultured DRG neurons.

Carbonylcyanide p-trifluoromethoxyphenylhydrazone (FCCP, Sigma), antimycin A (Sigma) and oligomycin (Sigma) were used in this study to regulate the mitochondrial membrane potential. FCCP (uncoupler) has dissociable protons and permeates bilayers either as a protonated acid or conjugate base. By cycling across the membrane FCCP catalyzes the transport of protons into the matrix of the mitochondria. Thereby reducing the electrochemical gradient across the membrane and hence the membrane potential. Therefore, FCCP was used to induce mitochondrial depolarization (Fig. 13). Antimycin is an inhibitor of mitochondrial electron transport chain that acts at complex III. It binds to the Qi site of complex III, preventing the oxidation of unbiquinol to semiubiquinol. Subsequently, this inhibition disrupts the release of protons to maintain the proton gradient. Hence, there is a reduction in the electrochemical gradient, which is reflected in the reduction in membrane potential (Fig. 13). Oligomycin is an inhibitor of ATP synthase. It blocks the proton channel (F_0 subunit), which is necessary for the oxidative phosphorylation of ADP to ATP. This can cause a build up of the electrochemical gradient leading to a transient hyperpolarization of the mitochondrial membrane (Fig. 13).

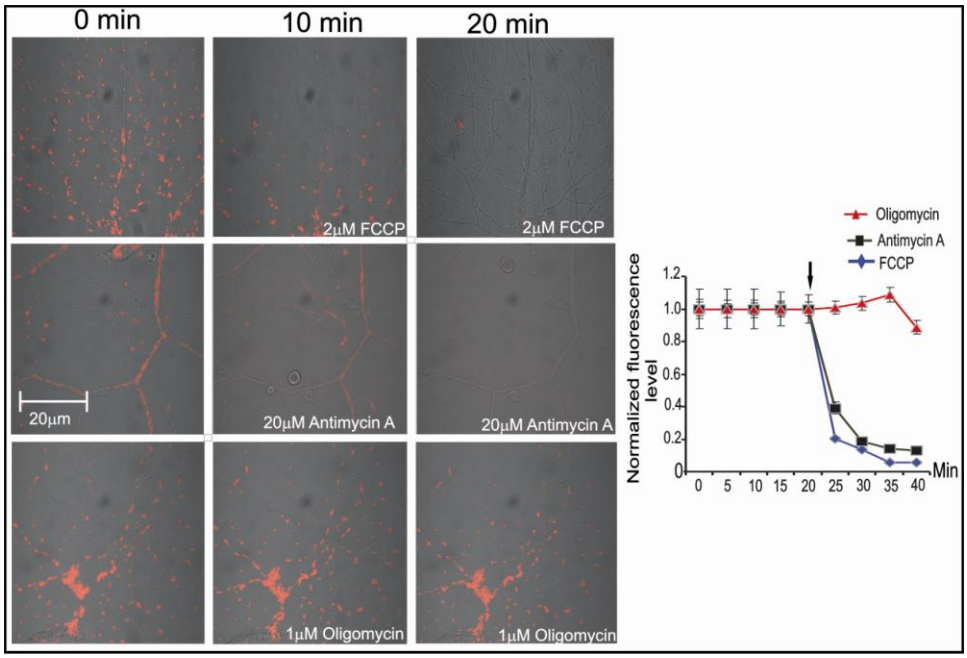

Fig. 13. Changes in the level of TMRM fluorescence (red) induced by FCCP, antimycin A or oligomycin in the axons of cultured DRG neurons. Black arrow indicates time of injection.

To validate the probe, DRG neurons were cultured in glass-bottom dishes (Willco, Ams) and stained with TMRM (as described). FCCP, antimycin A or oligomycin were injected into the F12 media to a final concentration of 2μM, 20μM or 1μM, respectively, following baseline measurements. Changes in fluorescence signals were then assessed using a Carl Zeiss LSM510 confocal. The pinhole diameter was adjusted to give an optical slice of 2μm. Fluorescence was excited in single-track mode with 543nm of HeNe1 laser (67% laser power). The emitted fluorescence was detected through emission filter LP 560. High resolution scanning was performed with a C-Aprochromat 63X/1.2w objective lens.

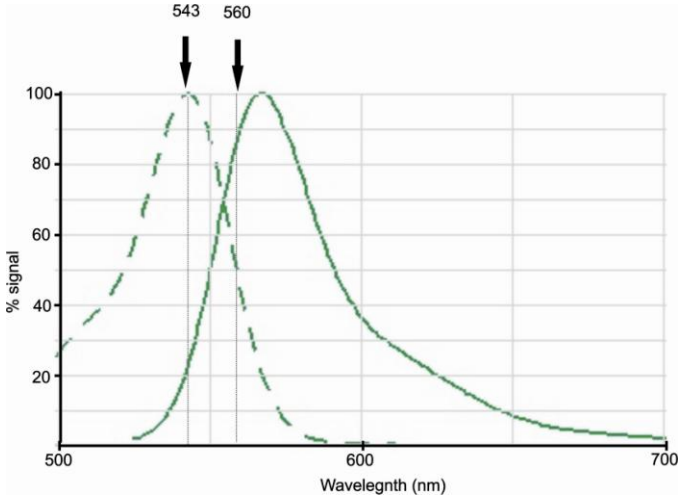

Fig. 14. Excitation (broken lines) and emission spectra for TMRM.

2.11. Assessing the rate of depolarization and hyperpolarization in STZ-induced diabetic neurons

Lumbar DRG sensory neurons from adult male Sprague-Dawley rats were isolated and dissociated. Rats were either age matched control or 3-5 month STZ- induced diabetic. Cells were plated onto poly-dL-ornithine hydrobromide and laminin-coated 25 mm glass-bottom dishes. Neurons were grown in defined Hams F-12 medium with N2 additives (no insulin), supplemented with neurotrophic factors: 0.1 ng/ml nerve growth factor, 1.0 ng/ml glial cell line-derived neurotrophic factor and 0.1 ng/ml neurotrophin-3 (all obtained from Sigma) and treated with either 10 mM D-glucose (control; with 10 nmol/l insulin) or 25 mM D-glucose (diabetic; no insulin) for 24 h. DRG neurons were then loaded with 3.0 nM TMRM for 1 hr and the fluorescence signal in the axons detected with a Carl Zeiss LSM510 confocal inverted microscope (microscope and spectra settings are described in the previous section). TMRM was utilized in sub quench mode – where decreased fluorescence intensity indicates reduced

mitochondrial inner membrane potential. Antimycin A (10μmol/l) + oligomycin (1 μmol/l) or oligomycin (1 μmol/l) were injected into the culture media following baseline fluorescence measurements. All axons in each field were assessed as average of fluorescence pixel intensity per axon length using the Carl Zeiss software package. Also, cultured DRG neurons from diabetic rats were treated with ciliary neurotrophic factor (CNTF, 10ng/ml), resveratrol (1μM) or pirenzepine (1μM), and the rate of depolarization and hyperpolarization assessed. This was to investigate the ability of these compounds to reverse abnormalities observed in the mitochondrial membrane potential.

2.12. Simultaneous assessment of plasma membrane potential and mitochondrial membrane potential

A single vial of plasma membrane potential indicator (PMPI) from Molecular Devices membrane potential assay kit, explorer format (R-7264) was reconstituted in 1ml distilled water, aliquoted and stored at -20°C (PMPI stock). For simultaneous detection of plasma membrane and mitochondrial membrane potential, 3.0 nmol/l TMRM was mixed with PMPI in F12 media (1:1000 dilution of PMPI stock). Cultured DRG neurons isolated from control rats were incubated with the TMRM and PMPI mixture at 37°C for at least 1h. FCCP or KCl or was injected into the media to a final concentration of 2μM (FCCP) or 35mM (KCl) following baseline fluorescence measurements. Changes in fluorescence were assessed with Carl Zeiss LSM510 confocal inverted microscope. The pinhole diameter was increased to give an optical slice of 7.5μm to allow collection of

defocused signal from individual mitochondria. Fluorescence was excited in single-track mode with 488nm band of argon laser. An argon bandwidth of 488nm was used to prevent overlap of the excitation and emission wavelength (Fig.15). Because the emission peaks of the two indicators are separated by only 20nm the spectra overlap was corrected by splitting the emitted epifluorescence with a 570nm dichroic mirror (splits emitted light which is guided into separate channels) and detected in channel 1 through an LP 585 filter (for TMRM) and channel 2 with BP 505-550 filter (for PMPI). Laser power was adjusted for optimal image and did not exceed 11%. High resolution scanning was performed with a C-Aprochromat 63X/1.2w objective lens. The amplifier gain was kept constant throughout.

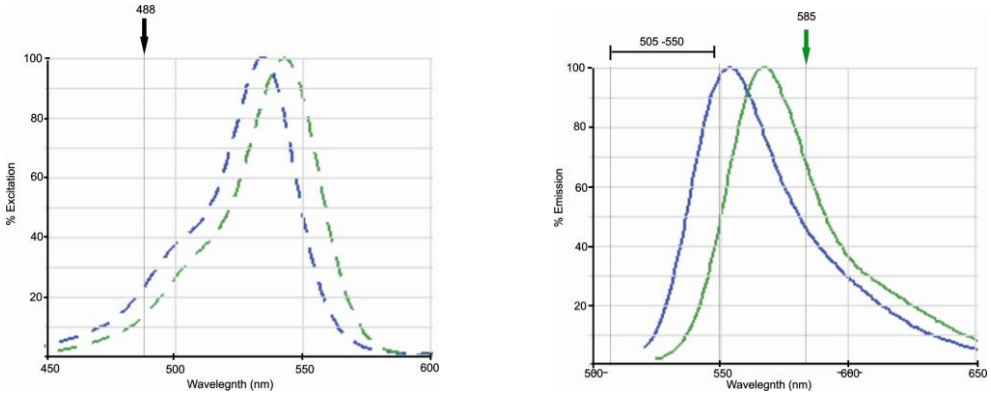

Fig. 15. Excitation and emission spectra for PMPI (Blue) and TMRM (Green).

2.13. Isolation of mitochondria from DRG's

Adult rat DRG were homogenized in mitochondria isolation buffer containing: 10 mM HEPES (pH 7.4), 200 mM mannitol, 70 mM sucrose, and 1 mM EGTA. The DRG homogenate was centrifuged at 800 x g for 10 min at 4°C followed by

centrifugation of the supernatant at 8000 x g for 15 min. The pellets (mitochondrial enriched fraction) were then re-suspended in mitochondrial isolation buffer. The mitochondrial-enriched fraction was then prepared for Western blot, proteomics or oxygraph measurements

2.14. Western blot

Samples for Western blots were obtained from sural nerve tissues, cell culture and mitochondria extracted from lumbar DRG (described above). Sural nerve tissues obtained from adult rats were cut into small pieces (1cm long) and homogenized in ice-cold neurofilament stabilization buffer containing: 0.1 M Pipes, 5 mM $MgCl_2$, 5 mM EGTA, 0.5 % Triton X-100, 20 % glycerol, 10 mM NaF, 1 μM PMSF and protease inhibitor cocktail (Fernyhough, Gallagher et al. 1999).The homogenate was immediately frozen and stored at -80°C. To extract samples from cell culture, DRG neurons from one or two adult rats were cultured in six-well plastic dishes for 24/48 hr. The dishes were placed on ice and the F12 media gently removed and replaced with 75μl ice-cold neurofilament stabilization buffer per well. The neurons were then scraped with a cell scraper. Scraping was repeated with another 75μl ice-cold neurofilament stabilization buffer and lysates collected into an Eppendorf tube. Proteins in all samples were assayed using DC protein assay (BioRad; Hercules, CA) and Western blot analysis performed as previously described (Towbin, Staehelin et al. 1979; Wataya, Nunomura et al. 2002). Proteins were resolved on an 8 % - 12 % SDS-PAGE gel, and electroblotted (30V, 16h) onto a nitrocellulose membrane. Blots were then

blocked in 5 % nonfat milk containing 0.05 % Tween overnight at 4°C, rinsed in phosphate buffered saline (pH 7.4) and then incubated with primary antibody overnight at 4°C (Table. 3). Levels of total extracellular signal-regulated kinase (T-ERK; Covance, Berkeley, CA; 1:2000) were detected and used as a loading control (our previous work has shown no change in expression in diabetes and under a range of conditions in our cultures). After 6 washes of 10 min in PBS–Tween and PBS, secondary antibody was applied for 1 hr at room temperature. The blots were rinsed, incubated in Super Signal West Pico (Pierce biotechnology, Rockford, IL) and imaged using the BioRad Fluor-S image analyzer.

2.15. PROTEOMICS

Preparation of isolated mitochondria from DRG and isotopically labeled S16 cells.

Mitochondrial preparations from DRG were isolated as described. Immortalized S16 Schwann cells were cultured in low glucose DMEM containing 125 mg/l 13C6-lysine (K6) and 84 mg/l 13C6,15N4-arginine (R10) (Cambridge Isotopes, Andover, MA), 10% dialyzed fetal calf serum (Atlas Biologicals, Fort Collins, CO) and antibiotics (Zhang, Yu et al. 2010). Crude mitochondria from labeled cells were obtained by differential centrifugation and purified through a discontinuous Nycodenz gradient (Oates 2008). For quantitative analysis of the DRG mitochondrial proteome, the K6R10 labeled mitochondria were used as a source of culture-derived isotope tags to serve as internal standards (Frezza, Cipolat et al. 2007). After assessing the protein concentration of the preparations,

the unlabeled mitochondrial protein (K0R0) obtained from each of the control (n=4), diabetic (n=3) and diabetic + insulin (n=4) treatments were mixed in a 2:1 ratio with K6R10 labeled mitochondria. Total protein (60- 70 µg) was subjected to SDS-PAGE, the gel was stained with colloidal Coomassie blue and lanes were cut into 5 x 1 cm pieces. The proteins were analyzed by RP-HPLC/LTQ-FT MS/MS (using the SILAC approach).

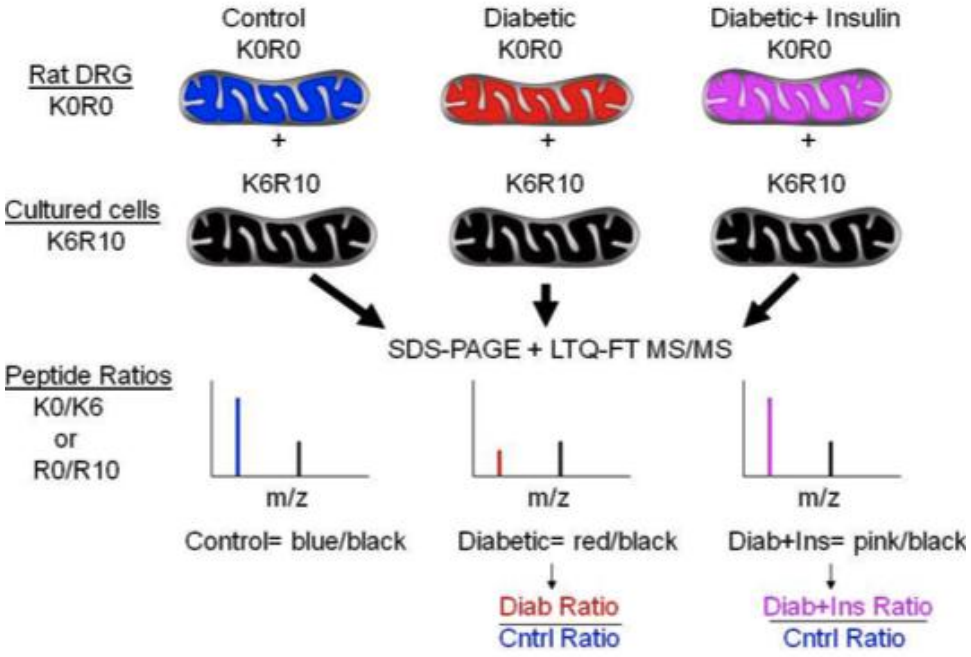

Fig. 16. Schematic for use of culture-derived isotope tags for quantitative proteomics. Unlabeled (K0R0) mitochondrial fractions were prepared from the lumbar DRGs obtained from each animal in the three treatment groups. Each K0R0 mitochondrial fraction was mixed in a 2:1 ratio with K6R10 labeled mitochondria obtained from S16 cells that had been metabolically labeled with 13C6 lysine (K6) or 13C6,15N4 arginine (R10) for 10 days. For each protein, the ratio of K0R0 to K6R10 quantifies the endogenous protein relative to the internal standard. Dividing the protein ratios obtained in the diabetic or diabetic + insulin treatment by those obtained from control animals cancels out the K6R10 internal standard and provides the fold control value.

2.16. Statistical analysis

Where appropriate, data were subjected to one-way ANOVA with *post-hoc* comparison using Tukey's test or regression analysis with a one-phase exponential decay parametric test with Fisher's parameter (GraphPad Prism 4, GraphPad Software Inc., San Diego, CA). In all other cases two-tailed Student's *t*-Tests were performed. To determine the threshold for statistical significance for the proteomic data proteins showing at least a 20 or 25% increase or decrease were grouped and compared to the entire dataset using a Kruskal-Wallis non-parametric ANOVA and Dunn's multiple comparison test. This analysis indicated that a minimum difference of 25% was necessary for a value to be considered statistically different from the data set.

Chapter 3:

4-Hydroxy-2-Nonenal Induces Mitochondrial Dysfunction and Aberrant Axonal Outgrowth in Adult Sensory Neurons that Mimics Features of Diabetic Neuropathy

NEUROTOXICITY RESEARCH (2010) 17:28–38

3.1. Introduction

Diabetic sensory neuropathy is one of the long-term clinical syndromes associated with poorly controlled diabetes mellitus (Said 2007; Yagihashi, Yamagishi et al. 2007). Sensory nerves from human patients with neuropathy show progressive nerve fiber loss, endoneurial microangiopathy, and demyelination which often precedes axonal degeneration of myelinated fibers (Malik, Tesfaye et al. 2005; Yagihashi, Yamagishi et al. 2007). Key features of the disease are the targeting of lumbar dorsal root ganglia (DRG) sensory neurons with the longest axons and the distal loss of sensory nerve endings in the epidermis with subsequent failure to regenerate and/or undergo collateral sprouting (Lauria, Morbin et al. 2003; Ebenezer, McArthur et al. 2007). Complex

metabolic pathways downstream of high glucose are involved in the etiology of this condition and include enhanced polyol pathway activity, increased non-enzymatic glycation of proteins, elevated oxidative stress, impaired neurotrophic support as well as changes in protein kinase C activity and/or MAP kinase activity (Brownlee 2001; Yagihashi, Yamagishi et al. 2007; Calcutt, Jolivalt et al. 2008; Tomlinson and Gardiner 2008). High [glucose]-induced generation of reactive oxygen species (ROS) by mitochondria has been proposed to link these mechanisms, suggesting a role for mitochondrial dysfunction in the etiology of this condition (Brownlee 2001). However, the link between the generation of ROS and nerve damage associated with this condition is still not clear.

4-hydroxy-2-nonenal (4-HNE) is a highly reactive α,β- unsaturated aldehyde formed from the breakdown of polyunsaturated fatty acids in cholesterol esters, phospholipids and triglycerides (Uchida 2003). It is a major product of lipid peroxidation and the pathway for its production and biotransformation has been well characterized (Uchida 2003; Carini, Aldini et al. 2004; Petersen and Doorn 2004). 4-HNE exhibits a variety of biological activities including inhibition of protein and DNA synthesis (Sayre, Lin et al. 2006), inactivation of enzymes (Isom, Barnes et al. 2004) and formation of protein adducts with amino acid residues such as cysteine, histamine and lysine due to its strong electrophilic properties (Uchida 2003; Isom, Barnes et al. 2004). The presence of protein adducts have been used as biomarkers for the occurrence and extent of oxidative stress (Uchida 2003). Formation of adducts of 4-HNE has been implicated in the pathophysiology of several neurodegenerative disorders

including diabetic neuropathy (Petersen and Doorn 2004; Obrosova, Drel et al. 2005). Ex vivo, increased levels of lipid peroxidation products, including 4-HNE and its amino acid adducts have been shown in the sciatic nerve and retina of streptozotocin (STZ)-diabetic rats, a model of type 1 diabetes (Obrosova, Minchenko et al. 2001; Obrosova, Drel et al. 2005), and also, modification of sorbitol dehydrogenase subunits has been associated with increased levels of 4-HNE in cardiomyopathy in diabetes (Lashin, Szweda et al. 2006). 4-HNE has been shown to inhibit neurite outgrowth, disrupt microtubules and modify tubulin in Neuro 2A neuroblastoma cells (Neely, Sidell et al. 1999; Kokubo, Nagatani et al. 2008), and its cytotoxic and genotoxic effects have been demonstrated in cerebral endothelial cells (Karlhuber, Bauer et al. 1997).

3.2. Rationale

In this study, we investigated the effect of treating normal neurons with 4-HNE (lipid peroxidation product) on axonal outgrowth and mitochondria activity. DRG neurons isolated from normal rodents were cultured in defined F12-media supplemented with neurotrophic factors (NTFs; 1nM insulin, 1ng/ml NGF, 10ng/ml GDNF and 10ng/ml NT-3) and then treated with 4-HNE. Phase contrast images were taken at 24 h, after which neurons were stained or harvested for biochemical analysis. Also, we determined the levels of adducts of 4-HNE in cultured neurons from diabetic rats.

Previous studies in our lab have demonstrated elevation of ROS in the axons of cultured DRG neurons isolated from STZ-induced diabetic rats mediated by

high glucose. The elevation of ROS in the axons of diabetic neurons was associated with impaired axonal outgrowth and aberrant dystrophic structures (Zherebitskaya, Akude et al. 2009), which is believed to predict the severity of the disease in the human condition (Lauria, Morbin et al. 2003). Additionally several studies have demonstrated an increase in oxidative stress under diabetic conditions (Obrosova, Drel et al. 2005). One of the next key steps in this area of research is to investigate the link between oxidative stress and axonal degeneration observed in neuropathy. An increase in ROS is believed to induce lipid peroxidation, which results in the production of 4-HNE (Petersen and Doorn 2004). 4-HNE reacts with protein residues resulting in the formation of adducts of 4-HNE (Uchida 2003). The increase in adducts of 4HNE has been demonstrated in the sciatic nerves and retina of STZ induced diabetic rats (Obrosova, Drel et al. 2005); however the protein targets and the long term implication is not known.

Since the mitochondria are one of the main sources of ROS (Brownlee 2001), we believe mitochondrial proteins may be particularly susceptible to the effects of oxidative stress. Therefore, we tested the hypothesis that the elevation of 4-HNE in diabetes will result in the formation of adducts on key mitochondrial proteins thereby modifying their structure and function. We believe the impairment of mitochondrial function is an important step that precedes the process of nerve degeneration.

3.3. Aims/objectives:

- To determine the effect of elevated levels of 4-HNE on axonal growth and neuronal survival in cultured DRG neurons isolated from normal neurons.
- To demonstrate the presence of adducts of 4-HNE in cultured DRG neurons treated with 4-HNE through Western blot and immunostaining.
- To compare effects of direct 4-HNE treatments of normal neurons with the phenotype of DRG cultures derived from STZ-induced diabetic rats. Immunofluorescent images will be taken and abnormal morphological features that develop in the axons compared.
- To show the presence of adducts in the axons of cultured neurons isolated from STZ-induced diabetic rats by immunostaining.
- To demonstrate the presence of adducts in mitochondria isolated from diabetic and 4-HNE treated DRG neurons by Western blot.
- To confirm the formation of adducts of 4-HNE in the axonal mitochondria of 4-HNE treated neurons using antibodies to adducts of 4-HNE
- To determine the effect of 4-HNE on mitochondrial activity in the axons of 4-HNE treated neurons using Mitotracker green and CMXRos.

Approach

We used cultures of dissociated adult rat DRG to determine the regenerative capability of axons under diabetic conditions. This culture system mimics collatoral sprouting, the process that occurs constantly to permit and maintain innervation of target fields. Furthermore, this process is enhanced following peripheral nerve injury or loss of nerves innervating adjacent target fields (Skene 1989; Diamond, Foerster et al. 1992; Smith and Skene 1997). In response to injury, some peripheral neurons support the rapid extension of long and sparsely branched axons (Smith and Skene 1997), resulting in vigorous axon regeneration and re-expression of several growth-associated genes (Hoffman 1989; Schreyer and Skene 1991). Thus, the level of neurite outgrowth in culture can be used to determine the ability of DRG neurons to undergo collatoral sprouting and/or regenerate under various conditions. For example, Skene and colleagues have used length of the longest neurites in adult DRG culture to determine the growth capabilities of individual adult neurons in the presence and absence of changes in gene expression elicited by nerve injury (Smith and Skene 1997). In addition, it is accepted that when measuring total neurite outgrowth from this system that this is a good surrogate measure of collatoral sprouting.

3.4. Results

To demonstrate the elevation of adducts of 4-HNE in diabetic neurons (an indicator of oxidative stress), DRG neurons were cultured for 4 days from age matched control and 3-5 month STZ- induced diabetic rats and immunostained for neuron-specific β-tubulin III and adducts of 4-HNE. The control group exhibited normal axons with minimal swellings (abnormal structures along the

axons), whereas, neurons from diabetic rats presented with axonal swellings, which stained positive for adducts of 4-HNE (Fig. 17A; white arrows). These swelling are also present in the nerves of humans with diabetic neuropathy (Schmidt, Dorsey et al. 1997) and can predict the severity of the disease (Lauria, Morbin et al. 2003). Quantification of the number of swellings (Fig. 17B) and levels of adducts of 4-HNE (Fig. 17C) showed a significant increase in swellings and adduct formation in the axons of diabetic neurons compared with controls. Increased levels of adducts of 4-HNE may reflect an impaired capacity to scavenge free radicals. Therefore, the effect of diabetes and high glucose on the expression of MnSOD was assessed in isolated mitochondrial preparation from DRG neurons. Presented in Fig. 18 is Western blot data demonstrating a 32% decrease ($P<0.05$) in mitochondria isolated from DRG of STZ- induced diabetic rats, and this was prevented by insulin therapy. Experiments now determined whether elevation of 4-HNE levels was causally linked to impairment of axonal regeneration and the formation of aberrant axonal structures along the axons. Adult sensory neurons from normal adult rats and mice were cultured for 24 hr in defined F12 + N2 medium supplemented with a cocktail of neurotrophic factors and treated exogenously with 4-HNE concentrations ranging from 1.0 μM to 10 μM. Cell survival, axon morphology and level of axon outgrowth were assessed at 24 hr of culture. 4-HNE significantly impaired axonal outgrowth by approximately 50% at a concentration of 2.5 μM in the rat sensory neuron culture (Fig. 19B) whilst having no effect on neuronal survival at this concentration. Thus, EC_{50} for the inhibition of neurite outgrowth by 4-HNE was found to be

significantly lower than that for decreased neuronal survival (Fig. 19C). Impairment of axonal outgrowth in the rat culture was not significantly different from the mouse culture; however, there was a slight shift of the mouse dose response curve to the left (Fig. 19B and C, Dotted line). 4-HNE-treated cultures also exhibited aberrant axonal structures with phase dark swellings or dystrophic structures along axons, which were absent or minimal in control cultures (Fig. 19A and C, white arrows).

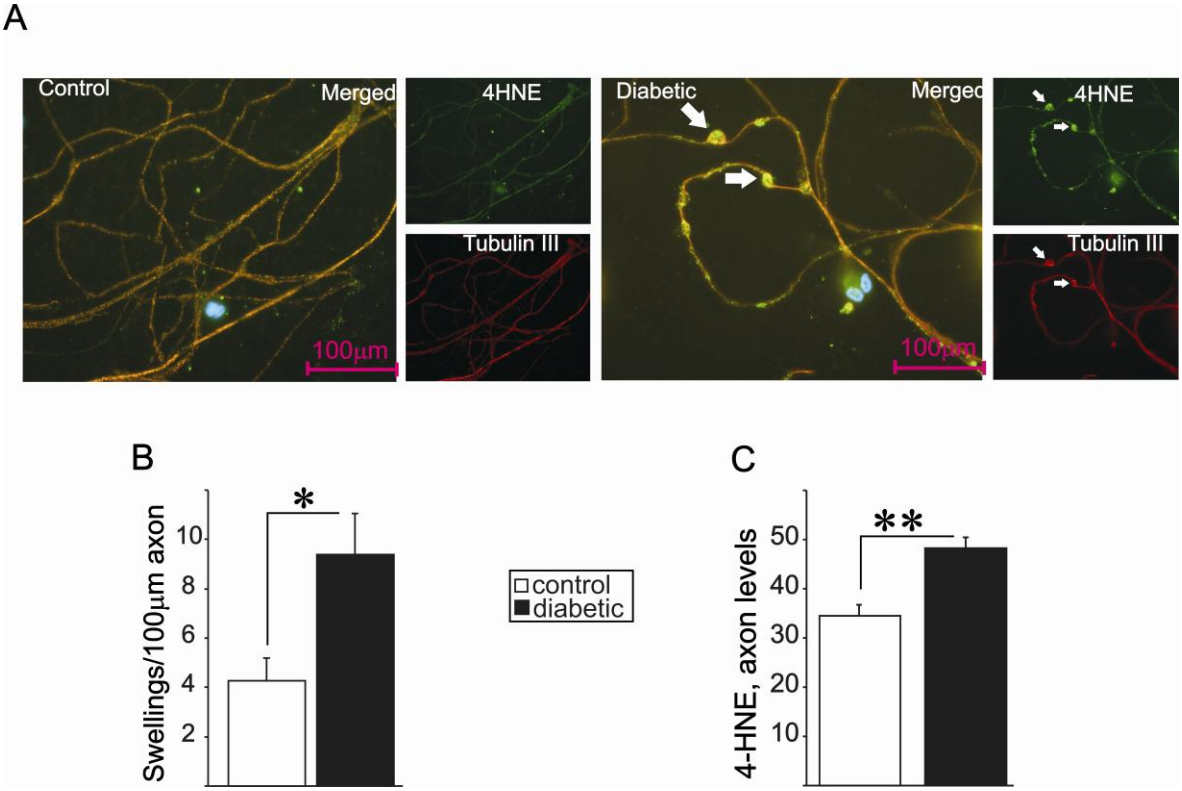

FIG. 17. Axons of neurons of STZ- induced diabetic rats exhibit swellings that express adducts of 4-HNE. (A) Representative immunofluorescent images derived from lumbar DRG sensory neurons cultured from age matched control and STZ-induced diabetic rats. Cells were grown for 4 days in F12+N2 defined medium with 10 mM D-glucose and with 10 nM insulin for controls, and 25 mM D-glucose without insulin for diabetic. Blue nuclei stains for DAPI. (B) and (C) are

quantification of number of swellings per 100 μm of axon length and 4-HNE level in axons. Values are means ± SEM, n = 3 replicates. * $p < 0.05$, ** $p < 0.001$.

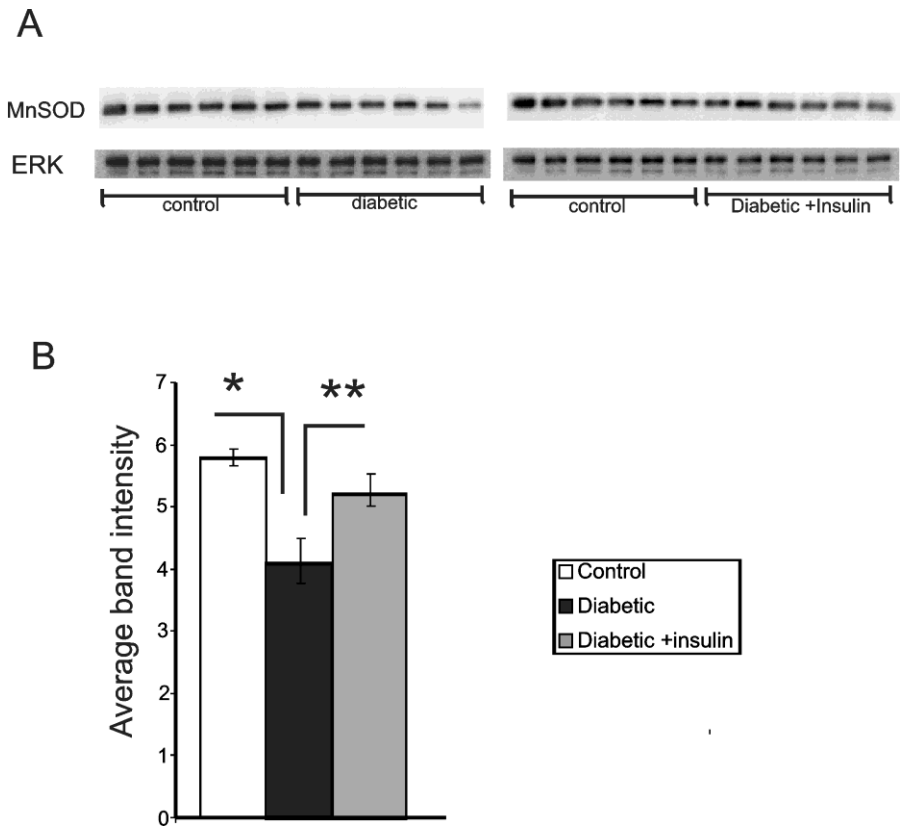

Fig. 18. MnSOD expression is reduced in mitochondria of DRG from STZ- induced diabetic rats. Mitochondria were purified from DRG isolated from 5 months control, STZ- induced diabetic or insulin treated diabetic rats. Proteins were resolved on a 12% SDS-PAGE gel and electroblotted (30V, 16 h) onto a nitrocellulose membrane. Blots were then blocked in 5% nonfat milk containing 0.05% Tween over- night at 4°C, rinsed in PBS (pH 7.4), and then incubated with rabbit anti-MnSOD polyclonal antibody (1:2,000 dilution) overnight at 4°C. Extracellular signal–regulated kinase (ERK; 1:2,000, Covance) was probed as a loading control (previously shown not to change in diabetes in DRG). The blots were rinsed, incubated in Super Signal West Pico (Pierce Biotechnology, Rockford, IL), and imaged using a BioRad Fluor-S image analyzer. Shown are the blots (A) and chart (B) in which MnSOD signal has been presented relative to total ERK

levels. Values are the means ± SE, n = 6. *P < 0.005 vs. control; **P < 0.05 vs. diabetic + insulin (one-way ANOVA with Tukey's test). DB, diabetic;; INS, insulin.

The effect of 4-HNE on axon outgrowth and morphology was compared with features of axon outgrowth produced by adult sensory neurons isolated from 3-5 month STZ- induced diabetic rats. Age matched control and diabetic neurons were incubated in defined F12 + N2 medium with normal glucose (10 mM) and high glucose (25 mM), respectively, and assessed at 3-4 days of culture. The longer growth period was required to allow time for high glucose concentration-dependent oxidative stress to develop and permit adducts of 4-HNE to build up and induce pathology. The diabetic neurons revealed approximately 50% reduction in axon outgrowth (Fig. 20B) and formation of phase dark swellings along axons (Fig. 20A) as observed under conditions of 4-HNE treatment in normal neurons. To determine the ability of diabetic neurons to recover from the inhibitory effect of 4-HNE, cultured DRG neurons were isolated from STZ-induced diabetic rats and treated with 4-HNE under conditions of 10mM or 25mM glucose. There was no significant difference in the axon outgrowth between the 4-HNE treated groups under 10mM glucose after 48 h (Fig. 21A). However, under 25mM there was approximately 44% ($P<0.05$) reduction in axonal growth at 48 h in 4-HNE treated groups compared with controls (Fig. 21B).

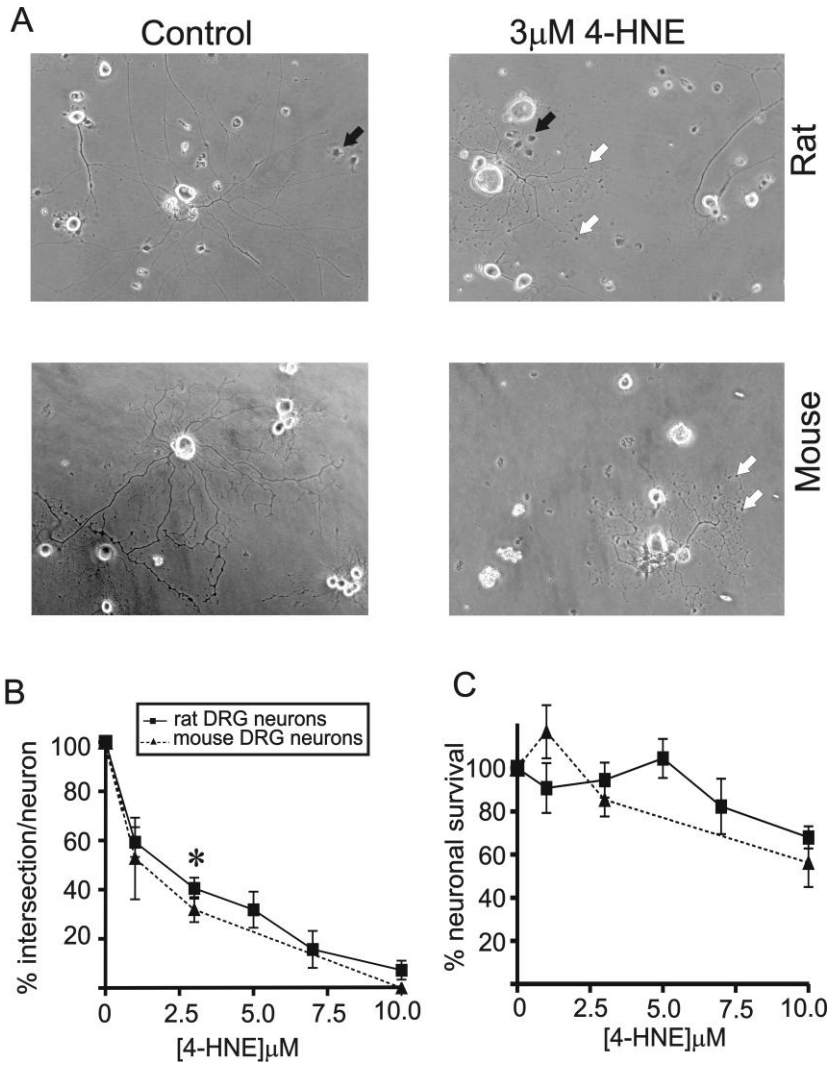

Fig. 19. Dose-dependent impairment of axon outgrowth by 4-HNE. (A) phase contrast images of 24 hr cultures of adult rat and mice DRG neurons. Neurons were grown in defined F12 media supplemented with N2 additives and neurotrophic factors (NTFs: 1 nM insulin, 1 ng/ml NGF, 10 ng/ml GDNF and 10 ng/ml NT-3) and treated with various concentrations 4-HNE. (B) and (C) are the quantification of total axon outgrowth and levels of survival of DRG neurons treated with 4-HNE. White arrows show swellings or dystrophic regions on the axons and black arrows show non-neurons. Broken line represents the mouse cultures and solid lines represent the rat cultures. Values are means $\pm$ SEM, n=4 replicate cultures. * $p < 0.05$ vs control in rat and mice, one-way ANOVA with Dunnetts test.

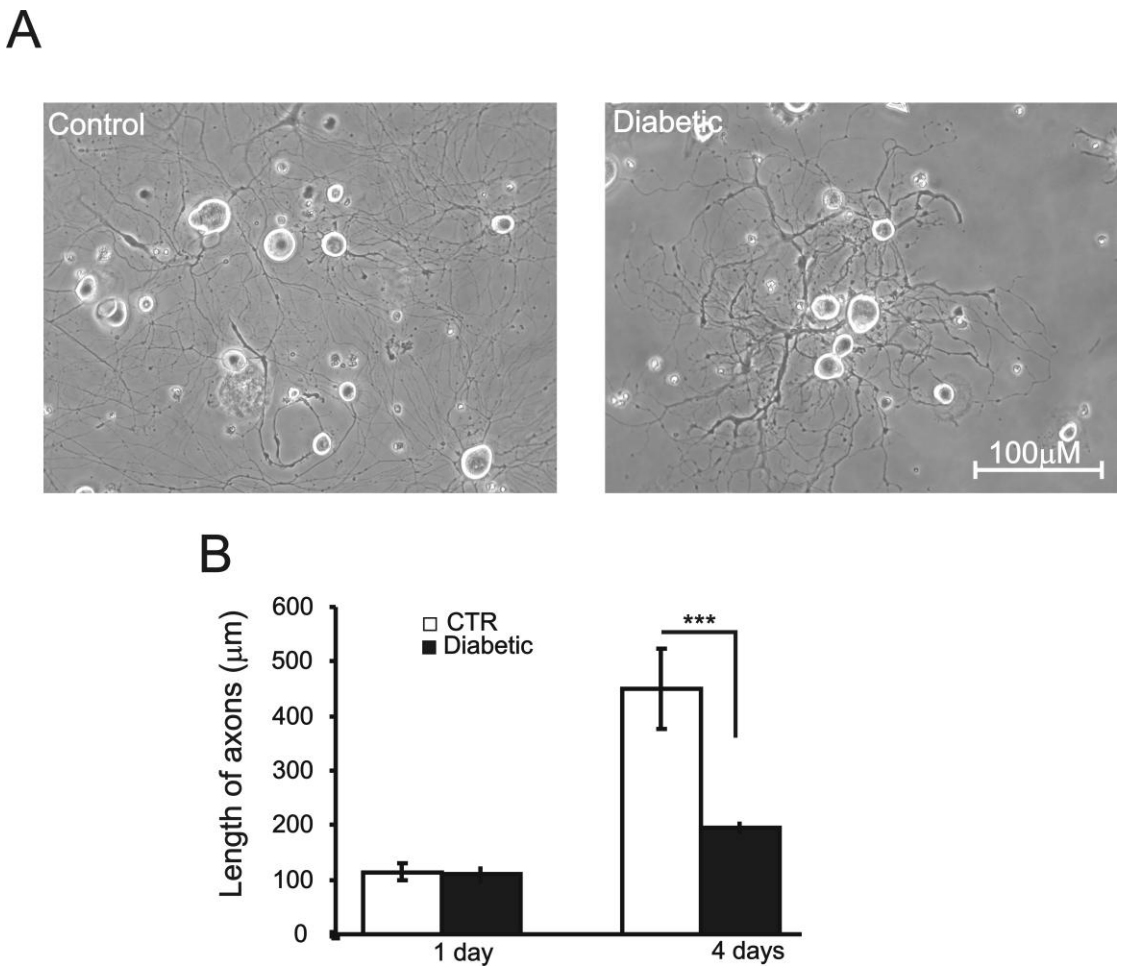

Fig. 20. Axon regeneration is impaired in cultured DRG neurons isolated from STZ-induced diabetic rats. (A) Phase contrast images of cultured DRG neurons isolated from STZ-induced diabetic rats taken on day 4 and (B) Shows the quantification of axon length in cultured DRG neurons isolated from STZ-induced diabetic rats on day 1 and day 4. Neurons were grown in defined F12 + N2 media supplemented with 10mM glucose (control) and 25mM glucose (diabetic). Values are means $\pm$ SEM, n= 3 replicate cultures. *** $p < 0.001$, t-test.

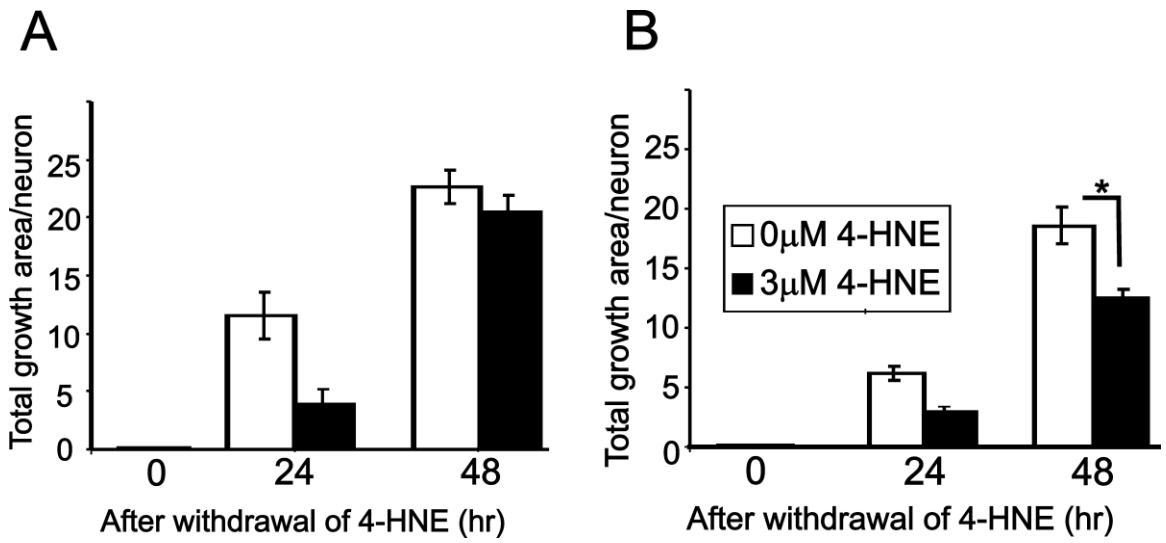

Fig. 21. High glucose increases the sensitivity of cultured diabetic DRG neurons to the inhibitory effect of 4-HNE. (A) Quantification of neurite outgrowth in diabetic neurons grown in 10mM D-glucose. Neurite outgrowth was measured 24 and 48 h following the removal of 4-HNE. (B**)** Quantification of neurite outgrowth of diabetic neurons grown in 25mM D-glucose. Neurite outgrowth was measured at 24 and 48 h following the removal of 4-HNE. Values are means $\pm$ SEM, n=3 replicate cultures. * $p < 0.05$, t-test. Neurons were grown in defined F12 media supplemented with N2 additives and treated with 3 μM 4-HNE.

In sensory neurons of diabetic rats, there is evidence to show that aberrant phosphorylation of neurofilament may contribute to the distal sensory axonopathy observed in diabetes (Fernyhough, Gallagher et al. 1999). Therefore, The ability of 4-HNE to form adducts on cytoskeletal proteins in rat sensory neurons and, as a result, to alter the phosphorylation of neurofilament proteins was investigated. Sensory neurons from normal rats were treated at 24 hr with 3 μM 4-HNE and immunostained (following 24 hr of treatment) for phosphorylated NFH (pNFH) and adducts of 4-HNE. Control cultures showed normal axons with minimal labeling of adducts of 4-HNE, whereas, 4-HNE-treated cultures showed large

numbers of aggregations or puncta comprising 4-HNE staining (Fig. 22A; white arrows). Quantification of levels of adducts of 4-HNE and pNFH signal showed a 2-fold increase in adduct formation compared to controls (Fig. 22B), and a significant increase in NFH phosphorylation in the 4-HNE treated groups (Fig. 22C). Shown in (Fig. 22D) is Western blot data confirming the presence of adducts of 4-HNE in DRG neurons treated exogenously with 4-HNE. There was a clear enhancement in adduct formation in the 4-HNE treated group, with discernable bands showing up around 25 KDa, 55 KDa, 70 KDa, and 130 KDa. These molecular weights are similar to those of cytochrome C oxidase, ATPase synthase, neurofilament L and neurofilament M, respectively.

Several studies have demonstrated that mitochondria are a significant source of ROS, and the elevation of ROS is associated with the increase in 4-HNE levels. Mitochondrial function has a central role in governing axon outgrowth, mainly through generation of ATP for actin treadmilling (Bernstein and Bamburg 2003). Therefore, owing to the critical role played by the mitochondria in providing energy needed for axon plasticity, the ability of 4-HNE to modify mitochondrial proteins was investigated.

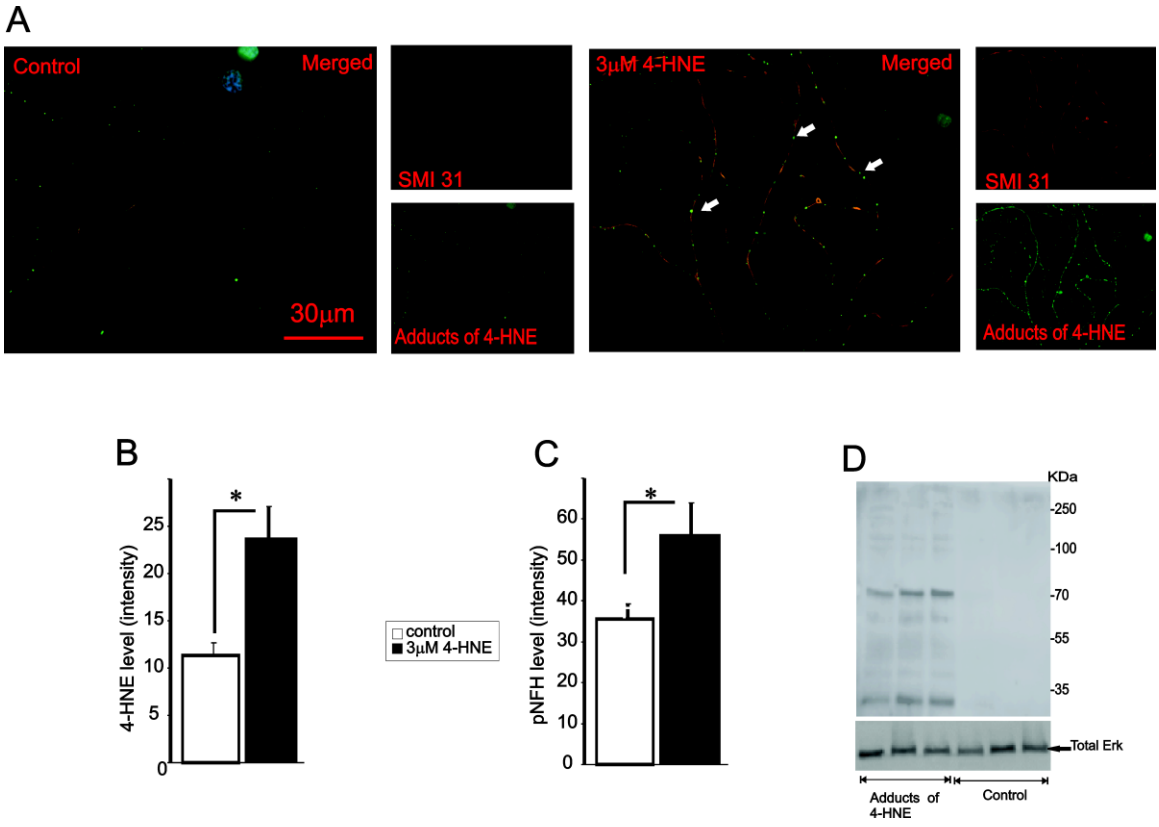

Fig. 22. 4-HNE treated adult rat DRG neurons show elevated levels of adducts of 4-HNE and abnormal neurofilament H phosphorylation. (A) Immunofluorescence images of 4-HNE treated DRG neurons isolated from lumbar DRG of adult rats. Neurons were stained for adducts of 4-HNE (green) and phosphorylated NFH using antibody SMI 31 (red). Yellow indicates the merged images of adducts of 4-HNE and phosphorylated NFH. Neurons were grown in defined F12 media supplemented with N2 additives and neurotrophic factors and treated with 3.0 μM 4-HNE. White arrows show accumulation of 4-HNE adducts. (B) and (C) are the quantification of levels of protein adducts and phosphorylated NFH in the axons, respectively. (D) Western blot showing adducts formation on various proteins in 4-HNE treated neurons. Values are means $\pm$ SEM, n=45 axons. * $p < 0.05$, t-test.

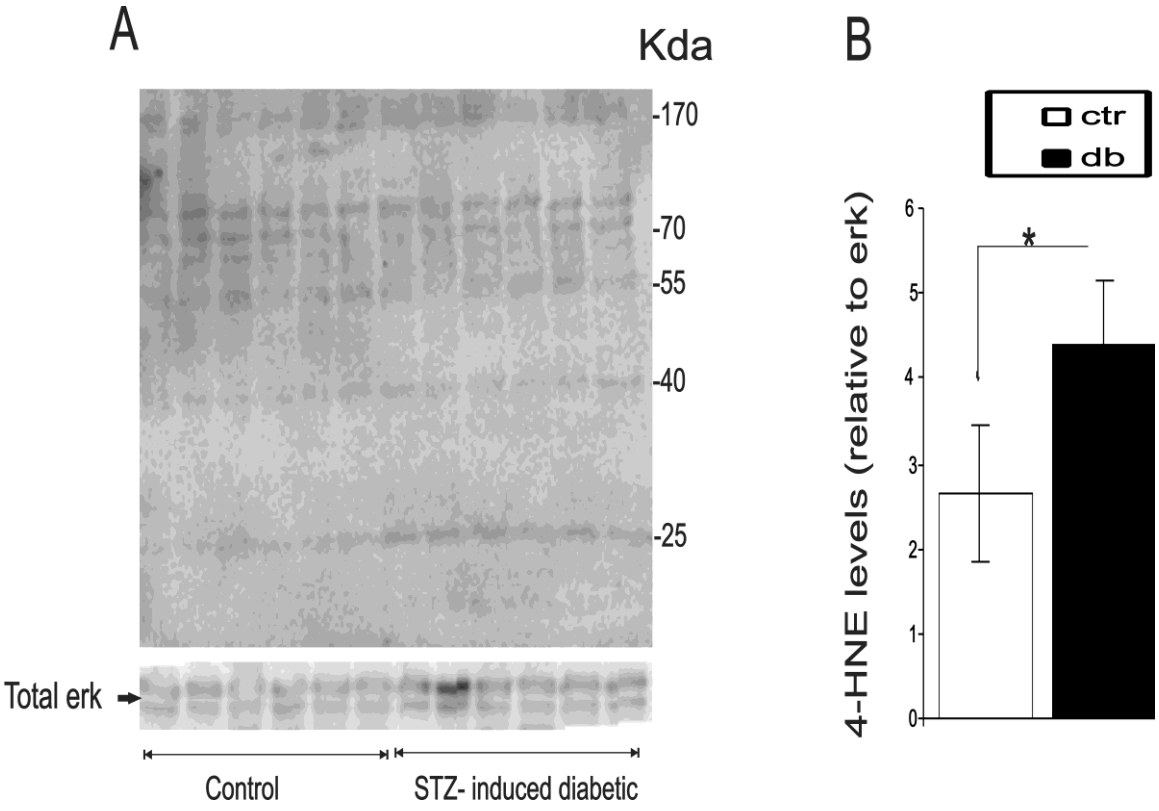

Fig. 23. Adducts of 4-HNE are formed on mitochondrial proteins**.** (A) Western blot showing protein adducts formation on mitochondrial proteins. Mitochondria were isolated from DRG of adult STZ-induced diabetic rats and age-matched controls using mitochondrial isolation buffer. (B) Is quantification of total levels of protein adducts in (A) in normal and STZ-induced diabetic DRG mitochondria. The band intensities from all the discernable bands in (A) were pooled together to generate (B). Values are means $\pm$ SEM, n = 6 .* $p < 0.05$**.**

To this end, mitochondria were isolated from normal and STZ-diabetic adult rat DRG and protein adducts of 4-HNE assessed by Western blot. The combined intensity of all the discernable bands on the blot showed an increase in adduct formation in mitochondrial from the DRG of the STZ-induced diabetic rat compared to the controls (Fig. 23A and B).

Also, the effect of 4-HNE adduct formation on the activity of mitochondria was analyzed in normal adult rat sensory neuron cultures. DRG neurons were treated with 3 μM 4-HNE at 24 hr and co-stained for actively respiring mitochondria using CMXRos and adducts of 4-HNE (following 24 hr of treatment). Control cultures exhibited normal axons with uniform labeling of actively respiring mitochondria and minimal swellings, which stained negatively for adducts of 4-HNE. In comparison, 4-HNE-treated cultures showed much less uniform staining for active mitochondria with a large number of axonal swellings that were filled with active mitochondria, which stained positively for adducts of 4-HNE (Fig. 24A). The accumulation of adducts of 4-HNE co-located with active mitochondria in the axonal swellings (Fig. 24A; white arrows).

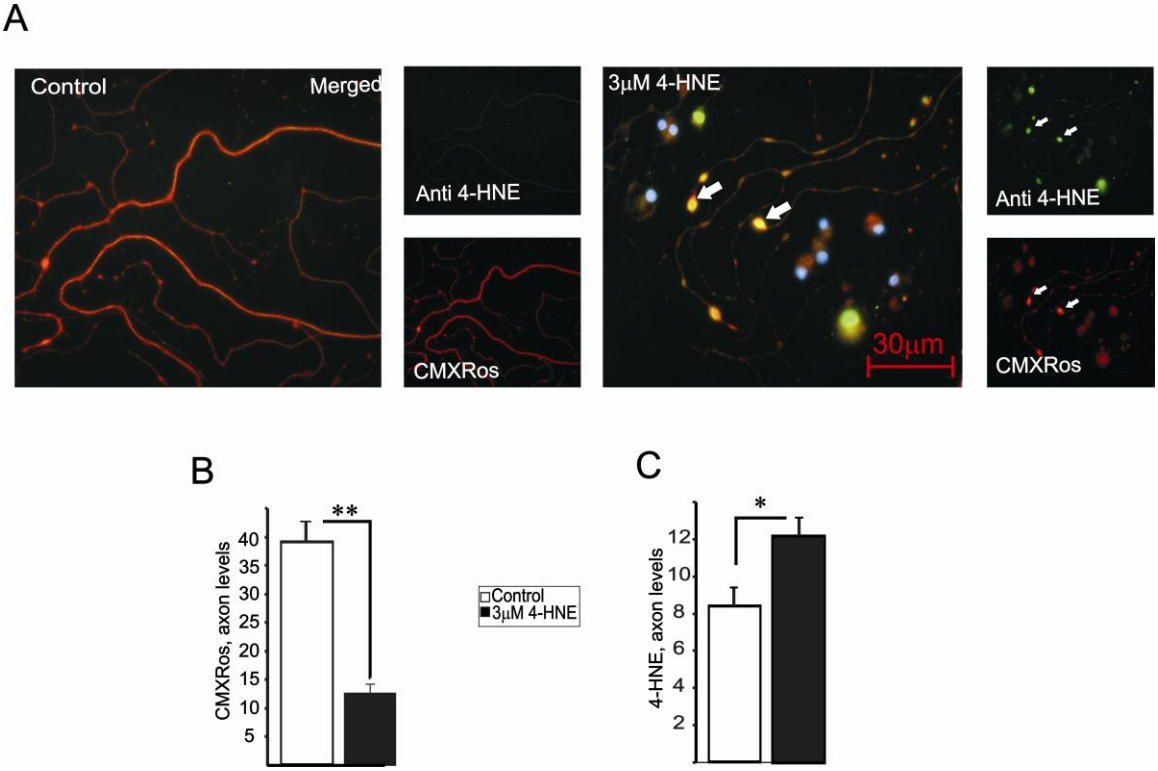

Fig. 24. 4-HNE induces the accumulation of active mitochondria in swellings along the axons of adult rat DRG neurons treated with 4-HNE. (A) Representative immunofluorescent images of 4-HNE treated DRG neurons isolated from lumbar DRG of adult rats. Neurons were stained for actively respiring mitochondria using CMXRos (red) and adducts of 4-HNE (green). The yellow stain represents the merged images and blue stain shows the nuclei. White arrows indicate the presence of axonal swellings. Neurons were grown in defined F12 media supplemented with N2 additives and neurotrophic factors and treated with 3.0 μM 4-HNE. Note: neurons were treated with 4-HNE at 24 hr of neuronal culture and immunofluorescent images taken at 24hr of treatment. (B) and (C) are the quantification of CMXRos levels and adducts of 4-HNE levels in the axons, respectively. Values are means $\pm$ SEM, n=48 axons. * $p < 0.05$ and ** $p < 0.01$.

Quantification of the fluorescence signal showed an association between increase in the formation of 4-HNE adducts in the axons (Fig. 24C) and a decrease in the levels of active mitochondria as indicated by CMXRos intensity levels (Fig. 24B).

We investigated if a decline in actively respiring mitochondrial levels resulted in a reduction in mitochondrial mass (active and inactive) in sensory neurons treated with 4-HNE. Sensory neurons were treated with 3 μM 4-HNE at 24 hr and co-stained with Mitotracker green dye and CMXRos (following 24 hr of treatment). Mitotracker green dye preferentially accumulates in mitochondria regardless of mitochondrial membrane potential, making it a tool for determining mitochondria mass. Mitochondrial mass as indicated by Mitotracker green intensity was evenly spread from the cell body to the axon terminals in the absence or presence of 4-HNE, however, a progressive decline in CMXRos signal intensity was observed towards the distal axonal regions in the 4-HNE

treated group (Fig. 25A.). There was no statistical difference between the treated and control groups with respect to Mitotracker green levels in the axons (Fig. 25B), however, CMXRos intensity levels declined significantly in the treated group compared to control (Fig. 25C).

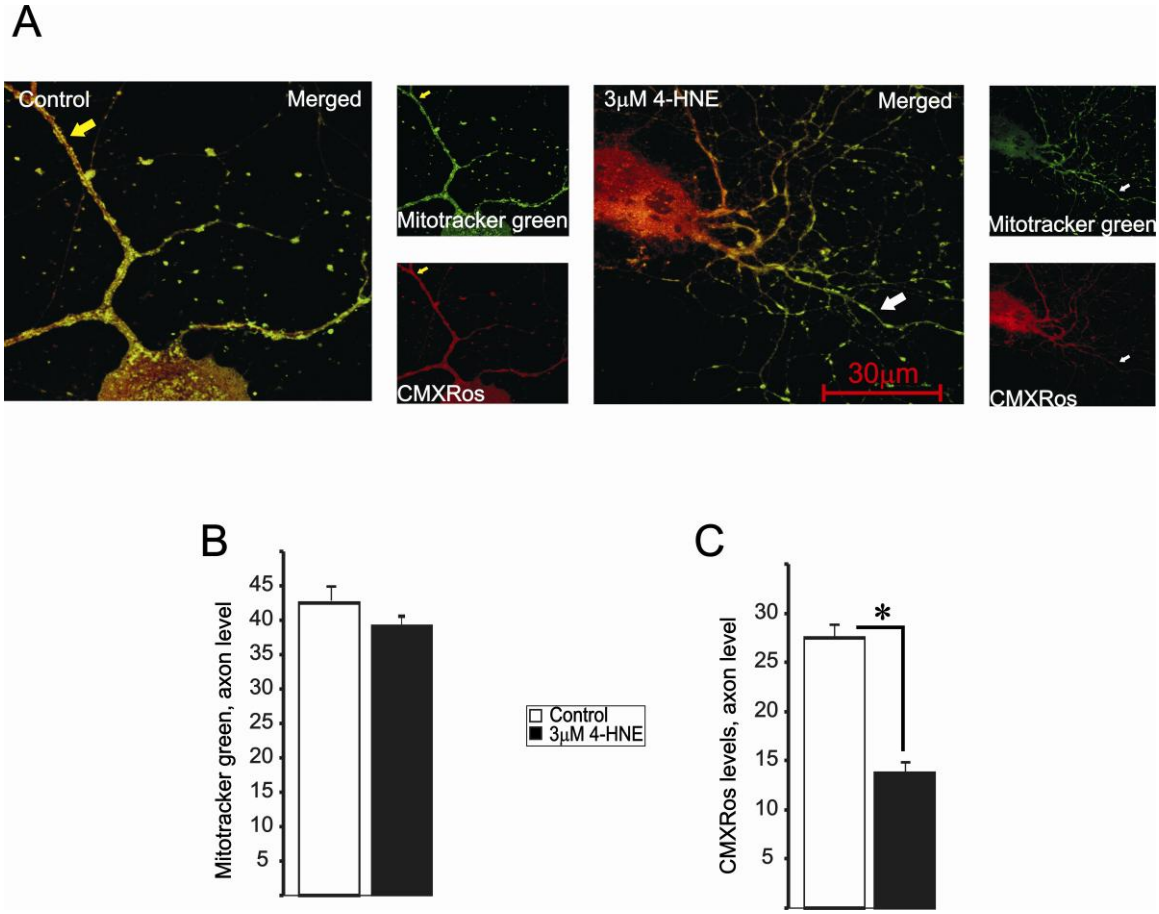

Fig. 25. 4-HNE induces the loss of actively respiring mitochondria at the distal ends of axons. (A) Representative immunofluorescent images of 4-HNE treated DRG neurons isolated from lumbar DRG of adult rats. Neurons were stained for actively respiring mitochondria using CMXRos (red) and mitochondrial mass using Mitotracker green (green). The yellow stain represents the areas of colocalization in the merged images. White arrows point to the areas along the axons where mitochondrial activity has been lost. Neurons were grown in defined F12 media supplemented with N2 additives and neurotrophic factors and treated with 3.0 μM 4-HNE. Note: neurons were

treated with 4-HNE at 24 hr of neuronal culture and immunofluorescent images taken at 24hr of treatment, (B) and (C) are the quantification of Mitotracker green and CMXRos levels in the axons, respectively. The asterisk shows cell body of neurons. Values are means ± SEM, n=48 axons. * $p < 0.05$, t-test.

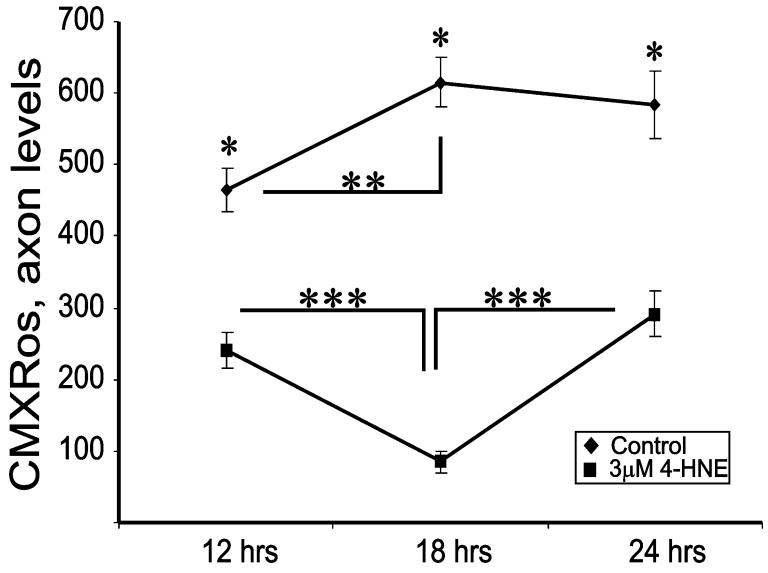

Fig. 26. Impairment of mitochondrial activity in 4-HNE treated neurons is reversed within 24 h. Neurons were grown in defined F12 media supplemented with N2 additives and neurotrophic factors and treated with 3.0 μM 4-HNE. Note: neurons were treated with 4-HNE and mitochondrial activity assessed at 12 h, 18 h and 24 h. Values are means ± SEM, n= 48 axons. *$p < 0.05$, ** $p < 0.01$ and ***$p < 0.001$,one-way ANOVA.

Finally, we determined if the suppression of mitochondrial activity is reversible over time. Sensory neurons were treated with 3 μM 4-HNE and mitochondria activity assessed. There was a significant 4-HNE-induced decrease in the levels of active mitochondria at 12 hr and 18 hr compared to controls, however,

mitochondrial activity levels began to recover at 24 hr even though the levels at this time point were still significantly lower than controls (Fig. 26).

3.5. DISCUSSION

There is increasing evidence of the role played by oxidative damage in the etiology of a range of neurodegenerative diseases, including development of diabetic neuropathy (Neely, Sidell et al. 1999; Obrosova, Drel et al. 2005). However the link between oxidative stress and nerve degeneration associated with neuropathy is not clearly understood. 4-HNE, a product of lipid peroxidation, forms adducts with key neuronal proteins (Uchida 2003; Petersen and Doorn 2004), and these adducts have been shown to be elevated in the peripheral nerves of STZ-induced diabetic rats (Obrosova, Drel et al. 2005). Protein adducts have also been detected in mouse sciatic nerves treated with 4-HNE (Wataya, Nunomura et al. 2002) and sciatic nerves and DRG of diabetic mice exposed to a high fat diet (a model of pre-diabetes) (Obrosova, Ilnytska et al. 2007). In the present study we show for the first time that 4-HNE directly impairs mitochondrial function and axonal regeneration in cultured adult DRG sensory neurons. 4-HNE triggered formation of amino acid adducts of neuronal proteins, including mitochondrial proteins, and this was associated with a distally directed reduction in the levels of active mitochondria in the axon, and the formation of abnormal axonal structures, which stained positively for adducts of 4-HNE. These structural abnormalities in the axons closely resembled dystrophic and 4-HNE labeled structures observed in the neurites of DRG neuronal cultures derived from STZ-induced diabetic rats (Fig.27). The ability of 4-HNE to form

adducts on neuronal proteins and impair mitochondrial activity is in good agreement with studies on other types of cells. For example, the Romani group showed specific modification of key mitochondrial proteins by 4-HNE leading to an impairment in enzymatic activity in the mitochondria of cardiac tissue in rodents with diabetes (Lashin, Szweda et al. 2006).

The axonal pathology induced by 4-HNE in the normal cultures closely paralleled axon damage generated in cultures of neurons from diabetic rats. Interestingly, the anatomical phenotype of these cultures described herein exhibited axonal morphologies that closely compare with axon pathology in human diabetic neuropathy where axonal swellings and dystrophy have been described in DRG, nerve and at distal sites within the epidermis (Schmidt, Dorsey et al. 1997; Lauria, Morbin et al. 2003; Ebenezer, McArthur et al. 2007). In diabetes it has been proposed that axonal pathology may be triggered by impaired mitochondrial function (Sasaki, Schmelzer et al. 1997; Brownlee 2001; Fernyhough, Huang et al. 2003; Verkhratsky and Fernyhough 2008). It has been theorized that high [glucose] drives excessive electron donation to the electron transport chain in mitochondria resulting in mitochondrial hyperpolarization and elevated production of ROS (Nishikawa, Edelstein et al. 2000). Brownlee et al. have proposed that this mitochondrial-dependent process is a central mediator of oxidative stress in complications of diabetes and could be a major generator of lipid peroxidation and 4-HNE (Brownlee 2001). The theory suggests that high [glucose] in tissue targets for diabetic complications leads to increased supply of NADH in the mitochondria, and that this increased electron availability and/or

saturation may cause partial reduction of oxygen to superoxide radicals in the proximal part of the electron transport chain. Subsequent large elevations in ROS and associated 4-HNE then may react with mitochondrial proteins and result in degeneration of tissue. These findings point to the central role played by the mitochondria, and in part 4-HNE, as a mediator of neurodegeneration in the PNS and a critical modulator of diabetic complications in neurons (Sasaki, Schmelzer et al. 1997; Brownlee 2001; Fernyhough, Huang et al. 2003; Verkhratsky and Fernyhough 2008).

The current study revealed that 4-HNE formed adducts and significantly impaired neurite outgrowth at concentrations as low as 3 μM in cultured adult DRG neurons treated with 4-HNE for a period of 24 hr. Also, significant neuronal death was observed at 4-HNE concentrations of 10 μM or higher in the DRG cultures. Other studies have reported impairment of neurite outgrowth in Neuro 2A cells incubated with 4-HNE for 1 hr and assessment of outgrowth made 24 hr later (Neely, Sidell et al. 1999). The former study showed no significant impairment of neurite outgrowth at 4-HNE concentrations below 25 μM, and found no significant cell death. These discrepancies could be the result of differences in cell types, period of 4-HNE exposure and extent of cell density (Kokubo, Nagatani et al. 2008). For example, within the present study there was enhanced sensitivity of the mouse DRG neuronal cultures to 4-HNE. It is worth noting that one of the key pathological features of diabetic neuropathy as observed in humans and in animal models involves the dying back of the longest axons, however, these neurons do not undergo any overt process of cell death

(Schmidt, Dorsey et al. 1997). Therefore, in our cultured DRG neurons, we determined the concentration of 4-HNE at which there was approximately 50% impairment in neurite outgrowth with no corresponding effect on neuronal survival. 4-HNE concentration of 2.5 μM appeared to be the ideal dose, however, we adjusted this to 3.0 μM taking into account the slight variability in neuronal numbers from different cultures.

The important finding in the present study was that 4-HNE was associated with a distally directed reduction in the levels of actively respiring mitochondria, and with the formation of swellings along the axons, further implicating the role of mitochondrial dysfunction in the etiology of the axon pathology. Also, the fact that the protein adducts of 4-HNE co-localized with actively respiring mitochondria in areas of swellings along the axons points to the fact that some mitochondrial proteins might have been modified. This result, with regard to the localization of mitochondria to sites of swellings along the axon, agrees with in vitro studies by the Connolly group (Greenwood, Mizielinska et al. 2007). Western blot analysis of mitochondria isolated from adult STZ-induced diabetic and normal rats indicate that one of the target proteins for 4-HNE adduction might be cytochrome C oxidase (Complex IV enzyme), although, other targets such as succinate dehydrogenase have been reported (Lashin, Szweda et al. 2006). Also, studies concerning adduction of 4-HNE to proteins have demonstrated its ability to inhibit a variety of enzymes including complex IV of the mitochondrial respiratory chain (Isom, Barnes et al. 2004). Cytochrome C is essential for the translocation of electrons between Complex III and IV, a key

process that generates the proton gradient that drives ATP synthase activity (Complex V) (Nicholls and Ward 2000). Modification of this key enzyme in the electron transport chain could result in diminished ATP production. A reduction in ATP synthesis in the axon from either disruption in proton gradient generation or improper mitochondrial localization could lead to decreased Na^+-K^+ ATPase function, resulting in a rise in intracellular Na^+ and a reversal of Na^+-Ca^{2+} exchanger function (Waxman 2006). The outcome could be an increase in intracellular Ca^{2+} to damaging levels, ultimately resulting in axonal degeneration (Duchen, Verkhratsky et al. 2008; Verkhratsky and Fernyhough 2008). It should be noted that abnormal Ca^{2+} homeostasis is also a key feature of sensory neuron dysfunction in animal models of type 1 and type 2 diabetes (Huang, Sayers et al. 2002; Verkhratsky and Fernyhough 2008). Moreover, we believe the presence of axonal swellings mediated by an accumulation of modified mitochondria and/or aberrantly phosphorylated neurofilament proteins could physically obstruct the movement of mitochondria towards the axonal terminals. Disruption of proper mitochondrial motility and localization is believed to interfere with normal axonal and synaptic function and could likely result in distal axonal degeneration (Baloh 2008).

3.6. Conclusions

We propose that increased intracellular levels of 4-HNE leads to the modification of key mitochondrial proteins through adduct formation, this causes a disruption in the activity and localization of mitochondria and could trigger an impaired bioenergetic state within axons, eventually leading to axonal

degeneration. The axonal degeneration induced by 4-HNE closely resembles aberrant axon morphology observed in neurons from a diabetic background; a key feature in both settings is the presence of 4-HNE-labeled axonal swellings. In summary, these results implicate lipid peroxidation and 4-HNE adduct formation, possibly targeted to the mitochondrion, in the neurodegenerative processes central to the etiology of diabetic sensory neuropathy.

Chapter 4:

Diminished Superoxide Generation is Associated with Respiratory Chain Dysfunction and Changes in the Mitochondrial Proteome of Sensory Neurons from Diabetic Rats

Diabetes. 2011 Jan; 60(1): 288-97

4.1. Introduction

Enhanced oxidative stress is thought to be a central pathological feature in the etiology of diabetic peripheral neuropathy (Vincent, Russell et al. 2004).To develop more targeted therapeutics toward ameliorating oxidative stress and the development of diabetic peripheral neuropathy, considerable effort has focused on identifying the cellular source of ROS over the past decade. Brownlee and colleagues suggested that mitochondrial superoxide generation might be a critical feature in the onset of diabetic complications (Nishikawa, Edelstein et al. 2000). In cultured endothelial cells, hyperglycemia induced excessive electron flux through the respiratory chain that promoted mitochondrial hyperpolarization and elevated ROS production (Du, Edelstein et al. 2000; Nishikawa, Edelstein et al. 2000). These investigators proposed that hyperglycemia increases

mitochondrial NADH levels and that increased electron availability and/or saturation caused partial reduction of oxygen to superoxide in the proximal part of the respiratory chain (Nishikawa, Edelstein et al. 2000). In support of this mechanism, epineurial arterioles serving the sciatic nerve of STZ-induced diabetic rats show increased levels of mitochondrial superoxide that is dependent on complex I activity (Coppey, Gellett et al. 2003). On the other hand, studies in diabetic retina suggest that metabolism of high glucose concentrations does not operate in a fashion that supports superoxide formation by the respiratory chain (Ola, Berkich et al. 2006). Similarly, in sensory neurons from STZ-induced diabetic rats, the mitochondrial membrane potential is depolarized and not hyperpolarized as observed in endothelial cells exposed to hyperglycemia (Srinivasan, Stevens et al. 2000; Huang, Price et al. 2003). Further, lumbar DRG from diabetic rats exhibit reduced respiratory chain activity that correlated with the down-regulation of select proteins within the electron transport chain complexes (Chowdhury, Zherebitskaya et al. 2010). These findings are aligned with studies in diabetic heart where mitochondrial respiration and enzymatic activities are reduced (Lashin, Szweda et al. 2006; Yang, Yeh et al. 2009). In addition, activities of citrate synthase and mitochondrial respiratory chain are decreased in skeletal muscle of patients with type 2 diabetes (Kruszynska, Mulford et al. 1998; Kelley, He et al. 2002; Mogensen, Sahlin et al. 2007). Therefore, production of mitochondrial superoxide may exhibit fundamental differences in cells that are targets of diabetic complications. Indeed, the tissue specific nature of mitochondrial remodeling in diabetes is directly underscored by

results from an unbiased proteomic study that identified a differential affect of diabetes on mitochondrial protein expression and oxidative capacity. For example, proteins associated with oxidative phosphorylation were more depressed and respiratory activity decreased in heart compared to liver mitochondria from diabetic Akita mice (Bugger, Chen et al. 2009).

4.2. Rationale

Since DRG sensory neurons are highly susceptible to glucotoxicity (Tomlinson and Gardiner 2008), we examined the effect of diabetes on mitochondrial proteome, respiratory capacity and superoxide production. DRG neurons isolated from normal or diabetic rats were cultured in F12 media containing 10mM or 25mM glucose; respectively. Changes in mitochondrial function and physiology were then assessed at 24 h of culture. Additionally, proteomic analysis was performed in mitochondria isolated from DRG to assess changes induced by diabetes. In our previous study, we showed that under hyperglycemic conditions ROS levels are elevated in diabetic neurons (Zherebitskaya, Akude et al. 2009), this was associated with an increase in the formation of adducts of 4-HNE on mitochondria proteins (Akude, Zherebitskaya et al. 2010) including proteins in the respiratory chain (Lashin, Szweda et al. 2006). Further, increases in the levels of 4-HNE were found to induce abnormal mitochondrial activity in the axons of cultured DRG neurons (Akude, Zherebitskaya et al. 2010). These results suggest that mitochondria proteins and respiratory chain activity in the axons of diabetic neurons may be particularly susceptible to the deleterious effects of oxidative stress. Therefore, we tested the

hypothesis that mitochondrial dysfunction in axons of sensory neurons in type 1 diabetes is due to abnormal activity of the respiratory chain and an altered mitochondrial proteome.

4.3. Aims / objectives

- To determine the effect of diabetes and insulin therapy on proteins involved in oxidative phosphorylation and mitochondrial dysfunction.
- To determine the effect of diabetes on mitochondrial membrane potential in the axons of cultured DRG neuron, where oxidative stress and degeneration are most clearly defined (Kennedy, Wendelschafer-Crabb et al. 1996; Polydefkis, Hauer et al. 2004; Zherebitskaya, Akude et al. 2009).
- To relate the effects of diabetes on mitochondrial proteome expression to mitochondrial physiology and function within the axon of DRG neurons.
- To determine if diabetes-induced abnormalities in respiratory chain was associated with ROS generation in the axons of cultured DRG neurons

Approach

We exploited the use of stable isotope labeling of cells in culture (SILAC) (Ong, Blagoev et al. 2002) to provide a set of culture-derived isotope tags (Ishihama, Sato et al. 2005) to serve as internal standards for a quantitative proteomic analysis. Also we used mitochondrial respiration assay and real-time fluorescence microscopy to demonstrate that in diabetes impaired respiratory chain function correlates with decreased protein expression and in mitochondria

of axons these deficits are associated with membrane depolarization and reduced respiratory chain-derived ROS generation.

4.4. Results

STZ-induced diabetic rats did not suffer weight loss during the study but showed reduced weight gain after 22 weeks of STZ-induced diabetes compared to age-matched controls (Table 3). Persistence of diabetes was indicated by elevated non-fasting blood glucose and glycated hemoglobin levels (Table 3). STZ-induced diabetic rats that received insulin supplementation for the final 4 weeks of a 22 week period of diabetes showed a partial, but statistically significant, recovery of body weight, blood glucose and glycated hemoglobin levels.

Table 3. Body weights, plasma glucose and glycated hemoglobin (HbA1c) of treatment groups.

	Body weight (g)	Blood glucose (mmol/l)	HbA1c (%)
	n = 10-13	n = 10-13	n = 9-10
Control	770.9 ± 57.9*	8.24 ± 0.89*	4.39 ± 0.28*
Diabetic	415.8 ± 33.9**	30.95 ± 2.71**	11.69 ± 0.97**
Diabetic + insulin	519.1 ± 42.0	14.81 ± 4.95	8.59 ± 1.17

Values are means ± SD. *p<0.001 vs other groups; **p<0.001 vs diabetic + insulin (one-way ANOVA with Tukey's test). Starting weights for the groups were 293 ± 8.8 g (mean ± SD; n=38). Non-fasting blood sugar concentration was measured using the Accu-Chek Compact Plus

glucometer (Roche, Laval, QC, Canada) and blood glycated hemoglobin (HbA1c) levels by the A1cNow+ system (Bayer Healthcare, Sunnyvale, CA).

To quantitatively assess the effect of diabetes and insulin therapy on the mitochondrial proteome of lumbar DRG, we labeled S16 immortalized Schwann cells with isotopic forms of lysine (K6) and arginine (R10) and isolated labeled mitochondria to serve as internal standards (Fig. 27A). We examined the quantitative accuracy of this approach by mixing the K6R10: K0R0 mitochondria in ratios of 0.75:1, 1.5:1 and 3:1. The K6/K0 or R10/R0 ratios for individual peptides were obtained from MaxQuant analysis and a linear response was observed after plotting the average peptide ratio obtained from each mixture against the known mixing ratio. A 25% decrease in protein expression was quantifiable. Unlabeled (K0R0) DRG mitochondria from the three treatments were then individually mixed in a 2:1 ratio with the K6R10 mitochondria prior to SDS-PAGE and LTQ-FT MS/MS analysis. From over 43,600 identified peptides, 12,785 SILAC pairs were sequenced and approximately 60% identified. After culling out contaminants (n=30), reverse-decoy hits (n=13) and proteins identified by only a single unique peptide, we identified 672 proteins of which 334 (49.6%) were quantified by at least one unique peptide identified in samples from at least two animals. The median number of quantified ratios for the three treatments was: control (n=5), diabetic (n=8) and diabetic + insulin (n=7). Of the total proteins identified, 206 (30%) were annotated as mitochondrial/glycolytic and 151 were quantified (73%). To provide a global view of the effect of diabetes and

insulin therapy on protein expression, the expression ratios were binned and a frequency distribution assessed (Fig. 27B).

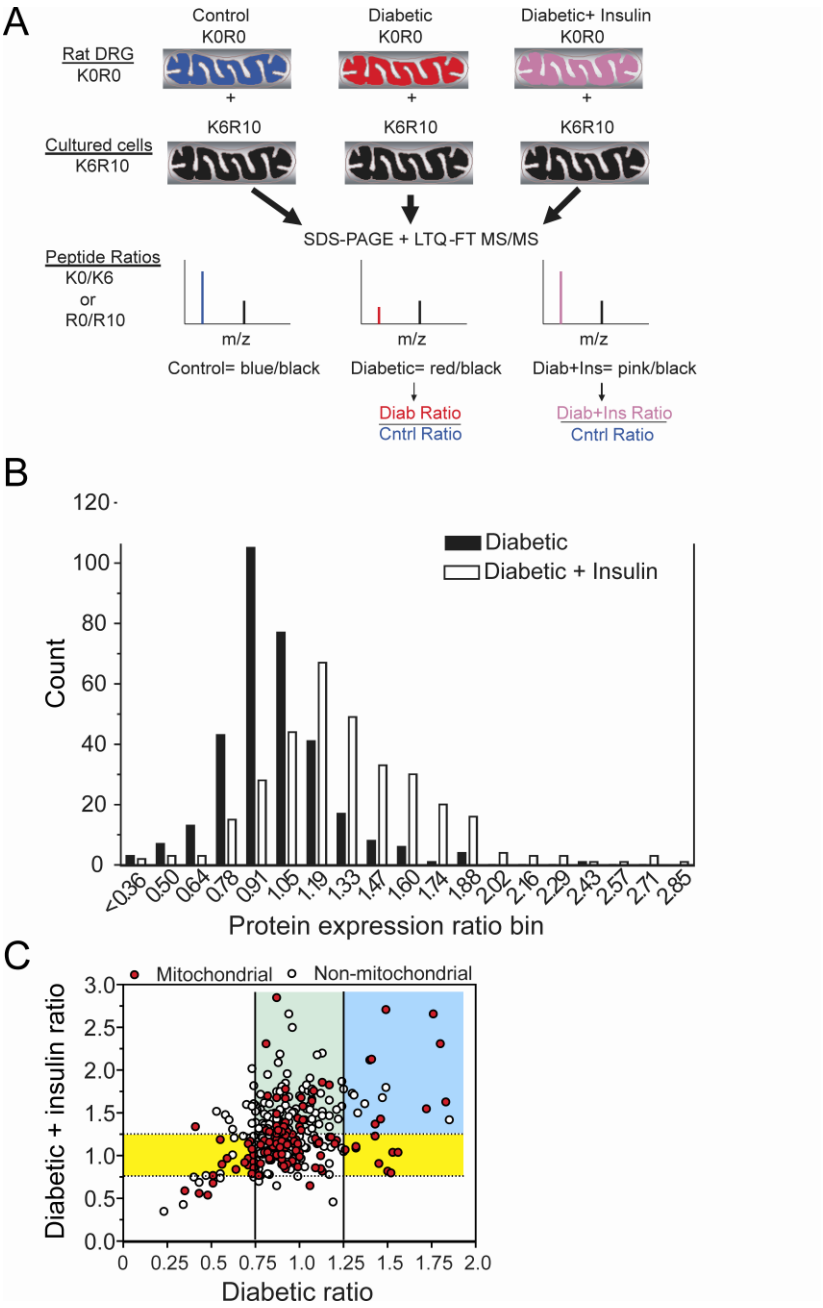

FIG. 27. In *(A)* Schematic for use of culture-derived isotope tags for quantitative proteomics and overview of results. Unlabeled (K0R0) mitochondrial fractions were prepared from the lumbar DRGs obtained from each animal in the three treatment groups. Each K0R0 mitochondrial fraction was mixed in a 2:1 ratio with K6R10 labeled mitochondria obtained from S16 cells that had been metabolically labeled with $^{13}C_6$ lysine (K6) or $^{13}C_6$,$^{15}N_4$ arginine (R10) for 10 days. The proteins were resolved by SDS-PAGE, digested with trypsin and analyzed by RP-HPLC/LTQ-FT MS/MS. For each protein, the ratio of K0R0 to K6R10 quantifies the endogenous protein relative to the internal standard. Dividing the protein ratios obtained in the diabetic or diabetic + insulin treatment by those obtained from control animals cancels out the K6R10 internal standard and provides the fold control value. *(B)* Effect of diabetes and insulin therapy on mitochondrial protein expression. The protein expression ratios from the diabetic and diabetic + insulin treatments were binned and the number of proteins per bin counted. *(C)* To determine the effect of diabetes and insulin therapy on mitochondrial versus non-mitochondrial proteins, the expression ratio for each protein was plotted against each treatment. Solid and dotted lines demarcate the threshold necessary for proteins to show a significant change in the diabetic and diabetic + insulin treatments, respectively. Proteins in-between dotted and solid lines did not change with either treatment. Yellow shading indicates proteins that were significantly up or down regulated by diabetes and normalized by insulin therapy. Blue shading indicates proteins that were increased by diabetes but not normalized by insulin therapy. Green shading indicates proteins not affected by diabetes but increased by insulin therapy.

In general, diabetes had a more pronounced effect on decreasing protein expression. Insulin therapy induced a rightward shift toward normalizing expression and promoted a significant increase in protein expression. Pathway analysis found that proteins associated with mitochondrial dysfunction, oxidative phosphorylation and ubiquinone biosynthesis (primarily complex 1 proteins) were

the most significantly over-represented and showed the greatest percentage of proteins that underwent significant down-regulation (Table 4).

Table 4. Over-represented canonical pathways identified in the proteomic analysis.

Canonical Pathways	Significance	Ratio, %	Total Genes
Mitochondrial dysfunction	3.16×10^{-11}	7.2	171
Oxidative phosphorylation	3.98×10^{-7}	5.4	166
Ubiquinone biosynthesis	7.94×10^{-6}	5.0	119
Methane metabolism	1.25×10^{-4}	4.0	66
Breast cancer regulation by stathmin1	1.59×10^{-4}	4.6	199
Integrin signaling	1.99×10^{-4}	3.5	200
Butanoate metabolism	6.31×10^{-4}	3.0	132
14-3-3-mediated signaling	6.31×10^{-4}	4.4	114
Propanoate metabolism	7.94×10^{-4}	3.1	130
Citrate cycle	7.94×10^{-4}	5.2	58
Valine, leucine and isoleucine degradation	1.00×10^{-3}	3.6	111
Fatty acid metabolism	1.25×10^{-3}	2.6	192
Phenylalanine metabolism	1.25×10^{-3}	2.8	109

Ketone body biology	2.51×10^{-3}	10.5	19
Fatty acid elongation	5.01×10^{-3}	4.4	45
Induction of apoptosis by HIV1	6.31×10^{-3}	4.6	65

Significance provides the confidence of the association as identified by the p value of the Fisher exact test. The ratio provides the percent of proteins associated with the pathway that underwent a significant change. The total genes column refers to all known genes to be linked to the pathway (not necessarily identified by the proteomic screen).

Consistent with the diabetic phenotype, proteins associated with ketone body biology were also over-represented and diabetes increased the expression of succinyl-CoA:3-ketoacid-coenzyme A transferase 1 (SCOT), which is critical in acetoacetate clearance.

To determine if diabetes and insulin therapy had a distinct effect on mitochondrial versus non-mitochondrial proteins, the expression ratios for each protein were plotted against each treatment (Fig. 27C). This analysis indicated that diabetes had little effect on the majority of mitochondrial and non-mitochondrial proteins that were quantified (region between solid and dotted lines). With rare exception, insulin therapy did not decrease protein expression but led to a significant increase in the expression of numerous non-mitochondrial proteins (green shading). Enrichment analysis of proteins in this region using the Biological Networks Gene Ontology (BiNGO) plugin of Cytoscape found that cluster frequency for proteins annotated to the biological process of translation

was 36.1%, a 7-fold enrichment. We also noted a small group of proteins that were significantly increased by diabetes but whose expression was unchanged by insulin (blue shading). BiNGO analysis of this subset of proteins indicated that small G-protein signaling and protein transport were the enriched processes.

Diabetes caused a statistically relevant change in 27% of quantified mitochondrial proteins and insulin therapy had an ameliorative effect that, in general, normalized this decrease (Fig. 27C), yellow shading. Consistent with another proteomic study of heart mitochondria (Bugger, Chen et al. 2009), bioinformatic analysis found that proteins associated with canonical pathways of mitochondrial dysfunction and oxidative phosphorylation were over-represented and mainly decreased in expression (Table 5). Representative examples from a diabetic animal show a 51% decrease in the complex 1 protein, NADH dehydrogenase Fe-S protein 3 (NDUFS3) and a 29% decline of Mn superoxide dismutase (Mn-SOD) (Fig. 28A & B). However, insulin therapy improved the deficits in NDUFS3 and Mn-SOD expression (Fig. 28C). This result was consistent with quantitative Western blotting, which showed diminished expression of some components of the mitochondrial electron transport chain. NDUFS3 (component of complex I) and COX IV (component of complex IV) were significantly decreased by 50 and 20%, respectively, whereas levels of ATP synthase subunit β and ERK remained unaltered (Fig. 29).

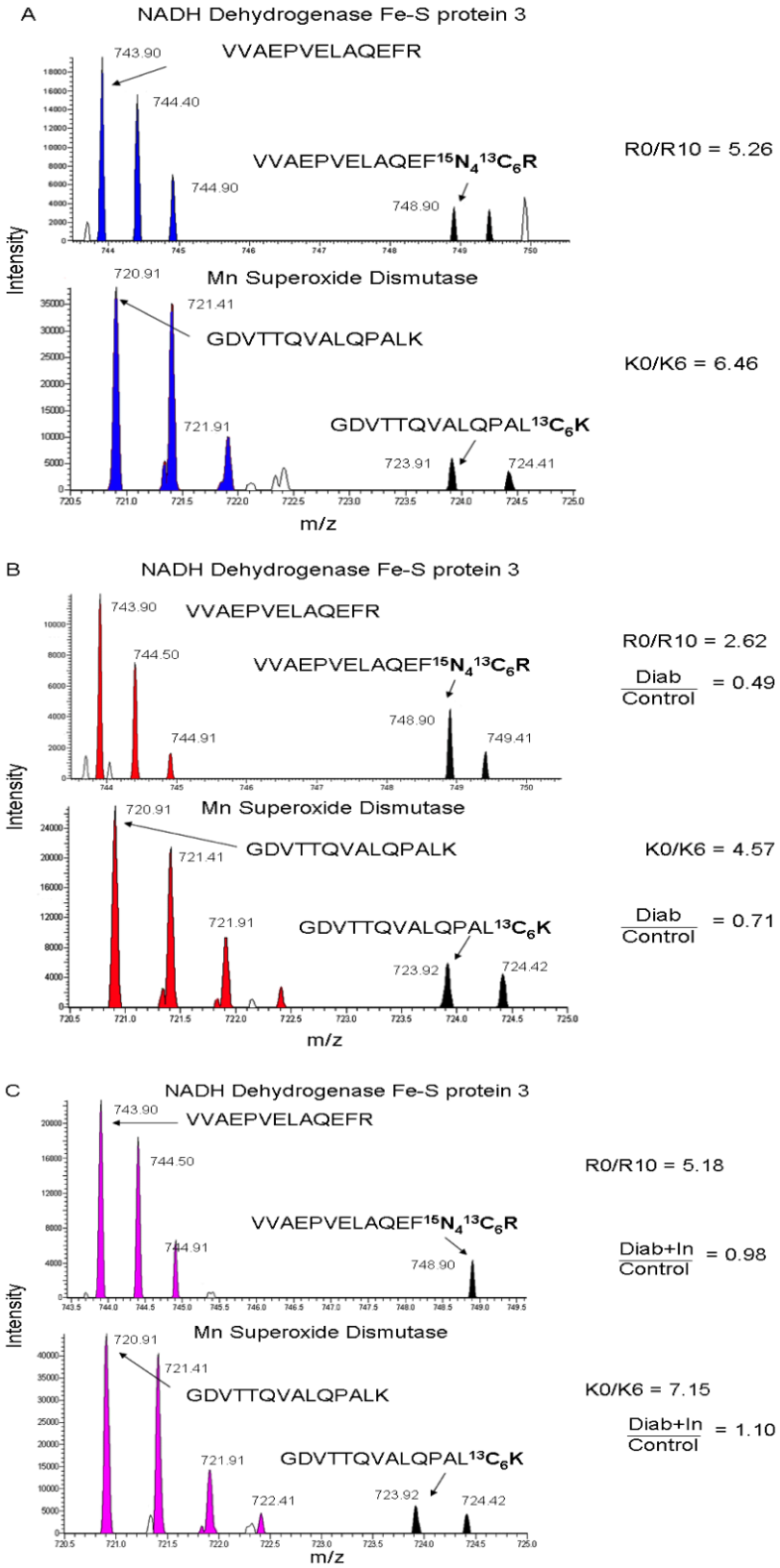
A
NADH Dehydrogenase Fe-S protein 3
743.90
VVAEPVELAQEFR
744.40
VVAEPVELAQEF15N4 13C6R
744.90
748.90
R0/R10 = 5.26
Intensity
720.91
Mn Superoxide Dismutase
721.41
GDVTTQVALQPALK
K0/K6 = 6.46
721.91
GDVTTQVALQPAL13C6K
723.91
724.41
m/z
B
NADH Dehydrogenase Fe-S protein 3
743.90
VVAEPVELAQEFR
R0/R10 = 2.62
744.50
VVAEPVELAQEF15N4 13C6R
Diab / Control = 0.49
748.90
744.91
749.41
Intensity
720.91
Mn Superoxide Dismutase
721.41
GDVTTQVALQPALK
K0/K6 = 4.57
721.91
GDVTTQVALQPAL13C6K
Diab / Control = 0.71
723.92
724.42
m/z
C
NADH Dehydrogenase Fe-S protein 3
743.90
VVAEPVELAQEFR
744.50
R0/R10 = 5.18
VVAEPVELAQEF15N4 13C6R
744.91
Diab+In / Control = 0.98
748.90
Intensity
720.91
Mn Superoxide Dismutase
721.41
GDVTTQVALQPALK
K0/K6 = 7.15
721.91
GDVTTQVALQPAL13C6K
Diab+In / Control = 1.10
722.41
723.92
724.42
m/z

FIG. 28. Representative peptide mass spectra showing the effect of diabetes and insulin therapy on NDUFS3 and MnSOD. *(A)* The upper spectrum shows the doubly charged ion of the unlabeled (m/z 743.90, blue) and R10 labeled (m/z 748.90, black) VVAEPVELAQEFR peptide of NDUFS3 from a control animal. Since the peptide is doubly charged, the mass difference is 5 atomic mass units and the other colored peaks represent the isotopic envelope of the monoisotopic peak. The lower spectrum shows the doubly charged ion of the unlabeled (m/z 720.91, blue) and K6 labeled (m/z 723.91, black) GDVTTQVALQPALK peptide of Mn-SOD from a control animal. Since the peptide is doubly charged, the mass difference is 3 atomic mass units and the other colored peaks represent the isotopic envelope of the monoisotopic peak. The R0/R10 and K0/K6 ratios for these peptides are indicated. *(B)* Upper and lower spectra show the same NDUFS3 and Mn-SOD peptides, but from a diabetic animal. The K0R0/K6R10 ratios for each peptide are indicated and the Diab/Control ratio were obtained after dividing by the control ratios from panel A. *(C)* Upper and lower spectra show the same NDUFS3 and Mn-SOD peptide, but from a diabetic + insulin treated animal. The K0R0/K6R10 ratios for each peptide are indicated and the Diab/Control ratio were obtained after dividing by the control ratios from panel A. Note that the intensity of the K6 and R10 peptides are very similar between the treatments (A - C) indicating that the changes in protein expression are minimally influenced by the internal standard.

Table 5. Effect of diabetes and insulin therapy on representative proteins annotated to oxidative phosphorylation and mitochondrial dysfunction.

		Fold Control		
Symbol	**Protein Description**	**Diabetic**	**Diabetic + Insulin**	**% Change**
ATP5C1	ATP synthase, F1 complex, gamma	0.90	1.29*	143

ATP5D	ATP synthase, F1 complex, delta subunit	0.69*	0.92	133
ATP5F1	ATP synthase, F0 complex, subunit B1	0.92	1.31*	142
ATP5I	ATP synthase, F0 complex, subunit E	0.75*	0.81	108
COX2	cytochrome c oxidase subunit 2	0.82	1.06	129
COX4I1	cytochrome c oxidase subunit IV isoform 1	0.71*	0.89	125
COX5A	cytochrome c oxidase subunit Va	0.83	1.28*	154
CPT1A	carnitine palmitoyltransferase 1A (liver)	0.51*	0.77	172
CYCS	cytochrome c, somatic	0.56*	0.9	160
HSD17B10	hydroxysteroid (17-beta) dehydrogenase 10	0.71*	1.14	160
ND4	NADH dehydrogenase, subunit 4 (complex I)	0.43*	0.56*	130
NDUFA10	NADH dehydrogenase 1 α subcomplex 10	0.73*	0.79	108
NDUFA13	NADH dehydrogenase 1 alpha subcomplex, 13	0.35*	0.59*	168
NDUFB10	NADH dehydrogenase 1 beta subcomplex, 10	0.94	1.4*	148
NDUFS1	NADH dehydrogenase Fe-S protein 1	0.78	0.91	116
NDUFS2	NADH dehydrogenase Fe-S protein 2	0.48*	0.54	113
NDUFS3	NADH dehydrogenase Fe-S protein 3	0.64*	0.84	131
NDUFS8	NADH dehydrogenase Fe-S protein 8	0.91	1.34*	147

PRDX3	peroxiredoxin 3	0.87	1.26*	145
PRDX5	peroxiredoxin 5	0.74*	0.86	116
SOD2	superoxide dismutase 2, mitochondrial	0.73*	1.08	148
UQCRC1	ubiquinol-cytochrome c reductase I	0.87	1.26*	145

Values shown are the mean and the asterisk (*) indicates proteins that showed a significant change in expression. Percent change represents effect of insulin treatment on the protein expression ratio measured from diabetic rats. Please see supplementary Table 1 for more complete information. Confirming (Zherebitskaya, Akude et al. 2009; Chowdhury, Zherebitskaya et al. 2010); confirming (Price, Zeef et al. 2006).

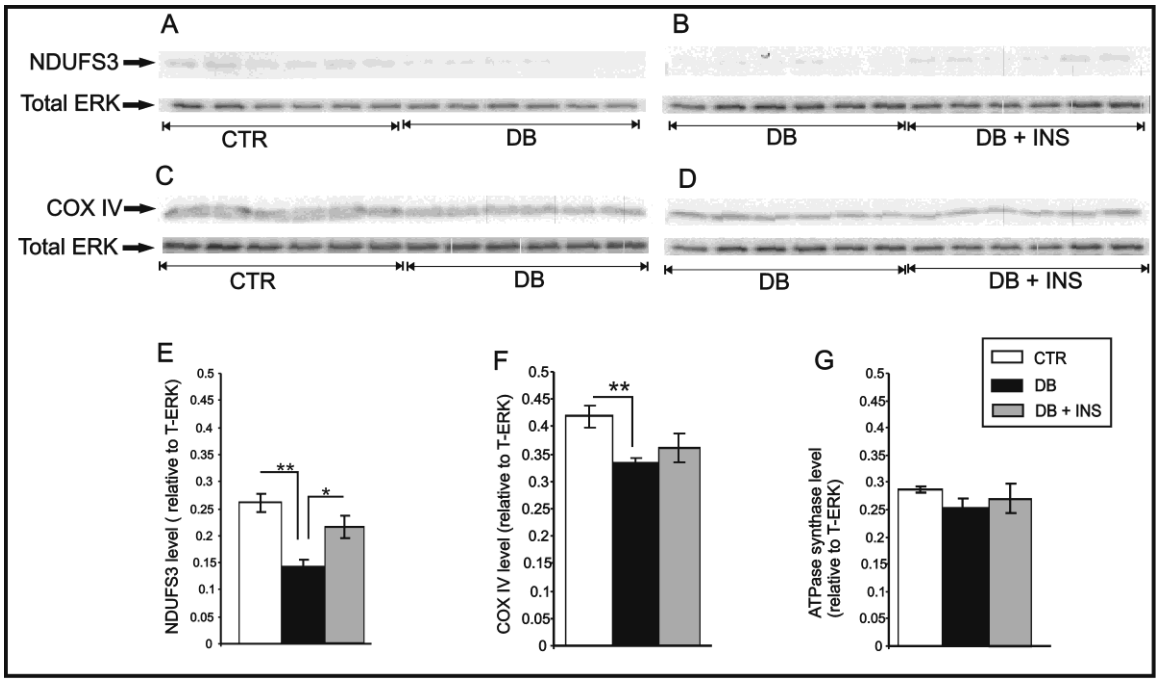

FIG. 29. Expression of components of the electron transport chain are reduced in DRG from STZ-induced diabetic rats. Shown are representative blots *(A–D)* and charts in which NDUFS3 *(E)*, COX IV *(F),* and ATP synthase β subunit signal *(G)* have been presented relative to total ERK level. Values are the means ± SEM, n = 6. **P < 0.005 vs. control (CTR), *P < 0.05 vs. Db + INS (one-way ANOVA with Tukey's post hoc test). Db,diabetic; Db + INS, diabetic with insulin implant.

Lumbar DRG from age-matched control and 22 week STZ-induced diabetic rats were analyzed for rates of oxygen consumption as shown in Fig. 30. Respiratory chain activity, whether coupled or uncoupled, was significantly depressed in diabetic samples. In agreement with the proteomic data and oxygen consumption results, the enzymatic activities of rotenone-sensitive NADH-cytochrome *c* reductase (Complex I) and cytochrome *c* oxidase (COX; Complex IV) as well as the Krebs cycle enzyme, citrate synthase, were significantly decreased in STZ-diabetic rats compared to control (Table 6).

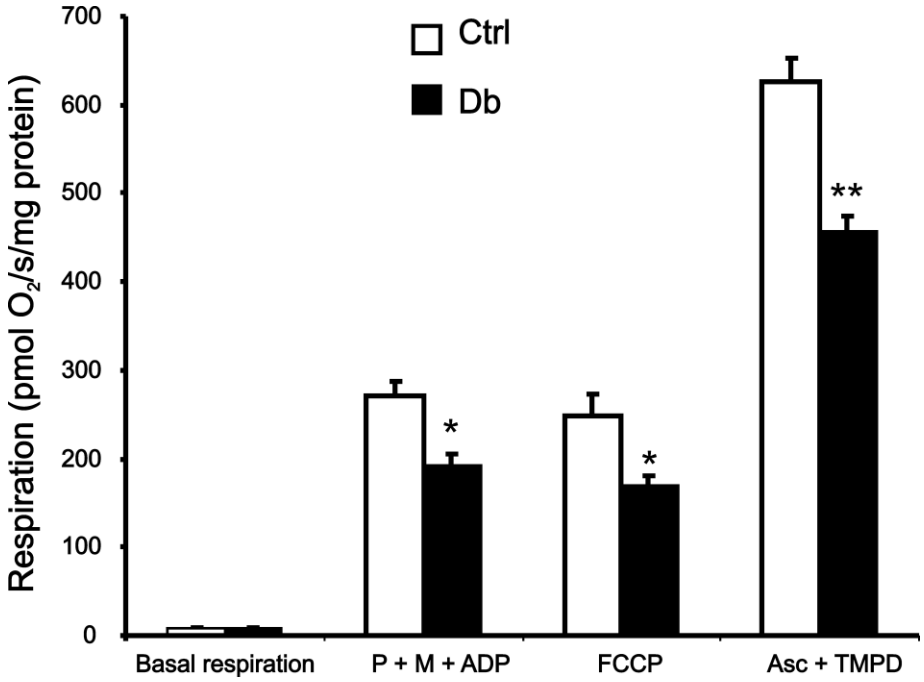

FIG. 30. The mitochondria of DRG sensory neurons exhibited lower respiratory chain activity. Oxygen consumption was assessed in freshly isolated mitochondria from lumbar DRG of age-matched control and 22 week diabetic rats using an OROBOROS oxygraph 2k. Coupled respiration rates were measured in the presence of pyruvate, P (10 mmol/l); malate, M (5.0 mmol/l) and ADP (2.0 mmol/l. Addition of FCCP (0.5 mmol/l) permits a measure of uncoupled

respiratory chain activity. Addition of ascorbate, Asc (5.0 mmol/l) and TMPD (0.5 mmol/l) permit an analysis of complex IV activity that was verified by specific inhibitors. Values are mean ± SEM; n = 5. *p < 0.05 versus controls.

Table 6. Enzymatic activities of mitochondrial respiratory chain complexes and Kreb's cycle enzyme, citrate synthase are decreased in isolated mitochondria from lumbar DRG of STZ-induced diabetic rats.

	Enzymatic activity (nmol/min/mg protein)	
Enzymes	Control	Diabetic
Complex I	182.29 ± 14.67	135.73 ± 21.55 *
Complex IV	1488.32 ± 155.44	1262.66 ± 99.19 *
Citrate synthase	239.94 ± 57.91	164.22 ± 18.86*

Enzymatic activity of complex I was assessed as rotenone-sensitive portion of NADH: cytochrome *c* reductase activity. Complex IV activity was measured at 550 nm following the reduction of oxidized cytochrome *c* and the activity of citrate synthase by following the color of thionitrobezoic acid at 412 nm. Values are means ± SD, n = 4-6. *P<0.05 vs control (Student's *t*–Test).

To determine differences in mitochondrial membrane potential, adult sensory neurons were cultured for 1 day from age matched control and 22 weeks STZ-

induced diabetic rats and loaded with TMRM. This dye was used at a sub-quench concentration where a decrease in fluorescence signal intensity indicated reduced mitochondrial inner membrane potential (Nicholls 2006). The live neurons were exposed to FCCP (uncoupler) or a combination of antimycin A (inhibitor of complex III) and oligomycin (inhibitor of ATP synthase) and the fluorescence signal in axons detected by confocal microscopy. Antimycin A blocks electron transfer leading to mitochondrial depolarization whereas oligomycin inhibits the ATPase and prevents reverse pumping of protons and associated generation of a proton gradient. Therefore, the mitochondrial membrane potential (and associated proton gradient) is completely dissipated in the presence of both these drugs. In the presence of FCCP or antimycin A + oligomycin, the rate of mitochondrial depolarization was more rapid in axons of normal neurons compared with diabetic neurons (Figs. 31 & 33). This suggests that prior to addition of antimycin A + oligomycin, the axonal mitochondria were more highly polarized in the normal neurons compared with the diabetic neurons. Nicholls and colleagues have demonstrated in cerebellar granular cells that low micromolar concentrations of FCCP causes depolarization of plasma membrane (Nicholls 2006). To ensure that changes in TMRM fluorescence observed after adding FCCP was a result of mitochondrial depolarization in our DRG culture, DRG neurons were stained simultaneously with PMPI and TMRM dyes. FCCP was injected into the culture media to final concentration of 2μM and changes in fluorescence signal assessed. FCCP caused a rapid decrease in TMRM fluorescence while having no significant effect on the PMPI fluorescence level

(Fig. 32A - C). Also, neurons were treated with 30mM KCl (depolarizes the plasma membrane). KCl was observed to induce a rapid increase in PMPI fluorescence level (Figs. 32D & E).

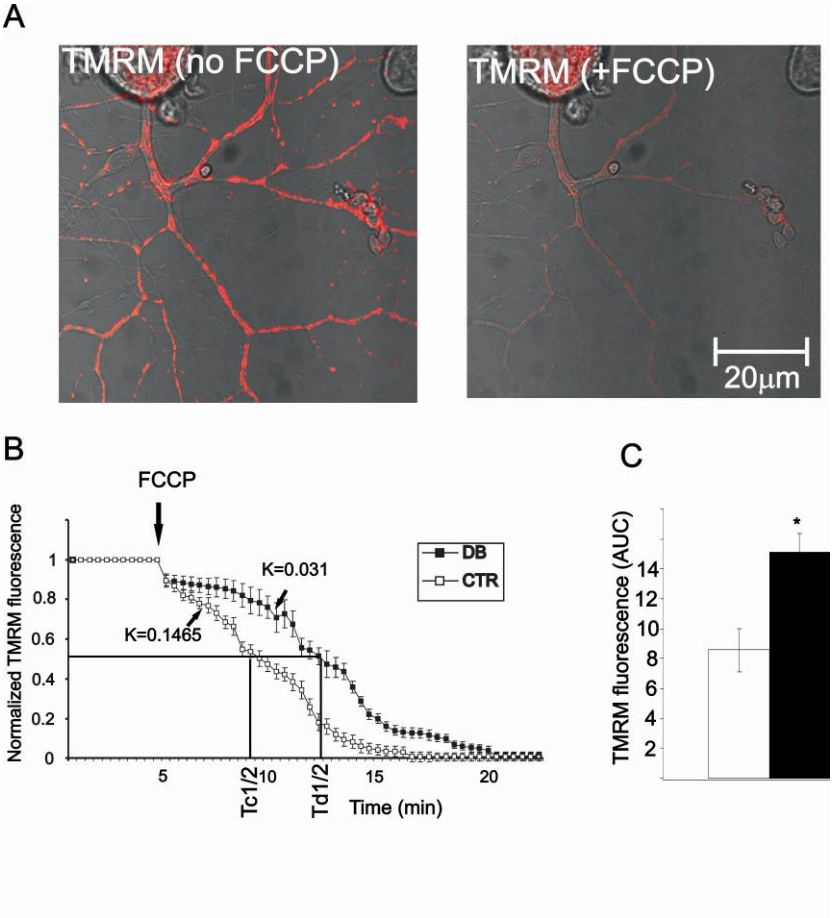

Fig. 31. The mitochondria in the axons of normal neurons show greater levels of FCCP-induced depolarization compared with neurons from diabetic rats. (*A)* Fluorescence video confocal microscopy of mitochondria in live cultures of DRG neurons isolated from adult age-matched or 3-5 month STZ-induced diabetic rats. *(B)* Quantification of TMRM fluorescence signal in the axons of cultured DRG neurons. The TMRM trace was characterized by non-linear regression (one phase exponential decay). Values are means ± SE, n= 50-65 axons, the rate constant of decay (K) = 0.1465 ± 0.0005 (control) and 0.031± 0.0006 (diabetic). Half-life of decay for control ($Tc_{1/2}$) =

4.73 min and diabetic ($Td_{1/2}$)= 12.5 min. The F (Fisher parameter)-ratio = 346.7, P < 0.0001, control vs diabetic. The F-ratio compares the goodness-of-fit of the two curves. *(C)* Shows the area under the TMRM fluorescence curve, the AUC was estimated from the baseline (at the point of injection) to a fluorescence level of 0.0 and between time points of 5.0 min and 20.0 min using sums-of-squares, P<0.001, t-test. The black arrow indicates point of injection of FCCP.

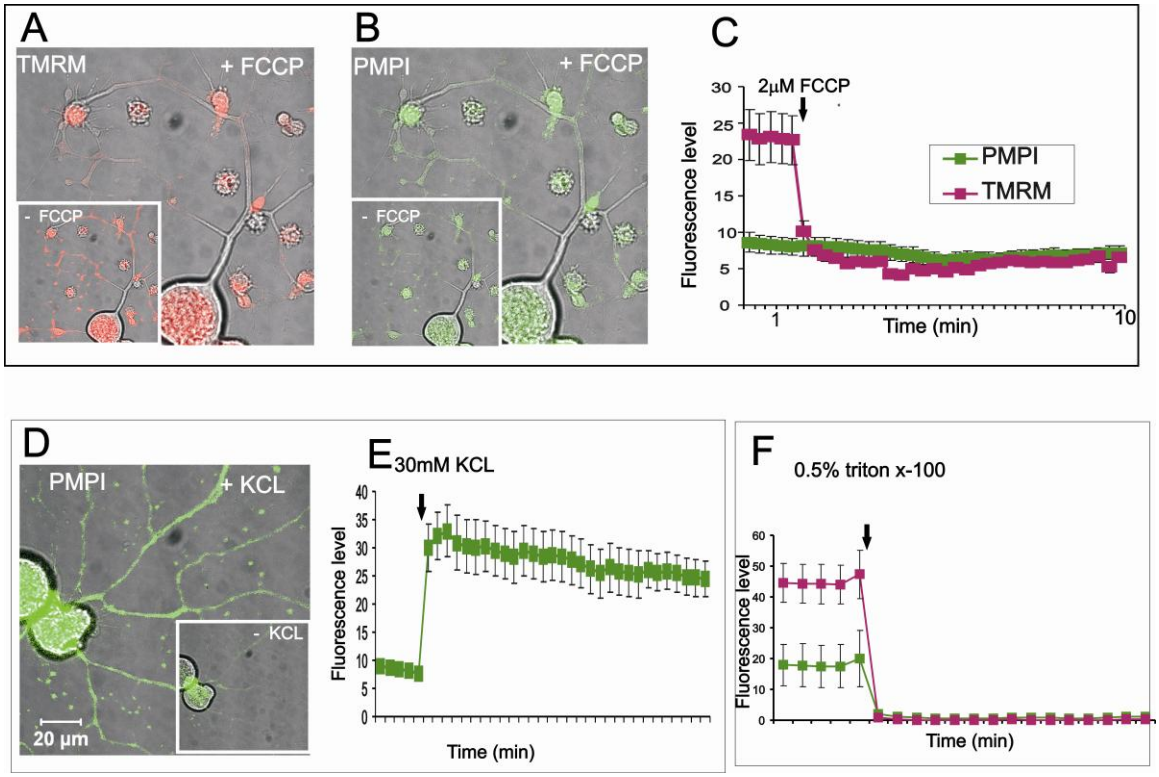

Fig. 32. Low micromolar concentrations of FCCP do not affect the plasma membrane potential in cultured DRG neurons. *(A)* Fluorescence images of TMRM, *(B)* PMPI in cultured DRG neurons isolated from control adult rats showing effect of FCCP. *(C)* Trace of TMRM and PMPI fluorescence following FCCP injection. *(D)* Fluorescence image of PMPI showing the effect of KCl. *(E)* Trace of PMPI fluorescence following KCl injection. *(F)* Fluorescence trace of TMRM and PMPI showing the effect of triton-X100. Inserts show fluorescence levels at baseline.

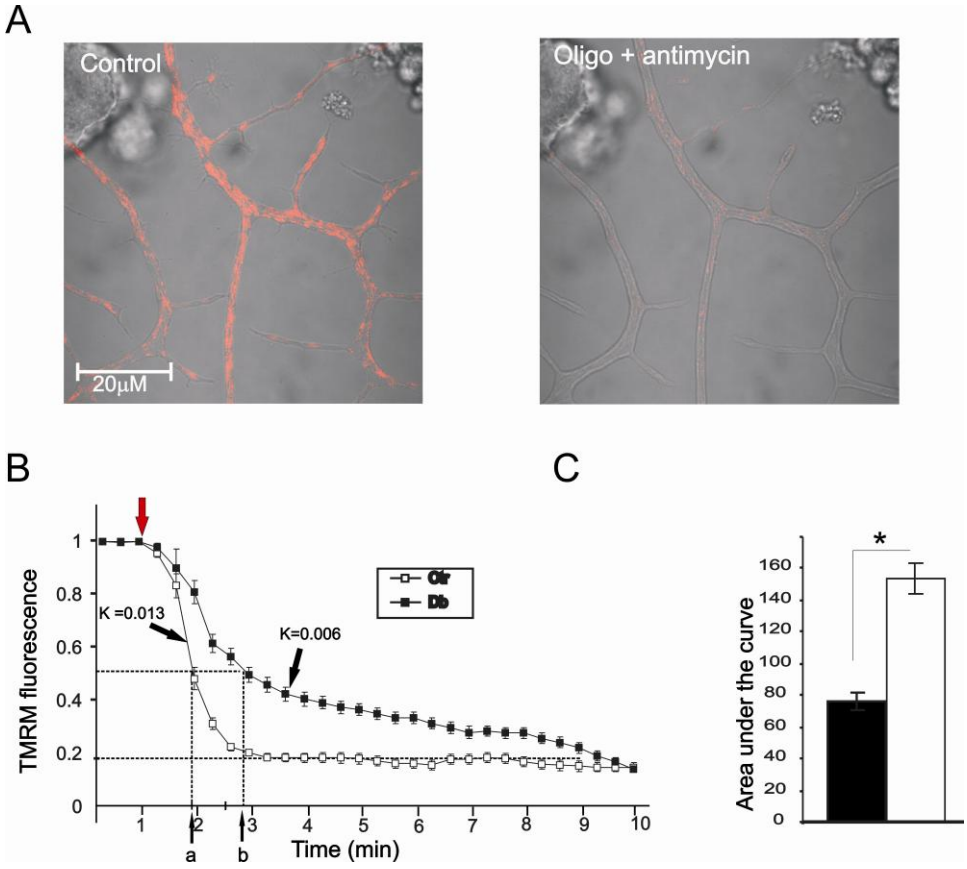

Fig. 33. The mitochondria in the axons of normal neurons show greater levels of antimycin A and oligomycin-induced depolarization compared with neurons from diabetic rats. *(A)* Images of fluorescence confocal microscopy using TMRM in live cultures of DRG neurons isolated from control adult rats showing effect of antimycin A and oligomycin. *(B)* Trace of TMRM fluorescence signal in the axons of cultured DRG neurons isolated from age matched controls and STZ-diabetic rats. *(C)* Shows the area under the TMRM fluorescence trace (AUC) for control (open bar) and diabetic (filled bar) neurons. The AUC was estimated from the baseline (at the point of injection) to a fluorescence level of 0.2 and between time points of 1.0 min and 6 min using sums-of-squares (shown by dotted line). Values are the means ± SEM, n = 65–80 axons; * $p < 0.001$ compared to control, t-test. The TMRM trace was characterized by non-linear regression (one phase exponential decay). The rate constant of decay (K) = 0.013 ± 0.0004 (control) and 0.006 ± 0.0001 (diabetic). Half-life of decay = 54.19 s (control) and 108.7 s (diabetic). The F (Fisher

parametric)-ratio = 409.5, P < 0.0001, control vs diabetic. The F-ratio compares the goodness-of-fit of the two curves. The red arrow indicates point of injection of antimycin A + oligomycin.

Mitochondrial physiology was further investigated by treating cultured neurons from control and diabetic rats with oligomycin alone. Blockade of the ATPase results in a build-up of the transmembrane proton gradient and induces hyperpolarization of the mitochondrial inner membrane as indicated by elevated TMRM fluorescence (Fig. 34) (Jekabsons and Nicholls 2004). In normal neurons a transient hyperpolarization was observed followed by a recovery due to adaption of the respiratory chain. For example, uncoupling proteins become active and dissipate the proton gradient under a high inner membrane potential (Azzu, Parker et al. 2008). Diabetic neurons exhibited a significantly greater level of hyperpolarization upon oligomycin application and the adaptive response was impaired (Fig. 34).

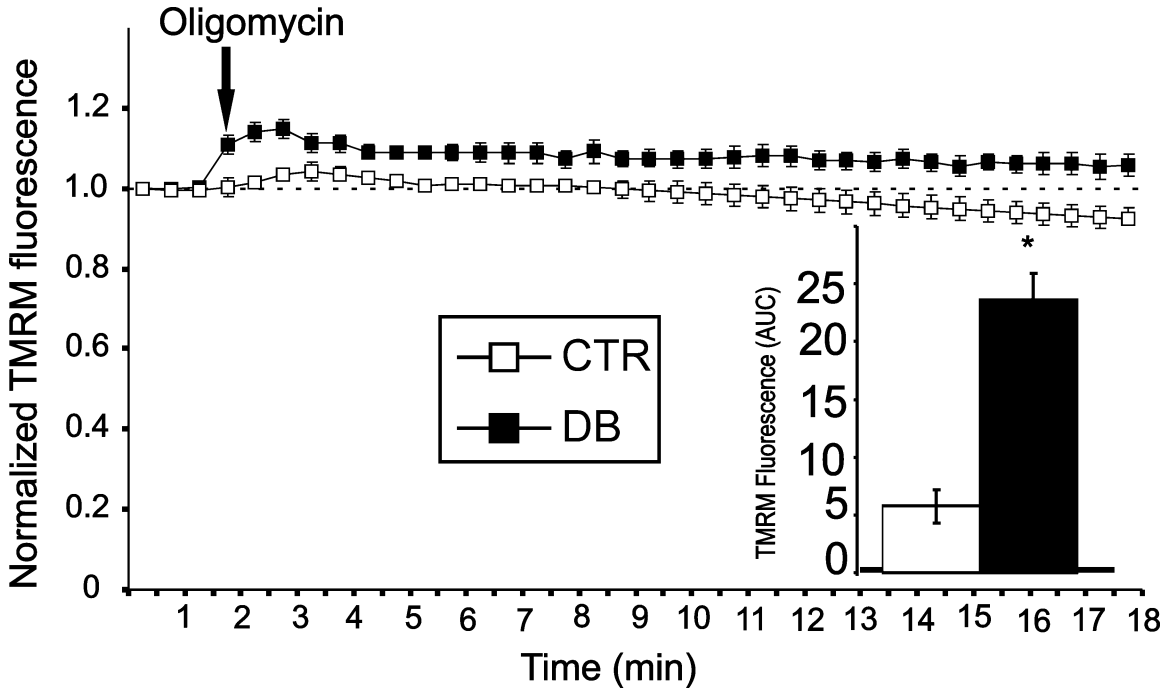

Fig. 34. Oligomycin induces greater hyperpolarization levels in the axons of STZ diabetic neurons compared with controls. TMRM fluorescence trace showing the effect of oligomycin is shown. TMRM fluorescence trace was characterized by one-exponential association. The rate constant /slope, (K) = 0.057± 0.012 (control) and 0.039 ± 0.007 (diabetic). The F (Fisher parameter)-ratio = 23.83, $P < 0.0001$, control vs diabetic. Inset shows the area under the TMRM fluorescence trace (AUC) for control (open bar) and diabetic (filled bar) neurons. The AUC was estimated from the baseline (at the point of injection, and between time points of 1.0 min and 4 min using sums-of-squares). Values are the means ± SEM, n = 65–80 axons,* $P < 0.01$ compared to control, t-Test. The black arrow indicates point of injection of oligomycin.

We determined if the respiratory chain was contributing to oxidative stress in diabetic neurons by loading cells with the mitochondrially-targeted ROS detector, MitoSOX red. A subset of diabetic neurons was pre-treated with oligomycin to hyperpolarize the inner mitochondrial membrane and maximize loading of MitoSOX red into the mitochondrial matrix. Neurons were treated with the uncoupler, carbonylcyanide-p-trifluoromethoxyphenylhydrazone (FCCP), to

dissipate the transmembrane electrochemical gradient and enhance the rate of electron transfer. Increased respiratory chain activity will lead to augmented electron leakage and associated generation of ROS, primarily superoxide. In normal neurons this was demonstrated with elevated FCCP-induced MitoSOX red fluorescence (Fig. 35E and F). Diabetic neurons, with or without prior oligomycin treatment, exhibited lower MitoSOX red fluorescence intensities indicative of reduced levels of superoxide being generated by the respiratory chain.

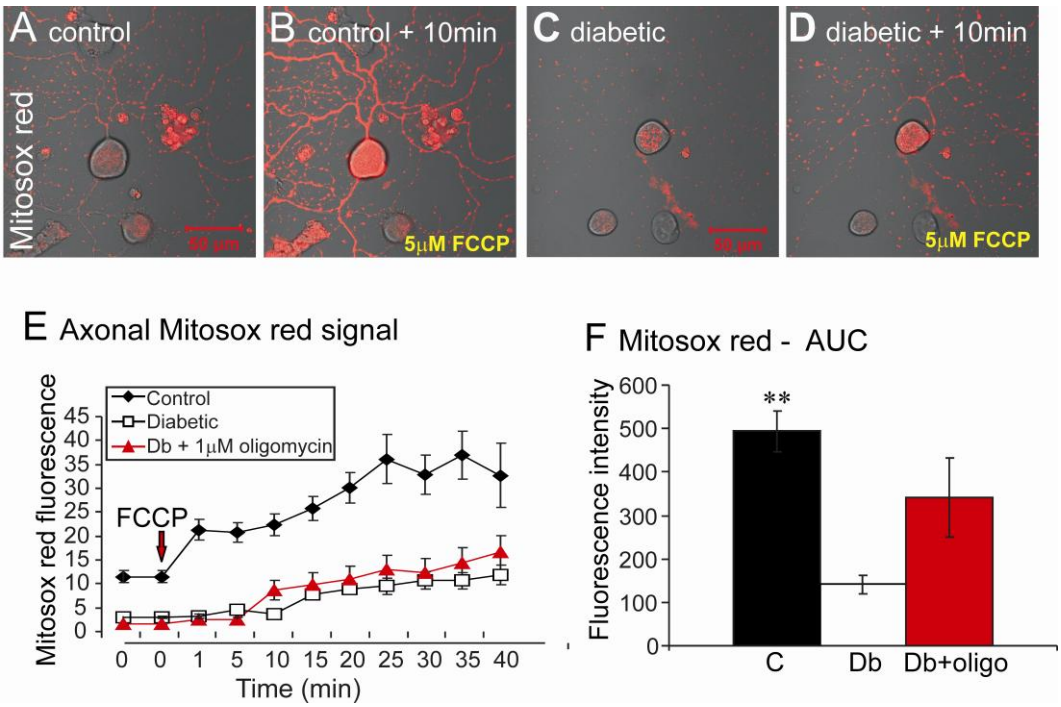

Fig. 35. Impaired respiratory function is associated with reduced ROS generation in the mitochondrial matrix of cultured neurons isolated from STZ-diabetic rats. . *(A-D)* Images of MitoSOX red fluorescence in cultures of DRG neurons showing effect of 5.0 μmol/l FCCP.

(E) Quantification of real-time MitoSOX red fluorescence levels in the axons of cultured DRG neurons after 5.0 μmol/l FCCP treatment. MitoSOX trace was characterized by non-linear regression. F-ratio = 32.48, $P < 0.0001$ (control vs. diabetic with or without oligomycin by oneway ANOVA). Values are the mean ± SEM, n= 18-73 axons. *(F)* Shows area under the curve for Mitosox red fluorescence intensity levels. Values are the mean ± SEM, n=35-73 axons; ** $P < 0.001$ compared to diabetic or diabetic + oligomycin treated cells by oneway ANOVA.

4.5. Discussion

The results show that respiratory chain components of the mitochondrial proteome are down regulated in DRG in diabetes and this phenotypic alteration was associated with impairment in respiratory chain activity. In addition, for the first time this study demonstrates that altered mitochondrial proteome expression was linked to altered mitochondrial physiology in axons of diabetic neurons.

We used SILAC to provide a set of culture-derived isotope tags (Ishihama, Sato et al. 2005) to serve as internal standards for quantifying the effect of diabetes on the composition of the mitochondrial proteome from DRG. One advantage of culture-derived isotope tags is the quantitative accuracy that can be achieved relative to label-free approaches (Geiger, Cox et al. 2010), especially for low abundant proteins. Despite our small sample size, a 25% change in expression was sufficient to reach statistical significance and the number of mitochondrial proteins that exceeded this threshold was similar to that previously reported in mitochondria isolated from heart tissue of diabetic Akita mice (Bugger, Chen et al. 2009). Further, the results of our unbiased quantification were in close agreement with those obtained by targeted immunoblot analyses for COX subunit IV, NDUFS3, ATP synthase and Mn-SOD in two prior studies (Zherebitskaya, Akude et al. 2009; Chowdhury, Zherebitskaya et al. 2010). Similar to a previous gene array study delineating alterations in mRNA expression in DRG from diabetic rats (Price, Zeef et al. 2006), the magnitude of changes observed in the mitochondrial proteins were rather modest and averaged 0.44 ± 0.16 fold in either direction. Interestingly, the gene array study

reported that after 2 months of diabetes, no modification occurred in gene expression of enzymes associated with the tricarboxylic acid (TCA) cycle. We also observed no changes in pyruvate dehydrogenase and 6 of 8 of the TCA cycle enzymes at the protein level, the exception being fumarate hydratase and succinyl Co-A ligase. Similarly, with the exception of hexokinase 1, the remaining glycolytic enzymes that were quantifiable did not alter in agreement with mRNA expression studies at 2 months of diabetes (Price, Zeef et al. 2006). We have previously reported that hexokinase 1 localizes to mitochondria of DRG (Gardiner, Wang et al. 2007) and this protein was reproducibly detected in the heavy mitochondrial fraction of all animals. Interestingly, although hexokinase gene and protein expression were not modified after 2-3 months of diabetes (Price, Zeef et al. 2006; Gardiner, Wang et al. 2007), expression was decreased after 22 weeks of diabetes in the present study. Since this was the only glycolytic enzyme that significantly changed, it is tempting to speculate that its lowered expression also has a function separate from glucose metabolism. In this regard, sensory neurons from diabetic adult animals have an impaired ability to support neurite development (Zherebitskaya, Akude et al. 2009) and directly inhibiting hexokinase activity blocks neurotrophin-induced neuritogenesis (Wang, Gardiner et al. 2008). In the cardiac system diminished mitochondrial respiratory function caused by diabetes has also been identified by proteomic and gene array techniques (Bugger and Abel 2008; Bugger, Chen et al. 2009). These broad changes in gene expression could be triggered by altered activity of key upstream regulators. For example, in human skeletal muscle in type 2 diabetes

the transcriptional regulator NRF-1 and the transcriptional co-activator peroxisome proliferator-activated receptor-gamma coactivator 1 α (PGC-1α) were down-regulated and corresponded with reduced expression of proteins that regulate cellular energy metabolism, including mitochondrial biogenesis and oxidative phosphorylation (Mootha, Lindgren et al. 2003; Patti, Butte et al. 2003). In fact, our preliminary data demonstrates a significant reduction in activity of AMP kinase, a regulator of PGC1-α, in DRG in type 1 diabetic rodents (Fig 36).

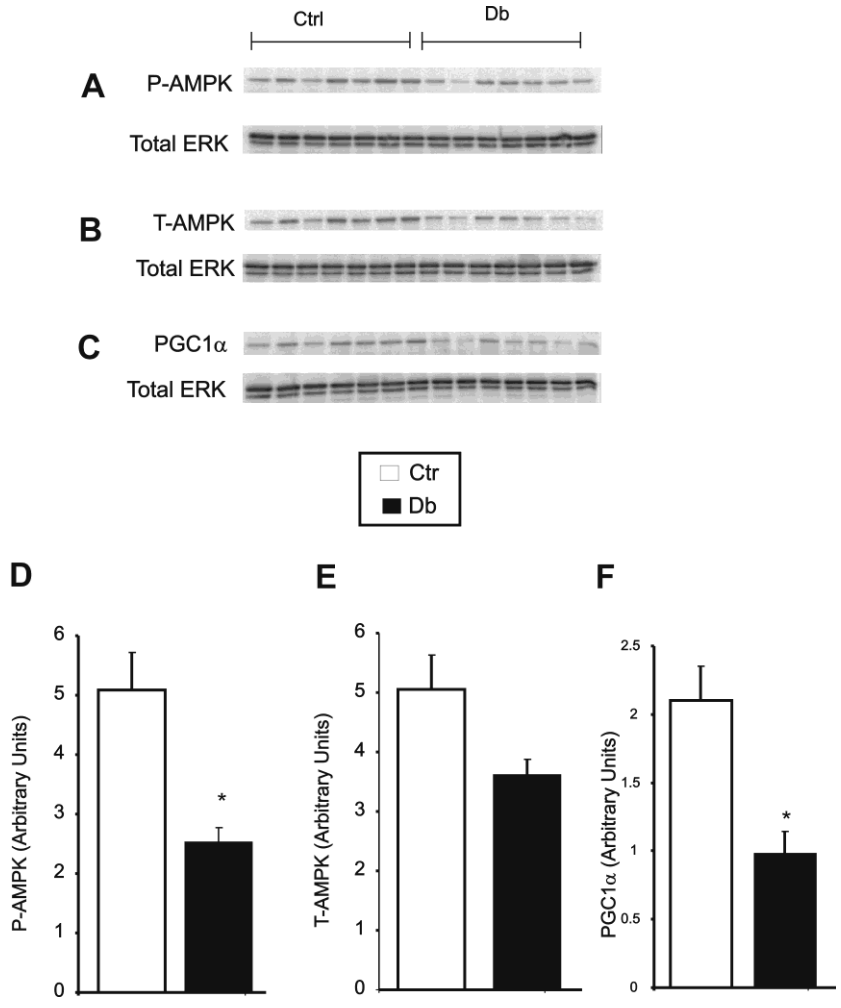

Fig. 36. Expression of some proteins that regulate cellular energy metabolism is reduced in DRG from STZ-induced diabetic rats. Shown are representative blots *(A–C)* and charts in which P-

AMPK *(D),* T-AMPK (E), and PGC1α (F) have been presented relative to total ERK level. Values are the means $\pm$ SEM, n = 6. **P < 0.05 vs diabetic.

Initial exposure to high glucose concentration over 1-4 weeks in DRG in diabetic rats is linked to up-regulation of glycolytic pathway expression (mRNA) (Price, Zeef et al. 2006). Studies in endothelial or Schwann cells demonstrate that acute exposure to glucose elevates ROS and respiratory chain activity, respectively (Nishikawa, Edelstein et al. 2000; Zhang, Yu et al. 2010). Therefore, in the short term hyperglycemia triggers enhanced glycolysis and associated respiratory chain activity (and possibly ROS). However, in the longer term the high intracellular glucose concentration provides an ample supply of ATP via several non-mitochondrial dependent pathways. Consequently, the metabolic phenotype of the cell adapts and functions in the absence of a dependence on the TCA cycle and oxidative phosphorylation for ATP production, possibly by initiating a process homologous to the 'Crabtree effect' (Ibsen 1961). Thus, rates of electron donation to the respiratory chain are sub-optimal in neurons in long term diabetic rats and may predispose to lower rates of mitochondrial respiratory chain activity and oxidative phosphorylation. Key metabolic activity sensors and/or regulators such as AMPK and NRF-1 are putative candidates for this modulation, although it is unlikely subsequent adapted metabolism of glucose is channeled through glycolysis in isolation. In this regard, elevated glucose flux through the aldehyde and aldose reductase pathway could be critical (Oates 2008; Ido, Nyengaard et al. 2010). For example, studies in lens (Obrosova, Faller et al. 1997), retina (Ola, Berkich et al. 2006) and cardiac tissue (Trueblood and

Ramasamy 1998) in medium to long term animal models of type 1 diabetes show that parts of glycolytic pathway function are depressed.

ROS production linked to enhanced electron leakage from the respiratory chain induced by uncoupling, and theoretically comprising superoxide, was lower in the axons of neurons from diabetic rats (Fig.35 A-D) confirming our mitochondrial physiology and proteomics work. The studies in Fig. 35 provide preliminary evidence that the sources of ROS in axons of diabetic neurons are not from aberrant respiratory chain function. Down-regulation of the respiratory chain machinery would be predicted to lead to depolarization of the mitochondrial membrane (Figs. 31 and 33), reduced rates of respiratory chain activity (Chowdhury, Zherebitskaya et al. 2010) (Fig. 30) and associated diminished electron leakage. The lower rate of loss of polarization status subsequent to uncoupling in Figs. 31 and 33 was not the result of resistance to uncoupling in the diabetic neurons since complementary measures of respiratory chain activity show lower rates of electron transfer in diabetic neurons (and see Figure 1 in (Chowdhury, Zherebitskaya et al. 2010)). These findings differ from those in cultured endothelial cells where high glucose concentration enhanced mitochondrial membrane potential and induced elevated ROS (Du, Edelstein et al. 2000; Nishikawa, Edelstein et al. 2000). Fig.34 reveals oligomycin treatment caused a greater level of mitochondrial inner membrane hyperpolarization above baseline in diabetic neurons compared with normal neurons further highlighting that adult sensory neurons with a history of diabetes and under high glucose concentration behave differently to endothelial cells. The adaption of

mitochondria in normal neurons to hyperpolarization was not observed in diabetic neurons, again stressing the aberrant phenotype of mitochondrial physiology. Uncoupling proteins such as adenine nucleotide transporters (ANT1/2) contribute to the dissipation of a high mitochondrial membrane potential (Azzu, Parker et al. 2008) and expression was depressed in diabetic mitochondria.

4.6. Conclusion

In conclusion, our proteomics data reveal a range of altered expression profiles in the mitochondrial proteome of DRG from diabetic rats. This modified expression pattern was associated with aberrant mitochondrial respiratory chain physiology and function. Under high glucose concentration the neuron cell body perceives that mitochondrial function can be downgraded, however, this may ignore the unique high energy requirements of the nerve ending and contribute to distal axon degeneration. For example, growth cone motility that underpins axonal plasticity and regeneration in the skin has an exceedingly high demand for ATP due to significant levels of actin treadmilling (Bernstein and Bamburg 2003). Impaired respiratory chain function did not elevate ROS generation even though oxidative stress was observed in axons. In fact, the lower rates of respiratory chain activity were linked to mitochondrial membrane depolarization, improper adaption to oligomycin-induced membrane hyperpolarization and reduced levels of superoxide derived from electron leakage during electron transport. In axons of neurons from long term diabetic rats sites of ROS production colocalize with the mitochondrial compartment (Zherebitskaya, Akude et al. 2009; Akude, Zherebitskaya et al. 2010). Therefore, alternative

mitochondrial-related sources of ROS should be considered. For example, NOX has been localized to the mitochondrial compartment of kidney cortex and mesanglial cells and mediates elevated ROS under high glucose concentration (Block, Gorin et al. 2009).

Chapter 5:

CNTF or Resveratrol Reverses Abnormalities in Mitochondrial Membrane Potential in Cultured DRG Neurons Isolated from STZ-induced Diabetic Rats

5.1. Introduction

There is evidence to suggest that mitochondria are dysfunctional under diabetic conditions (Fernyhough, Roy Chowdhury et al. 2010). Mitochondrial depolarization has been demonstrated in cultured STZ-induced diabetic rats, and this was corrected by systemic treatment with low dose insulin (Huang, Price et al. 2003). This sub-optimal functioning of the mitochondria could be critical in the process of nerve degeneration associated with neuropathy (Baloh 2008). Understanding the mechanisms involved in this process could reveal new therapeutic targets for the treatment of neuropathy.

Several agents are being studied as possible therapeutics for this condition. These include cytokines and resveratrol. CNTF is a 22-kDa cytokine member of the structurally related interleukin-6 (IL-6) family of related cytokines, which also includes leukemia inhibitory factor (LIF) (Calcutt, Jolivalt et al. 2008). It binds to the CNTFRα that is attached to the membrane surface via a glycosyl-

phosphotidyl inositol (Sleeman, Anderson et al. 2000).It is very similar to leptin in structure and function (Minokoshi, Kim et al. 2002). Resveratrol is an AMP kinase activator (Reznick and Shulman 2006) and it has been shown to induce mitochondrial biogenesis through the activation of peroxisome proliferator-activated receptor- coactivator (PGC)-1α, a member of a family of transcriptional coactivators that play a central role in the regulation of cellular energy metabolism (Liang and Ward 2006).

5.2. Rationale

In this chapter, we explored the ability of CNTF or resveratrol to reverse abnormalities in axonal mitochondrial membrane potential under diabetic conditions. Diabetic neurons were treated with / without CNTF or resveratrol, and the relative changes in the mitochondrial membrane potential assessed (as described in Chapter 4). Also, the ability of CNTF to reverse abnormalities in mitochondrial membrane potential induced by 4-HNE in DRG neurons isolated from normal rats was investigated. Previous studies in our lab have demonstrated that oxidative stress occurs in the axons of neurons isolated from STZ-induced diabetic rats (Zherebitskaya, Akude et al. 2009). The elevation of ROS (a consequence of oxidative stress) has also been shown to be associated with an increase in the lipid peroxidation product 4-HNE (Zherebitskaya, Akude et al. 2009). 4-HNE is a highly reactive compound, which has been demonstrated, to form adducts with several proteins thereby modifying their structure and function (Uchida 2003). Indeed our previous work has demonstrated the formation of adducts of 4-HNE on mitochondrial proteins under

diabetic conditions (Akude, Zherebitskaya et al. 2010), and this confirms work by other groups which demonstrated the formation of adducts on some proteins in the electron transport chain (Lashin, Szweda et al. 2006). Since the mitochondria are believed to be the primary source of ROS production (Brownlee 2001), it is logical to believe that mitochondrial proteins might particularly be susceptible to the deleterious effect of oxidative stress and its associated lipid peroxidation product. Proteomics studies performed on mitochondria isolated from diabetic DRG in chapter 4 showed the reduction in several mitochondrial proteins including proteins in the electron transport chain. One of the key pathways for the biogenesis of proteins in the electron transport chain involves the activation of AMP kinase, which in turn regulates other downstream factors such as PGC-1α. Since CNTF and resveratrol have exhibited the potential to correct some abnormalities associated with neuropathy, and coupled with the fact that CNTF and resveratrol exert some of their effects through the activation of AMP kinase (Watt, Dzamko et al. 2006) (Reznick and Shulman 2006), we propose that CNTF and/or resveratrol will reverse abnormalities in the mitochondrial membrane potential in diabetic neurons via an increase in biogenesis of proteins in the electron transport chain and oxidative phosphorylation.

5.3. Aim / objectives

- Investigate the ability of CNTF or resveratrol to reverse mitochondrial depolarization in axons of cultured DRG neurons isolated from STZ-induced diabetic rats.

- To investigate the association between elevated levels of 4-HNE and the reduction in mitochondrial membrane potential in the axons of DRG neurons
- To reverse 4-HNE induced mitochondrial depolarization in cultured DRG neurons using CNTF.

Approach

Mitochondrial membrane potential will be assessed by measuring the changes in rate of depolarization induced by a combination of antimycin A and oligomycin, and the differences in the level of hyperpolarization induced by oligomycin.

5.4. Results

To determine whether CNTF or resveratrol were capable of reversing abnormalities in mitochondrial membrane potential in diabetic neurons, adult sensory neurons were cultured for 1 day from age matched control and 3-5 months STZ-induced diabetic rats. During this period diabetic neurons were treated with/without drug (CNTF, 10 ng/ml and resveratrol, 1μM). After 24 hr the cells were loaded with TMRM and mitochondrial physiology assessed. The live neurons were exposed to a combination of antimycin A (inhibitor of complex III) and oligomycin (inhibitor of ATP synthase) and the fluorescence signal in axons detected by confocal microscopy. The rate of depolarization induced by antimycin A + oligomycin in the axons of diabetic neuron treated with CNTF or resveratrol was more rapid compared with diabetic neurons with no treatment

(Figs. 37 and 39). The rate of depolarization in CNTF or resveratrol treated neurons was comparable to that of normal neurons (Figs. 37 and 39). These findings indicate that CNTF or resveratrol induced the reversal of the lowered state of membrane polarization in diabetic neurons.

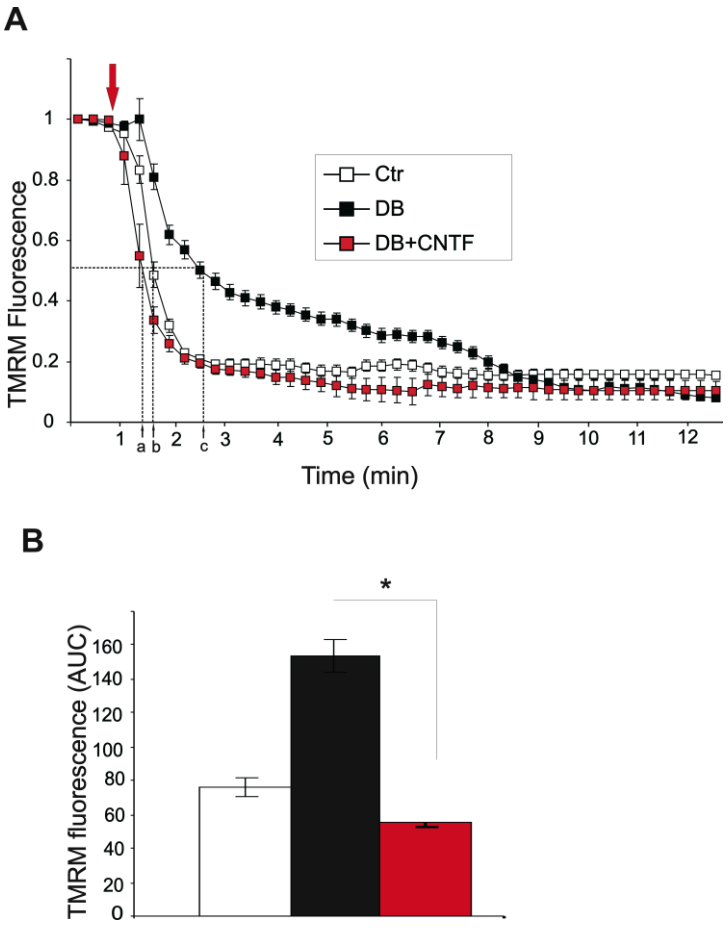

Fig. 37. CNTF normalizes abnormalities in the rate of depolarization in the axons of diabetic neurons. *(A)* Trace of TMRM fluorescence signal in the axons of cultured DRG neurons isolated from age matched controls and STZ-diabetic rats (with or without CNTF). *(B)* Shows the area under the TMRM fluorescence trace (AUC) for control (open bar), diabetic (black bar) and diabetic with CNTF (red bar). The TMRM trace was characterized by non-linear regression (one

phase exponential decay). The rate constant of decay (K) = 0.01217 ± 0.0006 (control), 0.0054 ± 0.0001 (diabetic) and .01516± .0008. Half-life of decay = 33 s (control), 96s (diabetic) and 25s (diabetic + CNTF). The F (Fisher parameter)-ratio = 319.2, P < 0.0001, diabetic vs diabetic + CNTF. The AUC was estimated from the baseline (at the point of injection) to a fluorescence level of 0.1 and between time points of 1.0 min and 9 min using sums-of-squares. Values are the means ± SEM, n = 45–65 axons; * p < 0.001 diabetic vs diabetic + CNTF, t-test. The red arrow indicates point of injection of antimycin A + oligomycin.

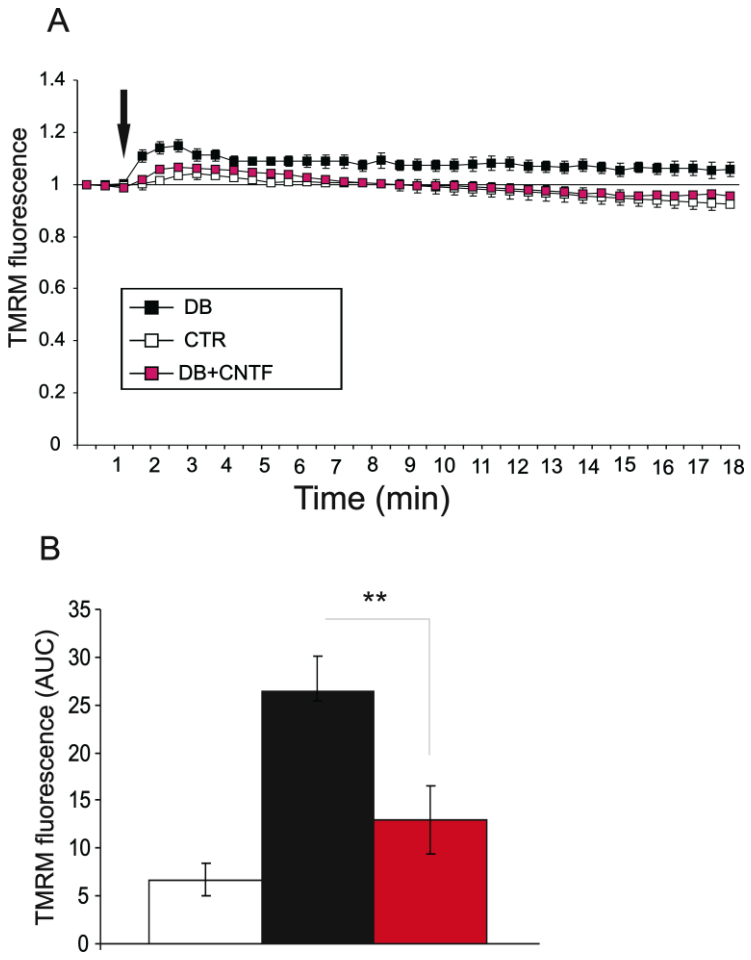

Fig. 38. CNTF normalizes abnormal levels of hyperpolarization induced by oligomycin in the axons of STZ diabetic neurons. *(A)* TMRM fluorescence trace showing the effect of oligomycin is shown. TMRM fluorescence trace was characterized by one-exponential association. The rate constant /slope, (K) = 0.057± 0.012 (control), 0.039 ± 0.007 (diabetic) and 0.050 ± 0.008 (diabetic

+ CNTF) . The F (Fisher parameter)-ratio = 23.83, P < 0.0001, control vs diabetic. *(B)* Shows the area under the TMRM fluorescence trace (AUC) for control (open bar) and diabetic (filled bar) neurons. The AUC was estimated from the baseline (at the point of injection, and between time points of 1.0 min and 6 min using sums-of-squares. Values are the means ± SEM, n = 44–53 axons,** P < 0.01 compared to control, t-Test. The black arrow indicates point of injection of oligomycin.

Reversal of abnormal mitochondrial physiology by CNTF or resveratrol was further investigated by hyperpolarizing the mitochondrial membrane in cultured neurons from control and diabetic rats with oligomycin alone. In normal neurons a transient hyperpolarization was observed followed by a recovery due to adaption of the respiratory chain. Diabetic neurons exhibited a significantly greater level of hyperpolarization upon oligomycin application and the adaptive response was impaired. However, upon treating diabetic neurons with CNTF or resveratrol, the level of oligomycin induced hyperpolarization was marginal and this was followed by a recovery to baseline levels, similar to that observed in control neurons (Figs. 38 and 40).

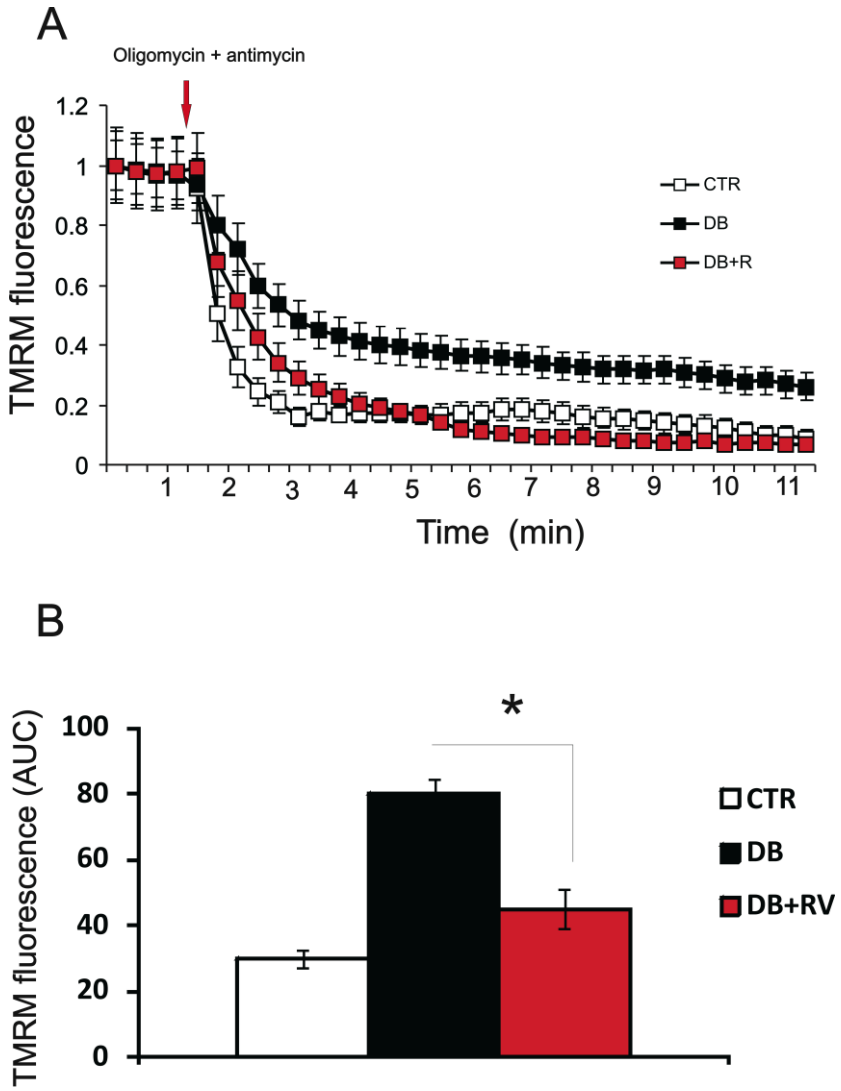

Fig. 39. Resveratrol normalizes abnormalities in the rate of depolarization in the axons of diabetic neurons. *(A)* Trace of TMRM fluorescence signal in the axons of cultured DRG neurons isolated from age matched controls and STZ-diabetic rats (with or without resveratrol). *(B)* Shows the area under the TMRM fluorescence trace (AUC) for control (open bar), diabetic (black bar) and diabetic with resveratrol (red bar). The TMRM trace was characterized by non-linear regression (one phase exponential decay). The rate constant of decay (K) = 0.01217 ± 0.0006 (control), 0.0054 ± 0.0001 (diabetic) and .01516± .0008. Half-life of decay = 33 s (control), 96s (diabetic) and 25s (diabetic + resveratrol). The F (Fisher parameter)-ratio = 319.2, P < 0.0001, diabetic vs

diabetic + resveratrol. The AUC was estimated from the baseline (at the point of injection) to a fluorescence level of 0.1 and between time points of 1.0 min and 9 min using sums-of-squares. Values are the means ± SEM, n = 45–65 axons; * p < 0.001 diabetic vs diabetic + resveratrol, t-test. The red arrow indicates point of injection of antimycin A + oligomycin.

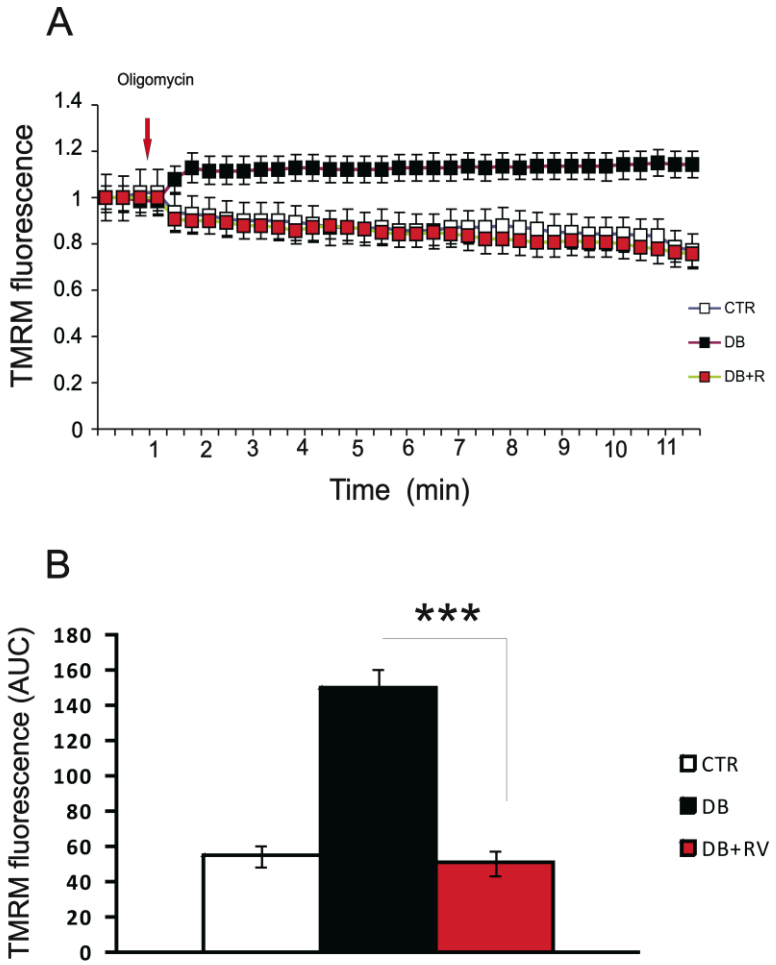

Fig. 40. Resveratrol normalizes abnormal levels of hyperpolarization induced by oligomycin in the axons of STZ diabetic neurons. *(A)* TMRM fluorescence trace showing the effect of oligomycin is shown. One- phase exponential association characterized TMRM fluorescence trace. The rate constant /slope, (K) = 0.057± 0.012 (control), 0.039 ± 0.007 (diabetic) and 0.050 ± 0.008 (diabetic + resveratrol) .The F (Fisher parameter)-ratio =233, P < 0.0001, control vs diabetic. *(B)* Shows

the area under the TMRM fluorescence trace (AUC) for control (open bar) , diabetic (black bar) and diabetic + resveratrol (red). The AUC was estimated from the baseline (at the point of injection, and between time points of 1.0 min and 6 min using sums-of-squares. Values are the means ± SEM, n = 44–53 axons,*** P < 0.01 compared to control, t-Test. The black arrow indicates point of injection of oligomycin.

As proof of principle, we determined if CNTF was capable of reversing 4-HNE induced abnormalities in mitochondrial membrane potential. Cultured neurons from normal rats were treated with/ without 4-HNE exogenously and the mitochondrial membrane potential in the axons assessed. The rate of depolarization induced by antimycin A + oligomycin was significantly slower in 4-HNE treated neurons compared with the non-treated neurons (Fig. 41). Subsequently, neurons were isolated from normal rats, treated exogenously with 4-HNE, exposed to CNTF and the mitochondrial membrane potential in the axons assessed. The rate of depolarization in the 4-HNE treated neurons was significantly greater in the presence of CNTF compared with non-treated neurons (Fig. 42).

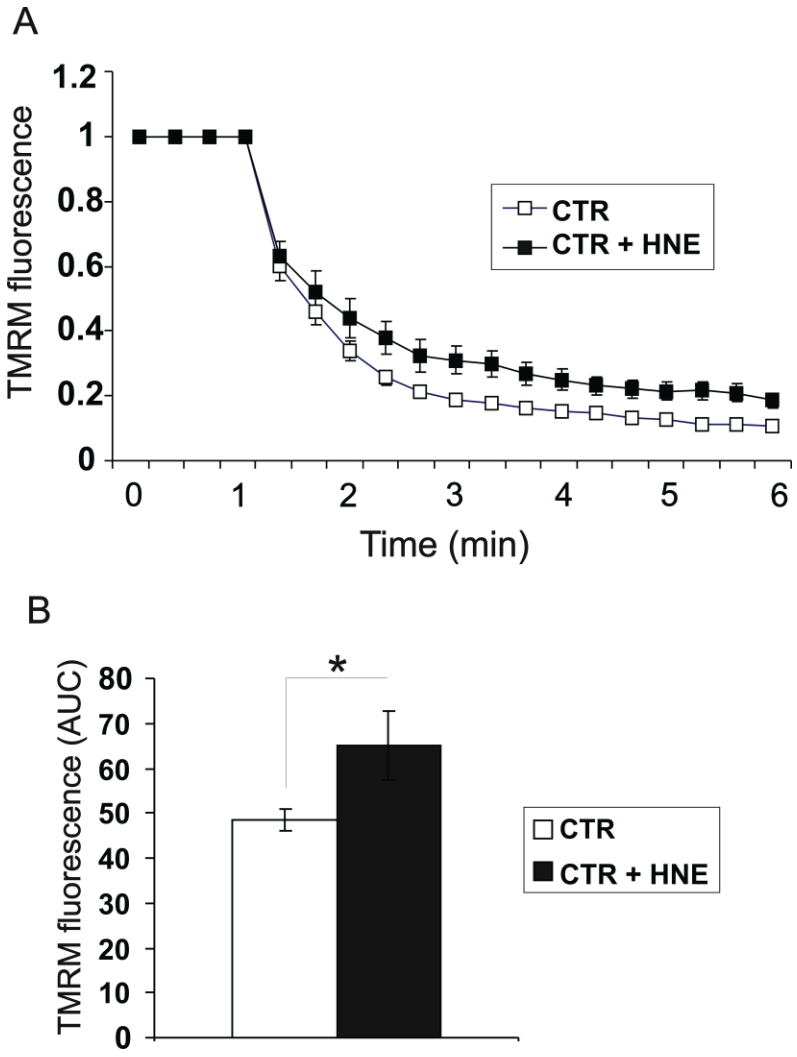

Fig. 41. Rate of mitochondrial depolarization is slower in DRG neurons treated with 4-HNE. *(A)* Trace of TMRM fluorescence signal in the axons of cultured DRG neurons treated with / without 4-HNE. *(B)* Shows the area under the TMRM fluorescence trace (AUC) for control (open bar) and 4-HNE treated neurons (filled bar). The AUC was estimated from the baseline (at the point of injection) to a fluorescence level of 0.1 and between time points of 1.0 min and 6 min using sums-of-squares (shown by dotted line). Values are the means ± SEM, n = 35–43 axons; * $p < 0.05$ compared with control, t-test. The TMRM trace was characterized by non-linear regression (one phase exponential decay). The rate constant of decay (K) = 0.011 ± 0.0004 (control) and 0.018 ± 0.0007 (control+4-HNE). Half-life of decay = 38.48 s (control) and 57 s (+ 4-HNE). The F (Fisher parametric)-ratio = 411.5, $P < 0.0001$, control vs control+4-HNE

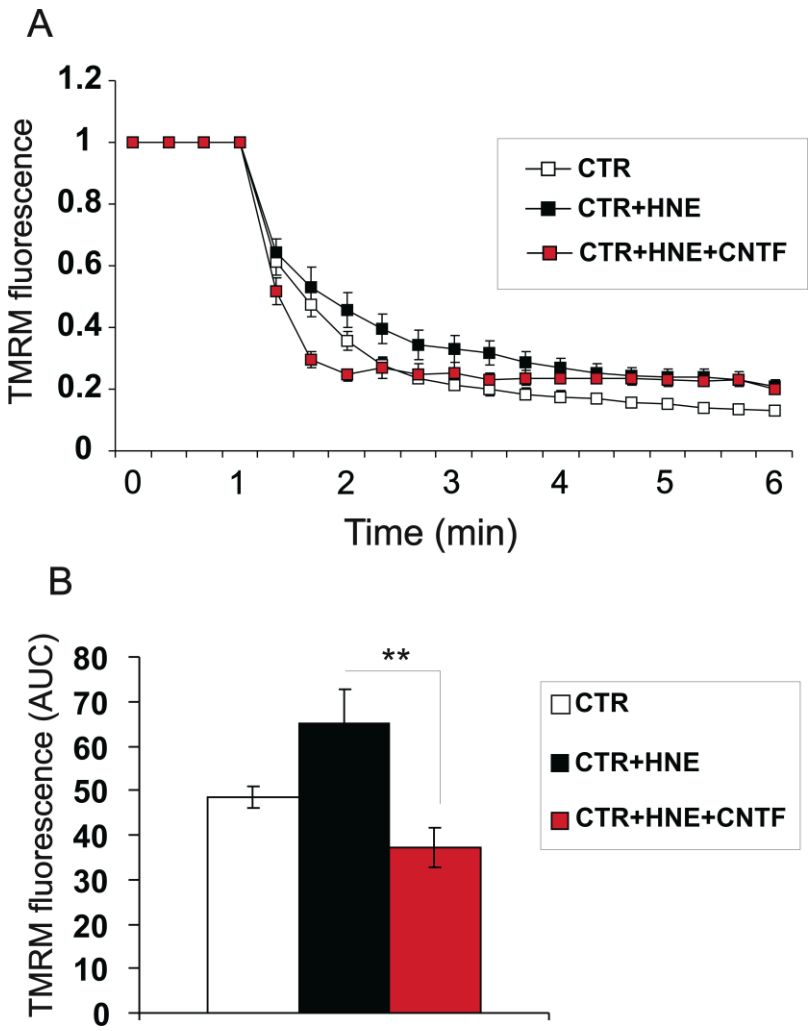

Fig. 42. CNTF normalizes abnormalities in the rate of depolarization in the axons of 4-HNE treated neurons. *(A)* Trace of TMRM fluorescence signal in the axons of 4-HNE treated DRG neurons (with or without CNTF). *(B)* Shows the area under the TMRM fluorescence trace (AUC) for control (open bar), control + 4-HNE (black bar) and control+4-HNE+CNTF (red bar). The TMRM trace was characterized by non-linear regression (one phase exponential decay). The rate constant of decay (K) = 0.018 ± 0.0007 (control), 0.011 ± 0.0001 (control + 4-HNE) and .045± .0003 (control +4-HNE+CNTF). Half-life of decay = 33 s (control), 57s (control+4-HNE) and 15.24s (control+4-HNE+ CNTF). The F (Fisher parameter)-ratio = 122.7, $P < 0.0001$, control+4-HNE vs control +4-HNE+ CNTF. The AUC was estimated from the baseline (at the point of injection) to a fluorescence level of 0.1 and between time points of 1.0 min and 6 min using sums-of-squares. Values are the means ± SEM, n = 31-45 axons; ** $p < 0.001$, control+4-HNE vs control+ 4-HNE + CNTF, t-test.

5.5. Discussion

This study demonstrates that abnormalities in mitochondrial physiology are corrected by CNTF and resveratrol in the axons of diabetic neurons. Additionally, we show that reduction in membrane potential induced by the treatment with 4-HNE is corrected by the co-treatment of neurons with CNTF. This result provides further evidence to support the fact that mitochondria are dysfunctional under conditions of oxidative stress putatively mediated by 4-HNE and/or the diabetic state. CNTF and resveratrol were employed to correct abnormalities in mitochondrial physiology in the axons of diabetic neurons. These drugs have demonstrated in the past to correct several abnormalities associated with neuropathy in vivo and in vitro (Kumar, Kaundal et al. 2007; Calcutt, Jolivalt et al. 2008). CNTF has effects throughout the nervous system, muscle and other systems(Vergara and Ramirez 2004). In the PNS, CNTF is localized in the Schwann cells, and an aldose reductase inhibitor can prevent its depletion (Kobayashi and Mizisin 2000). There is evidence to suggest that the lack of neurotrophic factors such as CNTF in peripheral nerve may contribute to the etiology of sensory neuropathy (Calcutt, Muir et al. 1992). Reduction of CNTF activity has been demonstrated in diabetic rats after 1-2months of hyperglycemia (Calcutt, Muir et al. 1992). Also various morphological abnormalities have been observed in the axons of CNTF null mice (Gatzinsky, Holtmann et al. 2003; Mizisin, Vu et al. 2004). Treatment of diabetic rats exogenously with CNTF improves nerve conduction, reduces nerve regeneration deficits and prevents several sensory disorders associated with neuropathy (Mizisin, Vu et al. 2004).

However, the mechanism underlying the ability of CNTF to reverse these abnormalities is not clearly understood. In isolated mouse skeletal muscle, the acute administration of CNTF was shown to increase AMPK activity and stimulated the expression of mitochondrial oxidative genes (Watt, Dzamko et al. 2006). Additionally, PGC-1α has been demonstrated to be upregulated in brown adipose tissues of mice administered with recombinant CNTF (Reznick and Shulman 2006; Liu, Gao et al. 2007). This supports the concept that CNTF induces mitochondrial biogenesis through the activation of AMPK and the upregulation of PGC-1α.

Resveratrol is an activator of AMP Kinase (Reznick and Shulman 2006) and it's been shown to attenuate deficits in conduction velocities and nerve blood flow, reduce diabetic neuropathic pain and several functional biochemical parameters associated with neuropathy (Kumar, Kaundal et al. 2007). Additionally, resveratrol administered systemically attenuates the cold allodynia and thermal hyperalgesia in STZ-induced diabetic rats (Sharma, Anjaneyulu et al. 2006). In the present study, we show that the rate of antimycin+oligomycin-induced depolarization of the mitochondrial membrane was significantly greater in diabetic neurons treated with CNTF or resveratrol. This suggests that CNTF and resveratrol were able to reverse the abnormalities in the mitochondrial membrane potential associated with diabetes. This adds to the fact that the drugs herein may have therapeutic potential for the treatment of diabetic neuropathy. This result was expected owing to the ability of CNTF or resveratrol to induce mitochondrial biogenesis through the activation of AMPK, and it's in good

agreement with our earlier study, which demonstrated the association between the lowered mitochondrial membrane potential in the axons of diabetic neurons and a reduction in levels of mitochondrial proteins involved in the process of oxidative phosphorylation (Chapter 4).

Also, treatment of diabetic neurons with CNTF or resveratrol was associated with a lowering of the hyperpolarized state induced by oligomycin. This suggests that CNTF or resveratrol were able to dissipate the high proton gradient induced by oligomycin in diabetic neurons. This could be attributed to the increase in biogenesis of proteins such as ANT1/2, which is involved in the process of dissipating the proton gradient across the mitochondrial membrane (Azzu, Parker et al. 2008). ANT1/2 have been shown in previous studies to be down regulated under diabetic conditions.

Our study showing that 4-HNE induces a reduction in mitochondrial membrane potential is important in that it shows the link between the elevation of ROS (Zherebitskaya, Akude et al. 2009) in diabetic neurons and the depolarization of the mitochondrial membrane. This work is in good agreement with our previous study (Akude, Zherebitskaya et al. 2010) and study by the Swzeda group (Lashin, Szweda et al. 2006), which demonstrated the formation of adducts of 4-HNE on key mitochondrial proteins leading to loss of activity. A study by Dyck et al. showed in cardiomyocytes that the 4-HNE forms adducts with LKB1, this enzyme functions as a tumor suppressor but has been shown to activate AMPK (Katajisto, Vallenius et al. 2007). The formation of 4-HNE adducts was shown to inhibit LKB1 activity and subsequently AMPK activity (Dolinsky, Chan et al.

2009). Therefore, it is very tempting to speculate from our results that 4-HNE reduced the mitochondrial membrane potential by inhibiting the activity of AMPK resulting in the reduction of mitochondrial biogenesis. This is supported by the fact that administration of CNTF in cultured DRG neurons treated with 4-HNE was able reverse the lowered state of mitochondrial membrane potential in the axons.

Impaired mitochondrial biogenesis due to diabetes and high glucose concentration could result in suboptimal activity of the electron transport chain thereby causing a reduction in the proton gradient across the mitochondrial inner membrane (mitochondrial depolarization) and ATP production. It is worth noting that about half of the ATP produced in neurons are consumed by the growth cone (Bernstein and Bamburg 2003). Due to the high energy demand of the axonal terminal, a decrease in energy production will induce an adaptive response involving the fragmentation of mitochondria (mitochondrial fission). There is evidence to suggest that mitochondrial fission and fusion play an important role in the pathogenesis of a number of neurodegenerative disorders (Frank 2006; Baloh, Schmidt et al. 2007). Mitochondrial fission could result in the formation of small-sized mitochondria, which may readily translocate to areas such as the axonal terminal where they may help regulate energy demand and balance (Fernyhough, Huang et al. 2003). Although mitochondrial fission may initially help in the distribution of energy in the neuron under conditions of reduced ATP production (Overly, Rieff et al. 1996), it causes the clustering of small mitochondrial along the axons that might impair trafficking of mitochondria

from the cell body, increase ROS generation, induced abnormal calcium regulation and further reduce energy levels in the axons (Baloh, Schmidt et al. 2007; Baloh 2008). In fact, inhibiting fission and promoting fusion (Westermann 2009) reduced ROS levels, and in cultured DRG neurons, genetic modification in the fusion inducing protein mitofusin-2 (MNF-2) resulted in clustering of small mitochondrial and aberrant trafficking of mitochondria along the axons (Baloh, Schmidt et al. 2007; Baloh 2008). Charcot Marie Tooth disease mimics diabetic neuropathy in that it affects the longest axons. Mitochondria fission in this disease induced by an increase in nitrosative and proteotoxic stress, caused the induction of the dynamin-related protein 1 (Drp 1) (Germain 2008) , which is a key regulator of mitochondrial fission (Baloh 2008). In cultured DRG neurons upregulation of Drp 1 is believed to regulate initial mitochondrial fission, and this is followed by the activation of Bim and Bax resulting in apoptosis (Leinninger, Backus et al. 2006). Although initial fragmentation and clustering of small mitochondria have been demonstrated in vivo in diabetes (Schmidt, Dorsey et al. 1997) clear evidence of apoptosis of DRG neurons is still lacking.

5.6. Conclusion

We demonstrated that CNTF and resveratrol, two drugs that are activators of AMPK and have reversed several abnormalities in diabetic neuropathy, are capable of reversing abnormities in mitochondrial physiology. This suggests that they might exert some of their effects by normalizing mitochondrial function. We also demonstrated that 4-HNE induced mitochondrial depolarization in a manner that mimics that observed under diabetic conditions. This indicates that 4-HNE

might be an important link between the elevation of ROS under diabetic conditions and the impairment of mitochondrial function under diabetic conditions. The fact that CNTF reversed this abnormality induced by 4-HNE indicates that 4-HNE might be interfering with a key process involved in mitochondrial biogenesis.

6.0. Summary of Conclusions

The overall objective of these studies was to investigate the link between hyperglycemia-induced increase in ROS levels and the process of nerve degeneration in diabetes. The increase in oxidative stress was associated with the elevation of 4-HNE in the axons of cultured diabetic neurons under hyperglycemic conditions. 4-HNE, applied exogenously to cultured DRG neurons in this study impaired axonal regeneration without significantly affecting neuronal survival. Also, 4-HNE induced abnormal swellings along the axons of 4-HNE neurons, which mimicked abnormalities present in the human condition. 4-HNE formed adducts with neurofilament H proteins and possibly inducing aberrant phosphosphorylation of these proteins. Neurofilament proteins are important constituents of the axonal cylinder and the levels and phosphorylation status of these proteins is believed to determine axonal caliber. In diabetes there is a 2-3 fold increase in neurofilament phosphorylation in the DRG of sensory neurons and this abnormality leads to the formation of aberrant neurofilament proteins, which are a key component of the cytoskeleton. 4-HNE formed adducts on mitochondrial proteins, and the formation of these adducts on mitochondrial proteins was closely associated with the loss of mitochondrial activity, which was more prominent at the distal ends of the axons compared with the proximal sections. This indicates that 4-HNE might exert it effects by impairing mitochondrial function.

Our proteomics data reveal a range of altered expression profiles in the mitochondrial proteome of DRG from diabetic rats. This modified expression pattern was associated with aberrant mitochondrial respiratory chain physiology and function. Impaired respiratory chain function did not elevate ROS generation within the mitochondrial matrix even though oxidative stress was observed in axons. In fact, the lower rates of respiratory chain activity were linked to mitochondrial membrane depolarization, improper adaption to oligomycin-induced membrane hyperpolarization and reduced levels of superoxide derived from electron leakage during electron transport. Finally, we demonstrated that CNTF and resveratrol, two drugs that act to increase mitochondrial biogenesis and reverse several abnormalities in diabetic neuropathy, are capable of reversing abnormalities in the mitochondrial membrane potential. This suggests that they might exert some of their effects by normalizing mitochondrial function. Additionally, the 4-HNE induced abnormality in mitochondrial membrane potential, was reversed by CNTF. The fact that 4-HNE induced mitochondrial depolarization in the neurons suggest that it might be central to the process of mitochondrial dysfunction in diabetes. We believe 4-HNE might be working at two levels – (a) impairing mitochondrial activity directly by forming adducts with key proteins in the respiratory chain, or (b) interfering with the signaling process involved in mitochondrial biogenesis. This indicates that 4-HNE is an important link between the elevation of ROS and the impairment of mitochondrial function under diabetic conditions.

7.0. Biblography

Abbott, C. A., L. Vileikyte, et al. (1998). "Multicenter study of the incidence of and predictive risk factors for diabetic neuropathic foot ulceration." Diabetes Care **21**(7): 1071-1075.

Akerblom, H. K., M. Knip, et al. (1997). "Interaction of genetic and environmental factors in the pathogenesis of insulin-dependent diabetes mellitus." Clin Chim Acta **257**(2): 143-156.

Akude, E., E. Zherebitskaya, et al. (2010). "4-Hydroxy-2-nonenal induces mitochondrial dysfunction and aberrant axonal outgrowth in adult sensory neurons that mimics features of diabetic neuropathy." Neurotox Res **17**(1): 28-38.

Alin, P., U. H. Danielson, et al. (1985). "4-Hydroxyalk-2-enals are substrates for glutathione transferase." FEBS Lett **179**(2): 267-270.

Amos, A. F., D. J. McCarty, et al. (1997). "The rising global burden of diabetes and its complications: estimates and projections to the year 2010." Diabet Med **14 Suppl 5**: S1-85.

Antunes, F. and E. Cadenas (2000). "Estimation of H2O2 gradients across biomembranes." FEBS Lett **475**(2): 121-126.

Awasthi, Y. C., R. Sharma, et al. (2003). "Role of 4-hydroxynonenal in stress-mediated apoptosis signaling." Mol Aspects Med **24**(4-5): 219-230.

Azzu, V., N. Parker, et al. (2008). "High membrane potential promotes alkenal-induced mitochondrial uncoupling and influences adenine nucleotide translocase conformation." Biochem J **413**(2): 323-332.

Bain, S. C., J. B. Prins, et al. (1992). "Insulin gene region-encoded susceptibility to type 1 diabetes is not restricted to HLA-DR4-positive individuals." Nat Genet **2**(3): 212-215.

Baloh, R. H. (2008). "Mitochondrial dynamics and peripheral neuropathy." Neuroscientist **14**(1): 12-18.

Baloh, R. H., R. E. Schmidt, et al. (2007). "Altered axonal mitochondrial transport in the pathogenesis of Charcot-Marie-Tooth disease from mitofusin 2 mutations." J Neurosci **27**(2): 422-430.

Behse, F., F. Buchthal, et al. (1977). "Nerve biopsy and conduction studies in diabetic neuropathy." J Neurol Neurosurg Psychiatry **40**(11): 1072-1082.

Bernstein, B. W. and J. R. Bamburg (2003). "Actin-ATP hydrolysis is a major energy drain for neurons." J Neurosci **23**(1): 1-6.

Bianchi, R., B. Buyukakilli, et al. (2004). "Erythropoietin both protects from and reverses experimental diabetic neuropathy." Proc Natl Acad Sci U S A **101**(3): 823-828.

Block, K., Y. Gorin, et al. (2009). "Subcellular localization of Nox4 and regulation in diabetes." Proc Natl Acad Sci U S A **106**(34): 14385-14390.

Boushel, R., E. Gnaiger, et al. (2007). "Patients with type 2 diabetes have normal mitochondrial function in skeletal muscle." Diabetologia **50**(4): 790-796.

Bradley, J., P. K. Thomas, et al. (1990). "Morphometry of endoneurial capillaries in diabetic sensory and autonomic neuropathy." Diabetologia **33**(10): 611-618.
Brown, M. J., A. J. Sumner, et al. (1980). "Distal neuropathy in experimental diabetes mellitus." Ann Neurol **8**(2): 168-178.
Brownlee, M. (2001). "Biochemistry and molecular cell biology of diabetic complications." Nature **414**(6865): 813-820.
Brussee, V., G. Guo, et al. (2008). "Distal degenerative sensory neuropathy in a long-term type 2 diabetes rat model." Diabetes **57**(6): 1664-1673.
Bugger, H. and E. D. Abel (2008). "Molecular mechanisms for myocardial mitochondrial dysfunction in the metabolic syndrome." Clin Sci (Lond) **114**(3): 195-210.
Bugger, H., S. Boudina, et al. (2008). "Type 1 diabetic akita mouse hearts are insulin sensitive but manifest structurally abnormal mitochondria that remain coupled despite increased uncoupling protein 3." Diabetes **57**(11): 2924-2932.
Bugger, H., D. Chen, et al. (2009). "Tissue-specific remodeling of the mitochondrial proteome in type 1 diabetic akita mice." Diabetes **58**(9): 1986-1997.
Burczynski, M. E., G. R. Sridhar, et al. (2001). "The reactive oxygen species--and Michael acceptor-inducible human aldo-keto reductase AKR1C1 reduces the alpha,beta-unsaturated aldehyde 4-hydroxy-2-nonenal to 1,4-dihydroxy-2-nonene." J Biol Chem **276**(4): 2890-2897.
Calcutt, N. A., C. G. Jolivalt, et al. (2008). "Growth factors as therapeutics for diabetic neuropathy." Curr Drug Targets **9**(1): 47-59.
Calcutt, N. A., M. C. Jorge, et al. (1996). "Tactile allodynia and formalin hyperalgesia in streptozotocin-diabetic rats: effects of insulin, aldose reductase inhibition and lidocaine." Pain **68**(2-3): 293-299.
Calcutt, N. A., D. Muir, et al. (1992). "Reduced ciliary neuronotrophic factor-like activity in nerves from diabetic or galactose-fed rats." Brain Res **575**(2): 320-324.
Cameron, N. E., M. A. Cotter, et al. (1994). "Aldose reductase inhibition, nerve perfusion, oxygenation and function in streptozotocin-diabetic rats: dose-response considerations and independence from a myo-inositol mechanism." Diabetologia **37**(7): 651-663.
Cameron, N. E., S. E. Eaton, et al. (2001). "Vascular factors and metabolic interactions in the pathogenesis of diabetic neuropathy." Diabetologia **44**(11): 1973-1988.
Carini, M., G. Aldini, et al. (2004). "Mass spectrometry for detection of 4-hydroxy-trans-2-nonenal (HNE) adducts with peptides and proteins." Mass Spectrom Rev **23**(4): 281-305.
Chakrabarti, S., A. A. Sima, et al. (1987). "Aldose reductase in the BB rat: isolation, immunological identification and localization in the retina and peripheral nerve." Diabetologia **30**(4): 244-251.

Cheng, C. and D. W. Zochodne (2003). "Sensory neurons with activated caspase-3 survive long-term experimental diabetes." Diabetes **52**(9): 2363-2371.
Cheng, H. M. and R. G. Gonzalez (1986). "The effect of high glucose and oxidative stress on lens metabolism, aldose reductase, and senile cataractogenesis." Metabolism **35**(4 Suppl 1): 10-14.
Chopra, J. S., L. J. Hurwitz, et al. (1969). "The pathogenesis of sural nerve changes in diabetes mellitus." Brain **92**(2): 391-418.
Chowdhury, S. K., E. Zherebitskaya, et al. (2010). "Mitochondrial respiratory chain dysfunction in dorsal root ganglia of streptozotocin-induced diabetic rats and its correction by insulin treatment." Diabetes **59**(4): 1082-1091.
Christianson, J. A., J. M. Ryals, et al. (2003). "Beneficial actions of neurotrophin treatment on diabetes-induced hypoalgesia in mice." J Pain **4**(9): 493-504.
Coppey, L. J., J. S. Gellett, et al. (2001). "Effect of M40403 treatment of diabetic rats on endoneurial blood flow, motor nerve conduction velocity and vascular function of epineurial arterioles of the sciatic nerve." Br J Pharmacol **134**(1): 21-29.
Coppey, L. J., J. S. Gellett, et al. (2003). "Preventing superoxide formation in epineurial arterioles of the sciatic nerve from diabetic rats restores endothelium-dependent vasodilation." Free Radic Res **37**(1): 33-40.
Coppey, L. J., J. S. Gellett, et al. (2003). "Mediation of vascular relaxation in epineurial arterioles of the sciatic nerve: effect of diabetes in type 1 and type 2 diabetic rat models." Endothelium **10**(2): 89-94.
Cotter, M. A., A. M. Jack, et al. (2002). "Effects of the protein kinase C beta inhibitor LY333531 on neural and vascular function in rats with streptozotocin-induced diabetes." Clin Sci (Lond) **103**(3): 311-321.
Cunha, J. M., C. G. Jolivalt, et al. (2008). "Elevated lipid peroxidation and DNA oxidation in nerve from diabetic rats: effects of aldose reductase inhibition, insulin, and neurotrophic factors." Metabolism **57**(7): 873-881.
Dabkowski, E. R., C. L. Williamson, et al. (2009). "Diabetic cardiomyopathy-associated dysfunction in spatially distinct mitochondrial subpopulations." Am J Physiol Heart Circ Physiol **296**(2): H359-369.
Dahlquist, G. G. (1997). "Viruses and other perinatal exposures as initiating events for beta-cell destruction." Ann Med **29**(5): 413-417.
Darrouzet, E., C. C. Moser, et al. (2001). "Large scale domain movement in cytochrome bc(1): a new device for electron transfer in proteins." Trends Biochem Sci **26**(7): 445-451.
Davies, J. L., Y. Kawaguchi, et al. (1994). "A genome-wide search for human type 1 diabetes susceptibility genes." Nature **371**(6493): 130-136.
de Cavanagh, E. M., L. Ferder, et al. (2008). "Renal mitochondrial impairment is attenuated by AT1 blockade in experimental Type I diabetes." Am J Physiol Heart Circ Physiol **294**(1): H456-465.
De Feyter, H. M., E. Lenaers, et al. (2008). "Increased intramyocellular lipid content but normal skeletal muscle mitochondrial oxidative capacity throughout the pathogenesis of type 2 diabetes." FASEB J **22**(11): 3947-3955.

Diamond, J., A. Foerster, et al. (1992). "Sensory nerves in adult rats regenerate and restore sensory function to the skin independently of endogenous NGF." J Neurosci **12**(4): 1467-1476.
Dick, R. A., M. K. Kwak, et al. (2001). "Antioxidative function and substrate specificity of NAD(P)H-dependent alkenal/one oxidoreductase. A new role for leukotriene B4 12-hydroxydehydrogenase/15-oxoprostaglandin 13-reductase." J Biol Chem **276**(44): 40803-40810.
Dolinsky, V. W., A. Y. Chan, et al. (2009). "Resveratrol prevents the prohypertrophic effects of oxidative stress on LKB1." Circulation **119**(12): 1643-1652.
Drel, V. R., N. Mashtalir, et al. (2006). "The leptin-deficient (ob/ob) mouse: a new animal model of peripheral neuropathy of type 2 diabetes and obesity." Diabetes **55**(12): 3335-3343.
Du, X. L., D. Edelstein, et al. (2000). "Hyperglycemia-induced mitochondrial superoxide overproduction activates the hexosamine pathway and induces plasminogen activator inhibitor-1 expression by increasing Sp1 glycosylation." Proc Natl Acad Sci U S A **97**(22): 12222-12226.
Duchen, M. R., A. Verkhratsky, et al. (2008). "Mitochondria and calcium in health and disease." Cell Calcium **44**(1): 1-5.
Dyck, P. J., S. Hansen, et al. (1985). "Capillary number and percentage closed in human diabetic sural nerve." Proc Natl Acad Sci U S A **82**(8): 2513-2517.
Dyck, P. J., B. R. Zimmerman, et al. (1988). "Nerve glucose, fructose, sorbitol, myo-inositol, and fiber degeneration and regeneration in diabetic neuropathy." N Engl J Med **319**(9): 542-548.
Ebenezer, G. J., J. C. McArthur, et al. (2007). "Denervation of skin in neuropathies: the sequence of axonal and Schwann cell changes in skin biopsies." Brain **130**(Pt 10): 2703-2714.
Echtay, K. S., E. Winkler, et al. (2000). "Coenzyme Q is an obligatory cofactor for uncoupling protein function." Nature **408**(6812): 609-613.
Ellis, T. M. and M. A. Atkinson (1996). "Early infant diets and insulin-dependent diabetes." Lancet **347**(9013): 1464-1465.
Engelstad, J. K., J. L. Davies, et al. (1997). "No evidence for axonal atrophy in human diabetic polyneuropathy." J Neuropathol Exp Neurol **56**(3): 255-262.
Esterbauer, H., R. J. Schaur, et al. (1991). "Chemistry and biochemistry of 4-hydroxynonenal, malonaldehyde and related aldehydes." Free Radic Biol Med **11**(1): 81-128.
Fagerberg, S. E. (1959). "Diabetic neuropathy: a clinical and histological study on the significance of vascular affections." Acta Med Scand Suppl **345**: 1-97.
Fernyhough, P., A. Gallagher, et al. (1999). "Aberrant neurofilament phosphorylation in sensory neurons of rats with diabetic neuropathy." Diabetes **48**(4): 881-889.
Fernyhough, P., T. J. Huang, et al. (2003). "Mechanism of mitochondrial dysfunction in diabetic sensory neuropathy." J Peripher Nerv Syst **8**(4): 227-235.

Fernyhough, P., S. K. Roy Chowdhury, et al. (2010). "Mitochondrial stress and the pathogenesis of diabetic neuropathy." Expert Rev Endocrinol Metab **5**(1): 39-49.
Fernyhough, P., D. R. Smith, et al. (2005). "Activation of nuclear factor-kappaB via endogenous tumor necrosis factor alpha regulates survival of axotomized adult sensory neurons." J Neurosci **25**(7): 1682-1690.
Frank, S. (2006). "Dysregulation of mitochondrial fusion and fission: an emerging concept in neurodegeneration." Acta Neuropathol **111**(2): 93-100.
Frezza, C., S. Cipolat, et al. (2007). "Organelle isolation: functional mitochondria from mouse liver, muscle and cultured fibroblasts." Nat Protoc **2**(2): 287-295.
Fridovich, I. (1995). "Superoxide radical and superoxide dismutases." Annu Rev Biochem **64**: 97-112.
Gabbay, K. H., L. O. Merola, et al. (1966). "Sorbitol pathway: presence in nerve and cord with substrate accumulation in diabetes." Science **151**(707): 209-210.
Gabbay, K. H. and J. B. O'Sullivan (1968). "The sorbitol pathway. Enzyme localization and content in normal and diabetic nerve and cord." Diabetes **17**(5): 239-243.
Gardiner, N. J., P. Fernyhough, et al. (2005). "Alpha7 integrin mediates neurite outgrowth of distinct populations of adult sensory neurons." Mol Cell Neurosci **28**(2): 229-240.
Gardiner, N. J., Z. Wang, et al. (2007). "Expression of hexokinase isoforms in the dorsal root ganglion of the adult rat and effect of experimental diabetes." Brain Res **1175**: 143-154.
Gatzinsky, K. P., B. Holtmann, et al. (2003). "Early onset of degenerative changes at nodes of Ranvier in alpha-motor axons of Cntf null (-/-) mutant mice." Glia **42**(4): 340-349.
Geiger, T., J. Cox, et al. (2010). "Super-SILAC mix for quantitative proteomics of human tumor tissue." Nat Methods.
Germain, D. (2008). "Ubiquitin-dependent and -independent mitochondrial protein quality controls: implications in ageing and neurodegenerative diseases." Mol Microbiol **70**(6): 1334-1341.
Giannini, C. and P. J. Dyck (1995). "Basement membrane reduplication and pericyte degeneration precede development of diabetic polyneuropathy and are associated with its severity." Ann Neurol **37**(4): 498-504.
Giannini, C. and P. J. Dyck (1996). "Axoglial dysjunction: a critical appraisal of definition, techniques, and previous results." Microsc Res Tech **34**(5): 436-444.
Giardino, I., D. Edelstein, et al. (1996). "BCL-2 expression or antioxidants prevent hyperglycemia-induced formation of intracellular advanced glycation endproducts in bovine endothelial cells." J Clin Invest **97**(6): 1422-1428.
Greenwood, S. M., S. M. Mizielinska, et al. (2007). "Mitochondrial dysfunction and dendritic beading during neuronal toxicity." J Biol Chem **282**(36): 26235-26244.

Gumy, L. F., E. T. Bampton, et al. (2008). "Hyperglycaemia inhibits Schwann cell proliferation and migration and restricts regeneration of axons and Schwann cells from adult murine DRG." Mol Cell Neurosci **37**(2): 298-311.
Hartley, D. P., J. A. Ruth, et al. (1995). "The hepatocellular metabolism of 4-hydroxynonenal by alcohol dehydrogenase, aldehyde dehydrogenase, and glutathione S-transferase." Arch Biochem Biophys **316**(1): 197-205.
Haslbeck, K. M., B. Neundorfer, et al. (2007). "Activation of the RAGE pathway: a general mechanism in the pathogenesis of polyneuropathies?" Neurol Res **29**(1): 103-110.
Heimpel, S., G. Basset, et al. (2001). "Expression of the mitochondrial ADP/ATP carrier in Escherichia coli. Renaturation, reconstitution, and the effect of mutations on 10 positive residues." J Biol Chem **276**(15): 11499-11506.
Herlein, J. A., B. D. Fink, et al. (2009). "Superoxide and respiratory coupling in mitochondria of insulin-deficient diabetic rats." Endocrinology **150**(1): 46-55.
Hers, H. G. (1960). "[Aldose reductase.]." Biochim Biophys Acta **37**: 120-126.
Hoffman, P. N. (1989). "Expression of GAP-43, a rapidly transported growth-associated protein, and class II beta tubulin, a slowly transported cytoskeletal protein, are coordinated in regenerating neurons." J Neurosci **9**(3): 893-897.
Huang, T. J., S. A. Price, et al. (2003). "Insulin prevents depolarization of the mitochondrial inner membrane in sensory neurons of type 1 diabetic rats in the presence of sustained hyperglycemia." Diabetes **52**(8): 2129-2136.
Huang, T. J., N. M. Sayers, et al. (2002). "Diabetes-induced alterations in calcium homeostasis in sensory neurones of streptozotocin-diabetic rats are restricted to lumbar ganglia and are prevented by neurotrophin-3." Diabetologia **45**(4): 560-570.
Huang, T. J., N. M. Sayers, et al. (2005). "Neurotrophin-3 prevents mitochondrial dysfunction in sensory neurons of streptozotocin-diabetic rats." Exp Neurol **194**(1): 279-283.
Huang, T. J., A. Verkhratsky, et al. (2005). "Insulin enhances mitochondrial inner membrane potential and increases ATP levels through phosphoinositide 3-kinase in adult sensory neurons." Mol Cell Neurosci **28**(1): 42-54.
Ibsen, H. K. (1961). "The Crabtree effect: a review." Cancer Research **21**: 829-841.
Ido, Y., J. R. Nyengaard, et al. (2010). "Early neural and vascular dysfunctions in diabetic rats are largely sequelae of increased sorbitol oxidation." Antioxid Redox Signal **12**(1): 39-51.
Iizuka, S., W. Suzuki, et al. (2005). "Diabetic complications in a new animal model (TSOD mouse) of spontaneous NIDDM with obesity." Exp Anim **54**(1): 71-83.
Ishihama, Y., T. Sato, et al. (2005). "Quantitative mouse brain proteomics using culture-derived isotope tags as internal standards." Nat Biotechnol **23**(5): 617-621.

Isom, A. L., S. Barnes, et al. (2004). "Modification of Cytochrome c by 4-hydroxy-2-nonenal: evidence for histidine, lysine, and arginine-aldehyde adducts." J Am Soc Mass Spectrom **15**(8): 1136-1147.
Jakobsen, J. (1976). "Axonal dwindling in early experimental diabetes. I. A study of cross sectioned nerves." Diabetologia **12**(6): 539-546.
Jakobsen, J. (1976). "Axonal dwindling in early experimental diabetes. II. A study of isolated nerve fibres." Diabetologia **12**(6): 547-553.
Jakus, V. and N. Rietbrock (2004). "Advanced glycation end-products and the progress of diabetic vascular complications." Physiol Res **53**(2): 131-142.
Jekabsons, M. B. and D. G. Nicholls (2004). "In situ respiration and bioenergetic status of mitochondria in primary cerebellar granule neuronal cultures exposed continuously to glutamate." J Biol Chem **279**(31): 32989-33000.
Jiang, Y., N. A. Calcutt, et al. (2006). "Novel sites of aldose reductase immunolocalization in normal and streptozotocin-diabetic rats." J Peripher Nerv Syst **11**(4): 274-285.
Johnson, M. S., J. M. Ryals, et al. (2008). "Early loss of peptidergic intraepidermal nerve fibers in an STZ-induced mouse model of insensate diabetic neuropathy." Pain **140**(1): 35-47.
Kalichman, M. W., H. C. Powell, et al. (1998). "Reactive, degenerative, and proliferative Schwann cell responses in experimental galactose and human diabetic neuropathy." Acta Neuropathol **95**(1): 47-56.
Kamiya, H., W. Zhang, et al. (2006). "Degeneration of the Golgi and neuronal loss in dorsal root ganglia in diabetic BioBreeding/Worcester rats." Diabetologia **49**(11): 2763-2774.
Kamiya, H., W. Zhangm, et al. (2005). "Apoptotic stress is counterbalanced by survival elements preventing programmed cell death of dorsal root ganglions in subacute type 1 diabetic BB/Wor rats." Diabetes **54**(11): 3288-3295.
Karlhuber, G. M., H. C. Bauer, et al. (1997). "Cytotoxic and genotoxic effects of 4-hydroxynonenal in cerebral endothelial cells." Mutat Res **381**(2): 209-216.
Kasajima, H., S. Yamagishi, et al. (2001). "Enhanced in situ expression of aldose reductase in peripheral nerve and renal glomeruli in diabetic patients." Virchows Arch **439**(1): 46-54.
Katajisto, P., T. Vallenius, et al. (2007). "The LKB1 tumor suppressor kinase in human disease." Biochim Biophys Acta **1775**(1): 63-75.
Kawasaki, H., S. Murayama, et al. (1987). "Neurofibrillary tangles in human upper cervical ganglia. Morphological study with immunohistochemistry and electron microscopy." Acta Neuropathol **75**(2): 156-159.
Kelley, D. E., J. He, et al. (2002). "Dysfunction of mitochondria in human skeletal muscle in type 2 diabetes." Diabetes **51**(10): 2944-2950.
Kelly, M. A., M. L. Rayner, et al. (2003). "Molecular aspects of type 1 diabetes." Mol Pathol **56**(1): 1-10.
Kennedy, J. M. and D. W. Zochodne (2000). "The regenerative deficit of peripheral nerves in experimental diabetes: its extent, timing and possible mechanisms." Brain **123 (Pt 10)**: 2118-2129.

Kennedy, J. M. and D. W. Zochodne (2005). "Impaired peripheral nerve regeneration in diabetes mellitus." J Peripher Nerv Syst **10**(2): 144-157.
Kennedy, W. R., D. C. Quick, et al. (1982). "Peripheral neurology of the diabetic Chinese hamster." Diabetologia **23**(5): 445-451.
Kennedy, W. R., G. Wendelschafer-Crabb, et al. (1996). "Quantitation of epidermal nerves in diabetic neuropathy." Neurology **47**(4): 1042-1048.
King, H., R. E. Aubert, et al. (1998). "Global burden of diabetes, 1995-2025: prevalence, numerical estimates, and projections." Diabetes Care **21**(9): 1414-1431.
Kinoshita, J. H. (1990). "A thirty year journey in the polyol pathway." Exp Eye Res **50**(6): 567-573.
Kobayashi, H. and A. P. Mizisin (2000). "CNTFR alpha alone or in combination with CNTF promotes macrophage chemotaxis in vitro." Neuropeptides **34**(6): 338-347.
Kokubo, J., N. Nagatani, et al. (2008). "Mechanism of destruction of microtubule structures by 4-hydroxy-2-nonenal." Cell Struct Funct **33**(1): 51-59.
Kruszynska, Y. T., M. I. Mulford, et al. (1998). "Regulation of skeletal muscle hexokinase II by insulin in nondiabetic and NIDDM subjects." Diabetes **47**(7): 1107-1113.
Kumar, A., R. K. Kaundal, et al. (2007). "Effects of resveratrol on nerve functions, oxidative stress and DNA fragmentation in experimental diabetic neuropathy." Life Sci **80**(13): 1236-1244.
Lashin, O. M., P. A. Szweda, et al. (2006). "Decreased complex II respiration and HNE-modified SDH subunit in diabetic heart." Free Radic Biol Med **40**(5): 886-896.
Lauria, G., M. Morbin, et al. (2003). "Axonal swellings predict the degeneration of epidermal nerve fibers in painful neuropathies." Neurology **61**(5): 631-636.
Lee, A. Y. and S. S. Chung (1999). "Contributions of polyol pathway to oxidative stress in diabetic cataract." FASEB J **13**(1): 23-30.
Leinninger, G. M., C. Backus, et al. (2006). "Mitochondria in DRG neurons undergo hyperglycemic mediated injury through Bim, Bax and the fission protein Drp1." Neurobiol Dis **23**(1): 11-22.
Li, Y. M., T. Mitsuhashi, et al. (1996). "Molecular identity and cellular distribution of advanced glycation endproduct receptors: relationship of p60 to OST-48 and p90 to 80K-H membrane proteins." Proc Natl Acad Sci U S A **93**(20): 11047-11052.
Liang, H. and W. F. Ward (2006). "PGC-1alpha: a key regulator of energy metabolism." Adv Physiol Educ **30**(4): 145-151.
Liu, Q. S., M. Gao, et al. (2007). "The novel mechanism of recombinant human ciliary neurotrophic factor on the anti-diabetes activity." Basic Clin Pharmacol Toxicol **101**(2): 78-84.
Llewelyn, J. G., S. G. Gilbey, et al. (1991). "Sural nerve morphometry in diabetic autonomic and painful sensory neuropathy. A clinicopathological study." Brain **114 (Pt 2)**: 867-892.

Lorenzo, M., S. Fernandez-Veledo, et al. (2008). "Insulin resistance induced by tumor necrosis factor-alpha in myocytes and brown adipocytes." J Anim Sci **86**(14 Suppl): E94-104.
Low, P. A. and K. K. Nickander (1991). "Oxygen free radical effects in sciatic nerve in experimental diabetes." Diabetes **40**(7): 873-877.
Lowitt, S., J. I. Malone, et al. (1995). "Acetyl-L-carnitine corrects the altered peripheral nerve function of experimental diabetes." Metabolism **44**(5): 677-680.
Luckey, S. W. and D. R. Petersen (2001). "Metabolism of 4-hydroxynonenal by rat Kupffer cells." Arch Biochem Biophys **389**(1): 77-83.
Ludvigson, M. A. and R. L. Sorenson (1980). "Immunohistochemical localization of aldose reductase. I. Enzyme purification and antibody preparation--localization in peripheral nerve, artery, and testis." Diabetes **29**(6): 438-449.
Malik, R. A., J. Metcalfe, et al. (1992). "Skin epidermal thickness and vascular density in type 1 diabetes." Diabet Med **9**(3): 263-267.
Malik, R. A., P. G. Newrick, et al. (1989). "Microangiopathy in human diabetic neuropathy: relationship between capillary abnormalities and the severity of neuropathy." Diabetologia **32**(2): 92-102.
Malik, R. A., S. Tesfaye, et al. (2005). "Sural nerve pathology in diabetic patients with minimal but progressive neuropathy." Diabetologia **48**(3): 578-585.
Malik, R. A., A. Veves, et al. (1992). "Endoneurial capillary abnormalities in mild human diabetic neuropathy." J Neurol Neurosurg Psychiatry **55**(7): 557-561.
Malik, R. A., A. Veves, et al. (2001). "Sural nerve fibre pathology in diabetic patients with mild neuropathy: relationship to pain, quantitative sensory testing and peripheral nerve electrophysiology." Acta Neuropathol **101**(4): 367-374.
Mattson, M. P., S. W. Barger, et al. (1995). "Calcium, free radicals, and excitotoxic neuronal death in primary cell culture." Methods Cell Biol **46**: 187-216.
McCormack, J. G. and R. M. Denton (1990). "The role of mitochondrial Ca2+ transport and matrix Ca2+ in signal transduction in mammalian tissues." Biochim Biophys Acta **1018**(2-3): 287-291.
McCormack, J. G., A. P. Halestrap, et al. (1990). "Role of calcium ions in regulation of mammalian intramitochondrial metabolism." Physiol Rev **70**(2): 391-425.
McKinney, P. A., R. Parslow, et al. (1999). "Perinatal and neonatal determinants of childhood type 1 diabetes. A case-control study in Yorkshire, U.K." Diabetes Care **22**(6): 928-932.
Minokoshi, Y., Y. B. Kim, et al. (2002). "Leptin stimulates fatty-acid oxidation by activating AMP-activated protein kinase." Nature **415**(6869): 339-343.
Mitchell, D. Y. and D. R. Petersen (1987). "The oxidation of alpha-beta unsaturated aldehydic products of lipid peroxidation by rat liver aldehyde dehydrogenases." Toxicol Appl Pharmacol **87**(3): 403-410.

Mizisin, A. P. (2003). "Comparative neuropathology and diabetic autonomic neuropathy." Am J Pathol **163**(5): 1703-1706.
Mizisin, A. P., L. Li, et al. (1997). "Sorbitol accumulation and transmembrane efflux in osmotically stressed JS1 schwannoma cells." Neurosci Lett **229**(1): 53-56.
Mizisin, A. P., R. W. Nelson, et al. (2007). "Comparable myelinated nerve pathology in feline and human diabetes mellitus." Acta Neuropathol **113**(4): 431-442.
Mizisin, A. P., G. D. Shelton, et al. (2002). "Neurological complications associated with spontaneously occurring feline diabetes mellitus." J Neuropathol Exp Neurol **61**(10): 872-884.
Mizisin, A. P., Y. Vu, et al. (2004). "Ciliary neurotrophic factor improves nerve conduction and ameliorates regeneration deficits in diabetic rats." Diabetes **53**(7): 1807-1812.
Mogensen, M., K. Sahlin, et al. (2007). "Mitochondrial respiration is decreased in skeletal muscle of patients with type 2 diabetes." Diabetes **56**(6): 1592-1599.
Mootha, V. K., C. M. Lindgren, et al. (2003). "PGC-1alpha-responsive genes involved in oxidative phosphorylation are coordinately downregulated in human diabetes." Nat Genet **34**(3): 267-273.
Munusamy, S., H. Saba, et al. (2009). "Alteration of renal respiratory Complex-III during experimental type-1 diabetes." BMC Endocr Disord **9**: 2.
Murakawa, Y., W. Zhang, et al. (2002). "Impaired glucose tolerance and insulinopenia in the GK-rat causes peripheral neuropathy." Diabetes Metab Res Rev **18**(6): 473-483.
Nadkarni, D. V. and L. M. Sayre (1995). "Structural definition of early lysine and histidine adduction chemistry of 4-hydroxynonenal." Chem Res Toxicol **8**(2): 284-291.
Nagamatsu, M., K. K. Nickander, et al. (1995). "Lipoic acid improves nerve blood flow, reduces oxidative stress, and improves distal nerve conduction in experimental diabetic neuropathy." Diabetes Care **18**(8): 1160-1167.
Nagashima, K. and K. Oota (1974). "A histopathological study of the human spinal ganglia. 1. Normal variations in aging." Acta Pathol Jpn **24**(3): 333-344.
Neely, M. D., K. R. Sidell, et al. (1999). "The lipid peroxidation product 4-hydroxynonenal inhibits neurite outgrowth, disrupts neuronal microtubules, and modifies cellular tubulin." J Neurochem **72**(6): 2323-2333.
Nerup, J., P. Platz, et al. (1974). "HL-A antigens and diabetes mellitus." Lancet **2**(7885): 864-866.
Nicholls, D. G. (2004). "Mitochondrial dysfunction and glutamate excitotoxicity studied in primary neuronal cultures." Curr Mol Med **4**(2): 149-177.
Nicholls, D. G. (2006). "Simultaneous monitoring of ionophore- and inhibitor-mediated plasma and mitochondrial membrane potential changes in cultured neurons." J Biol Chem **281**(21): 14864-14874.
Nicholls, D. G. and S. L. Budd (2000). "Mitochondria and neuronal survival." Physiol Rev **80**(1): 315-360.

Nicholls, D. G. and M. W. Ward (2000). "Mitochondrial membrane potential and neuronal glutamate excitotoxicity: mortality and millivolts." Trends Neurosci **23**(4): 166-174.
Nieto-Vazquez, I., S. Fernandez-Veledo, et al. (2008). "Insulin resistance associated to obesity: the link TNF-alpha." Arch Physiol Biochem **114**(3): 183-194.
Nishikawa, T., D. Edelstein, et al. (2000). "Normalizing mitochondrial superoxide production blocks three pathways of hyperglycaemic damage." Nature **404**(6779): 787-790.
Norido, F., R. Canella, et al. (1984). "Development of diabetic neuropathy in the C57BL/Ks (db/db) mouse and its treatment with gangliosides." Exp Neurol **83**(2): 221-232.
Oates, P. J. (2002). "Polyol pathway and diabetic peripheral neuropathy." Int Rev Neurobiol **50**: 325-392.
Oates, P. J. (2008). "Aldose reductase, still a compelling target for diabetic neuropathy." Curr Drug Targets **9**(1): 14-36.
Oates, P. J. and B. L. Mylari (1999). "Aldose reductase inhibitors: therapeutic implications for diabetic complications." Expert Opin Investig Drugs **8**(12): 2095-2119.
Obrosova, I., X. Cao, et al. (1998). "Diabetes-induced changes in lens antioxidant status, glucose utilization and energy metabolism: effect of DL-alpha-lipoic acid." Diabetologia **41**(12): 1442-1450.
Obrosova, I., A. Faller, et al. (1997). "Glycolytic pathway, redox state of NAD(P)-couples and energy metabolism in lens in galactose-fed rats: effect of an aldose reductase inhibitor." Curr Eye Res **16**(1): 34-43.
Obrosova, I. G. (2002). "How does glucose generate oxidative stress in peripheral nerve?" Int Rev Neurobiol **50**: 3-35.
Obrosova, I. G., V. R. Drel, et al. (2005). "Oxidative-nitrosative stress and poly(ADP-ribose) polymerase (PARP) activation in experimental diabetic neuropathy: the relation is revisited." Diabetes **54**(12): 3435-3441.
Obrosova, I. G., L. Fathallah, et al. (1999). "Evaluation of a sorbitol dehydrogenase inhibitor on diabetic peripheral nerve metabolism: a prevention study." Diabetologia **42**(10): 1187-1194.
Obrosova, I. G., L. Fathallah, et al. (2001). "Taurine counteracts oxidative stress and nerve growth factor deficit in early experimental diabetic neuropathy." Exp Neurol **172**(1): 211-219.
Obrosova, I. G., O. Ilnytska, et al. (2007). "High-fat diet induced neuropathy of pre-diabetes and obesity: effects of "healthy" diet and aldose reductase inhibition." Diabetes **56**(10): 2598-2608.
Obrosova, I. G., J. G. Mabley, et al. (2005). "Role for nitrosative stress in diabetic neuropathy: evidence from studies with a peroxynitrite decomposition catalyst." FASEB J **19**(3): 401-403.
Obrosova, I. G., A. G. Minchenko, et al. (2001). "Antioxidants attenuate early up regulation of retinal vascular endothelial growth factor in streptozotocin-diabetic rats." Diabetologia **44**(9): 1102-1110.

Obrosova, I. G., C. Van Huysen, et al. (2002). "An aldose reductase inhibitor reverses early diabetes-induced changes in peripheral nerve function, metabolism, and antioxidative defense." FASEB J **16**(1): 123-125.
Ohnishi, T., C. C. Moser, et al. (2000). "Simple redox-linked proton-transfer design: new insights from structures of quinol-fumarate reductase." Structure **8**(2): R23-32.
Ola, M. S., D. A. Berkich, et al. (2006). "Analysis of glucose metabolism in diabetic rat retinas." Am J Physiol Endocrinol Metab **290**(6): E1057-1067.
Ong, S. E., B. Blagoev, et al. (2002). "Stable isotope labeling by amino acids in cell culture, SILAC, as a simple and accurate approach to expression proteomics." Mol.Cell Proteomics. **1**: 376-386.
Ota, M., K. Offord, et al. (1974). "Morphometric evaluation of first sacral ganglia of man." J Neurol Sci **22**(1): 73-82.
Ou, D., L. A. Mitchell, et al. (2000). "Cross-reactive rubella virus and glutamic acid decarboxylase (65 and 67) protein determinants recognised by T cells of patients with type I diabetes mellitus." Diabetologia **43**(6): 750-762.
Overly, C. C., H. I. Rieff, et al. (1996). "Organelle motility and metabolism in axons vs dendrites of cultured hippocampal neurons." J Cell Sci **109 (Pt 5)**: 971-980.
Patti, M. E., A. J. Butte, et al. (2003). "Coordinated reduction of genes of oxidative metabolism in humans with insulin resistance and diabetes: Potential role of PGC1 and NRF1." Proc Natl Acad Sci U S A **100**(14): 8466-8471.
Pecqueur, C., M. C. Alves-Guerra, et al. (2001). "Uncoupling protein 2, in vivo distribution, induction upon oxidative stress, and evidence for translational regulation." J Biol Chem **276**(12): 8705-8712.
Pecqueur, C., E. Couplan, et al. (2001). "Genetic and physiological analysis of the role of uncoupling proteins in human energy homeostasis." J Mol Med **79**(1): 48-56.
Perkins, B. A., D. A. Greene, et al. (2001). "Glycemic control is related to the morphological severity of diabetic sensorimotor polyneuropathy." Diabetes Care **24**(4): 748-752.
Petersen, D. R. and J. A. Doorn (2004). "Reactions of 4-hydroxynonenal with proteins and cellular targets." Free Radic Biol Med **37**(7): 937-945.
Polydefkis, M., J. W. Griffin, et al. (2003). "New insights into diabetic polyneuropathy." JAMA **290**(10): 1371-1376.
Polydefkis, M., P. Hauer, et al. (2004). "The time course of epidermal nerve fibre regeneration: studies in normal controls and in people with diabetes, with and without neuropathy." Brain **127**(Pt 7): 1606-1615.
Polydefkis, M., C. T. Yiannoutsos, et al. (2002). "Reduced intraepidermal nerve fiber density in HIV-associated sensory neuropathy." Neurology **58**(1): 115-119.
Price, S. A., L. A. Zeef, et al. (2006). "Identification of changes in gene expression in dorsal root ganglia in diabetic neuropathy: correlation with functional deficits." J Neuropathol Exp Neurol **65**(7): 722-732.

Qi, Z., H. Fujita, et al. (2005). "Characterization of susceptibility of inbred mouse strains to diabetic nephropathy." Diabetes **54**(9): 2628-2637.
Rabol, R., P. M. Hojberg, et al. (2009). "Improved glycaemic control decreases inner mitochondrial membrane leak in type 2 diabetes." Diabetes Obes Metab **11**(4): 355-360.
Reichard, J. F., J. A. Doorn, et al. (2003). "Characterization of multidrug resistance-associated protein 2 in the hepatocellular disposition of 4-hydroxynonenal." Arch Biochem Biophys **411**(2): 243-250.
Reznick, R. M. and G. I. Shulman (2006). "The role of AMP-activated protein kinase in mitochondrial biogenesis." J Physiol **574**(Pt 1): 33-39.
Russell, J. W., D. Golovoy, et al. (2002). "High glucose-induced oxidative stress and mitochondrial dysfunction in neurons." Faseb J **16**(13): 1738-1748.
Russell, J. W., K. A. Sullivan, et al. (1999). "Neurons undergo apoptosis in animal and cell culture models of diabetes." Neurobiol Dis **6**(5): 347-363.
Said, G. (1983). "[Etiology of peripheral neuropathies]." Presse Med **12**(11): 669-671.
Said, G. (2007). "Diabetic neuropathy--a review." Nat Clin Pract Neurol **3**(6): 331-340.
Said, G., A. Bigo, et al. (1998). "Uncommon early-onset neuropathy in diabetic patients." J Neurol **245**(2): 61-68.
Said, G., C. Goulon-Goeau, et al. (1992). "Severe early-onset polyneuropathy in insulin-dependent diabetes mellitus. A clinical and pathological study." N Engl J Med **326**(19): 1257-1263.
Said, G., G. Slama, et al. (1983). "Progressive centripetal degeneration of axons in small fibre diabetic polyneuropathy." Brain **106 (Pt 4)**: 791-807.
Sasaki, H., J. D. Schmelzer, et al. (1997). "Neuropathology and blood flow of nerve, spinal roots and dorsal root ganglia in longstanding diabetic rats." Acta Neuropathol **93**(2): 118-128.
Sayre, L. M., D. Lin, et al. (2006). "Protein adducts generated from products of lipid oxidation: focus on HNE and one." Drug Metab Rev **38**(4): 651-675.
Sazanov, L. A. and J. E. Walker (2000). "Cryo-electron crystallography of two sub-complexes of bovine complex I reveals the relationship between the membrane and peripheral arms." J Mol Biol **302**(2): 455-464.
Schmidt, R. E., D. Dorsey, et al. (1997). "Dystrophic axonal swellings develop as a function of age and diabetes in human dorsal root ganglia." J Neuropathol Exp Neurol **56**(9): 1028-1043.
Schmidt, R. E., D. A. Dorsey, et al. (2003). "Non-obese diabetic mice rapidly develop dramatic sympathetic neuritic dystrophy: a new experimental model of diabetic autonomic neuropathy." Am J Pathol **163**(5): 2077-2091.
Schmidt, R. E., K. G. Green, et al. (2009). "Neuritic dystrophy and neuronopathy in Akita (Ins2(Akita)) diabetic mouse sympathetic ganglia." Exp Neurol **216**(1): 207-218.
Schmidt, R. E., C. A. Parvin, et al. (2008). "Synaptic ultrastructural alterations anticipate the development of neuroaxonal dystrophy in sympathetic ganglia of aged and diabetic mice." J Neuropathol Exp Neurol **67**(12): 1166-1186.

Schmidt, R. E., S. B. Plurad, et al. (1991). "Effects of sorbinil, dietary myo-inositol supplementation, and insulin on resolution of neuroaxonal dystrophy in mesenteric nerves of streptozocin-induced diabetic rats." Diabetes **40**(5): 574-582.
Schmidt, R. E., S. B. Plurad, et al. (1993). "Effect of diabetes and aging on human sympathetic autonomic ganglia." Am J Pathol **143**(1): 143-153.
Schreyer, D. J. and J. H. Skene (1991). "Fate of GAP-43 in ascending spinal axons of DRG neurons after peripheral nerve injury: delayed accumulation and correlation with regenerative potential." J Neurosci **11**(12): 3738-3751.
Schuit, F., A. De Vos, et al. (1997). "Metabolic fate of glucose in purified islet cells. Glucose-regulated anaplerosis in beta cells." J Biol Chem **272**(30): 18572-18579.
Schultz, B. E. and S. I. Chan (2001). "Structures and proton-pumping strategies of mitochondrial respiratory enzymes." Annu Rev Biophys Biomol Struct **30**: 23-65.
Sensi, M., S. Morano, et al. (1998). "Reduction of advanced glycation end-product (AGE) levels in nervous tissue proteins of diabetic Lewis rats following islet transplants is related to different durations of poor metabolic control." Eur J Neurosci **10**(9): 2768-2775.
Sharma, A. K., S. Bajada, et al. (1981). "Influence of streptozotocin-induced diabetes on myelinated nerve fibre maturation and on body growth in the rat." Acta Neuropathol **53**(4): 257-265.
Sharma, A. K. and P. K. Thomas (1974). "Peripheral nerve structure and function in experimental diabetes." J Neurol Sci **23**(1): 1-15.
Sharma, A. K., P. K. Thomas, et al. (1983). "Peripheral nerve abnormalities in the diabetic mutant mouse." Diabetes **32**(12): 1152-1161.
Sharma, S., M. Anjaneyulu, et al. (2006). "Resveratrol, a polyphenolic phytoalexin, attenuates diabetic nephropathy in rats." Pharmacology **76**(2): 69-75.
Shen, W., J. Hao, et al. (2008). "A combination of nutriments improves mitochondrial biogenesis and function in skeletal muscle of type 2 diabetic Goto-Kakizaki rats." PLoS One **3**(6): e2328.
Shun, C. T., Y. C. Chang, et al. (2004). "Skin denervation in type 2 diabetes: correlations with diabetic duration and functional impairments." Brain **127**(Pt 7): 1593-1605.
Sidenius, P. and J. Jakobsen (1980). "Reduced perikaryal volume of lower motor and primary sensory neurons in early experimental diabetes." Diabetes **29**(3): 182-186.
Sima, A. A. and H. Kamiya (2006). "Diabetic neuropathy differs in type 1 and type 2 diabetes." Ann N Y Acad Sci **1084**: 235-249.
Sima, A. A., V. Nathaniel, et al. (1988). "Histopathological heterogeneity of neuropathy in insulin-dependent and non-insulin-dependent diabetes, and demonstration of axo-glial dysjunction in human diabetic neuropathy." J Clin Invest **81**(2): 349-364.
Sima, A. A., A. Prashar, et al. (1993). "Overt diabetic neuropathy: repair of axo-glial dysjunction and axonal atrophy by aldose reductase inhibition and its

correlation to improvement in nerve conduction velocity." Diabet Med **10**(2): 115-121.
Sima, A. A., W. Zhang, et al. (2004). "Molecular alterations underlie nodal and paranodal degeneration in type 1 diabetic neuropathy and are prevented by C-peptide." Diabetes **53**(6): 1556-1563.
Sima, A. A., W. Zhang, et al. (2000). "A comparison of diabetic polyneuropathy in type II diabetic BBZDR/Wor rats and in type I diabetic BB/Wor rats." Diabetologia **43**(6): 786-793.
Singh, R., A. Barden, et al. (2001). "Advanced glycation end-products: a review." Diabetologia **44**(2): 129-146.
Skene, J. H. (1989). "Axonal growth-associated proteins." Annu Rev Neurosci **12**: 127-156.
Sleeman, M. W., K. D. Anderson, et al. (2000). "The ciliary neurotrophic factor and its receptor, CNTFR alpha." Pharm Acta Helv **74**(2-3): 265-272.
Smith, D. S. and J. H. Skene (1997). "A transcription-dependent switch controls competence of adult neurons for distinct modes of axon growth." J Neurosci **17**(2): 646-658.
Srinivasan, S., M. Stevens, et al. (2000). "Diabetic peripheral neuropathy: evidence for apoptosis and associated mitochondrial dysfunction." Diabetes **49**(11): 1932-1938.
Stevens, M. J., I. Obrosova, et al. (2000). "Effects of DL-alpha-lipoic acid on peripheral nerve conduction, blood flow, energy metabolism, and oxidative stress in experimental diabetic neuropathy." Diabetes **49**(6): 1006-1015.
Sugimoto, K., Y. Nishizawa, et al. (1997). "Localization in human diabetic peripheral nerve of N(epsilon)-carboxymethyllysine-protein adducts, an advanced glycation endproduct." Diabetologia **40**(12): 1380-1387.
Sugimura, K. and P. J. Dyck (1981). "Sural nerve myelin thickness and axis cylinder caliber in human diabetes." Neurology **31**(9): 1087-1091.
Sumner, C. J., S. Sheth, et al. (2003). "The spectrum of neuropathy in diabetes and impaired glucose tolerance." Neurology **60**(1): 108-111.
Sutera, S. P., K. Chang, et al. (1992). "Concurrent increases in regional hematocrit and blood flow in diabetic rats: prevention by sorbinil." Am J Physiol **263**(3 Pt 2): H945-950.
Territo, P. R., S. A. French, et al. (2001). "Calcium activation of heart mitochondrial oxidative phosphorylation: rapid kinetics of mVO2, NADH, AND light scattering." J Biol Chem **276**(4): 2586-2599.
Tesfaye, S., L. K. Stevens, et al. (1996). "Prevalence of diabetic peripheral neuropathy and its relation to glycaemic control and potential risk factors: the EURODIAB IDDM Complications Study." Diabetologia **39**(11): 1377-1384.
Thomas, P. K., N. G. Beamish, et al. (1996). "Paranodal structure in diabetic sensory polyneuropathy." Acta Neuropathol **92**(6): 614-620.
Thomas, P. K. and R. G. Lascelles (1965). "Schwann-Cell Abnormalities in Diabetic Neuropathy." Lancet **1**(7400): 1355-1357.
Thornalley, P. J. (1988). "Modification of the glyoxalase system in human red blood cells by glucose in vitro." Biochem J **254**(3): 751-755.

Tilton, R. G., K. Chang, et al. (1995). "Inhibition of sorbitol dehydrogenase. Effects on vascular and neural dysfunction in streptozocin-induced diabetic rats." Diabetes **44**(2): 234-242.
Timperley, W. R., A. J. Boulton, et al. (1985). "Small vessel disease in progressive diabetic neuropathy associated with good metabolic control." J Clin Pathol **38**(9): 1030-1038.
Todd, J. A. (1996). "Transcribing diabetes." Nature **384**(6608): 407-408.
Tomlinson, D. R. (1999). "Mitogen-activated protein kinases as glucose transducers for diabetic complications." Diabetologia **42**(11): 1271-1281.
Tomlinson, D. R. and N. J. Gardiner (2008). "Glucose neurotoxicity." Nat Rev Neurosci **9**(1): 36-45.
Tomlinson, D. R., G. B. Willars, et al. (1992). "Aldose reductase inhibitors and diabetic complications." Pharmacol Ther **54**(2): 151-194.
Towbin, H., T. Staehelin, et al. (1979). "Electrophoretic transfer of proteins from polyacrylamide gels to nitrocellulose sheets: procedure and some applications." Proc Natl Acad Sci U S A **76**(9): 4350-4354.
Trueblood, N. and R. Ramasamy (1998). "Aldose reductase inhibition improves altered glucose metabolism of isolated diabetic rat hearts." Am J Physiol **275**(1 Pt 2): H75-83.
Tuck, R. R., J. D. Schmelzer, et al. (1984). "Endoneurial blood flow and oxygen tension in the sciatic nerves of rats with experimental diabetic neuropathy." Brain **107 (Pt 3)**: 935-950.
Uchida, K. (2003). "4-Hydroxy-2-nonenal: a product and mediator of oxidative stress." Prog Lipid Res **42**(4): 318-343.
Valls-Canals, J., M. Povedano, et al. (2002). "Diabetic polyneuropathy. Axonal or demyelinating?" Electromyogr Clin Neurophysiol **42**(1): 3-6.
Varela-Calvino, R., R. Ellis, et al. (2002). "Characterization of the T-cell response to coxsackievirus B4: evidence that effector memory cells predominate in patients with type 1 diabetes." Diabetes **51**(6): 1745-1753.
Vergara, C. and B. Ramirez (2004). "CNTF, a pleiotropic cytokine: emphasis on its myotrophic role." Brain Res Brain Res Rev **47**(1-3): 161-173.
Verkhratsky, A. and P. Fernyhough (2008). "Mitochondrial malfunction and Ca2+ dyshomeostasis drive neuronal pathology in diabetes." Cell Calcium **44**(1): 112-122.
Vincent, A. M., L. L. McLean, et al. (2005). "Short-term hyperglycemia produces oxidative damage and apoptosis in neurons." Faseb J **19**(6): 638-640.
Vincent, A. M., J. A. Olzmann, et al. (2004). "Uncoupling proteins prevent glucose-induced neuronal oxidative stress and programmed cell death." Diabetes **53**(3): 726-734.
Vincent, A. M., J. W. Russell, et al. (2004). "Oxidative stress in the pathogenesis of diabetic neuropathy." Endocr Rev **25**(4): 612-628.
Walker, D., A. Carrington, et al. (1999). "Structural abnormalities do not explain the early functional abnormalities in the peripheral nerves of the streptozotocin diabetic rat." J Anat **195 (Pt 3)**: 419-427.

Wang, Z., N. J. Gardiner, et al. (2008). "Blockade of hexokinase activity and binding to mitochondria inhibits neurite outgrowth in cultured adult rat sensory neurons." Neurosci Lett **434**(1): 6-11.
Wataya, T., A. Nunomura, et al. (2002). "High molecular weight neurofilament proteins are physiological substrates of adduction by the lipid peroxidation product hydroxynonenal." J Biol Chem **277**(7): 4644-4648.
Watt, M. J., N. Dzamko, et al. (2006). "CNTF reverses obesity-induced insulin resistance by activating skeletal muscle AMPK." Nat Med **12**(5): 541-548.
Waxman, S. G. (2006). "Ions, energy and axonal injury: towards a molecular neurology of multiple sclerosis." Trends Mol Med **12**(5): 192-195.
Wendelschafer-Crabb, G., W. R. Kennedy, et al. (2006). "Morphological features of nerves in skin biopsies." J Neurol Sci **242**(1-2): 15-21.
Westermann, B. (2009). "Nitric oxide links mitochondrial fission to Alzheimer's disease." Sci Signal **2**(69): pe29.
Williamson, J. R., K. Chang, et al. (1993). "Hyperglycemic pseudohypoxia and diabetic complications." Diabetes **42**(6): 801-813.
Wright, A. and H. Nukada (1994). "Sciatic nerve morphology and morphometry in mature rats with streptozocin-induced diabetes." Acta Neuropathol **88**(6): 571-578.
Yagihashi, S. (1997). "Pathogenetic mechanisms of diabetic neuropathy: lessons from animal models." J Peripher Nerv Syst **2**(2): 113-132.
Yagihashi, S. and M. Matsunaga (1979). "Ultrastructural pathology of peripheral nerves in patients with diabetic neuropathy." Tohoku J Exp Med **129**(4): 357-366.
Yagihashi, S., S. Yamagishi, et al. (2007). "Pathology and pathogenetic mechanisms of diabetic neuropathy: correlation with clinical signs and symptoms." Diabetes Res Clin Pract **77 Suppl 1**: S184-189.
Yamagata, K., N. Oda, et al. (1996). "Mutations in the hepatocyte nuclear factor-1alpha gene in maturity-onset diabetes of the young (MODY3)." Nature **384**(6608): 455-458.
Yang, J. Y., H. Y. Yeh, et al. (2009). "Insulin stimulates Akt translocation to mitochondria: implications on dysregulation of mitochondrial oxidative phosphorylation in diabetic myocardium." J Mol Cell Cardiol **46**(6): 919-926.
Yang, Y., R. Sharma, et al. (2003). "Lipid peroxidation and cell cycle signaling: 4-hydroxynonenal, a key molecule in stress mediated signaling." Acta Biochim Pol **50**(2): 319-336.
Yasuda, H. and P. J. Dyck (1987). "Abnormalities of endoneurial microvessels and sural nerve pathology in diabetic neuropathy." Neurology **37**(1): 20-28.
Yorek, M. A. (2003). "The role of oxidative stress in diabetic vascular and neural disease." Free Radic Res **37**(5): 471-480.
Yu, C., S. Rouen, et al. (2008). "Hyperglycemia and downregulation of caveolin-1 enhance neuregulin-induced demyelination." Glia **56**(8): 877-887.

Yu, X., Y. A. Tesiram, et al. (2007). "Early myocardial dysfunction in streptozotocin-induced diabetic mice: a study using in vivo magnetic resonance imaging (MRI)." Cardiovasc Diabetol **6**: 6.

Yue, D. K., M. A. Hanwell, et al. (1982). "The effect of aldose reductase inhibition on motor nerve conduction velocity in diabetic rats." Diabetes **31**(9): 789-794.

Zhang, L., C. Yu, et al. (2010). "Hyperglycemia alters the schwann cell mitochondrial proteome and decreases coupled respiration in the absence of superoxide production." J Proteome Res **9**(1): 458-471.

Zherebitskaya, E., E. Akude, et al. (2009). "Development of selective axonopathy in adult sensory neurons isolated from diabetic rats: role of glucose-induced oxidative stress." Diabetes **58**(6): 1356-1364.

Ziegler, D., P. Mayer, et al. (1988). "Evaluation of thermal, pain, and vibration sensation thresholds in newly diagnosed type 1 diabetic patients." J Neurol Neurosurg Psychiatry **51**(11): 1420-1424.

Zimmet, P. (2000). "Globalization, coca-colonization and the chronic disease epidemic: can the Doomsday scenario be averted?" J Intern Med **247**(3): 301-310.

Zochodne, D. W. and C. Nguyen (1999). "Increased peripheral nerve microvessels in early experimental diabetic neuropathy: quantitative studies of nerve and dorsal root ganglia." J Neurol Sci **166**(1): 40-46.

Zochodne, D. W., V. M. Verge, et al. (2001). "Does diabetes target ganglion neurones? Progressive sensory neurone involvement in long-term experimental diabetes." Brain **124**(Pt 11): 2319-2334.